quaternary

Article

Early–Middle Pleistocene Magnetostratigraphic and Rock Magnetic Records of the Dolynske Section (Lower Danube, Ukraine) and Their Application to the Correlation of Loess–Palaeosol Sequences in Eastern and South-Eastern Europe

Dmytro Hlavatskyi * and **Vladimir Bakhmutov**

Institute of Geophysics, National Academy of Sciences of Ukraine, 03142 Kyiv, Ukraine; bakhmutovvg@gmail.com
* Correspondence: hlavatskyi@gmail.com

Abstract: We present new palaeomagnetic and rock magnetic results with a stratigraphic interpretation of the late Early–Middle Pleistocene deposits exposed on the left bank of the River Danube at Dolynske, southern Ukraine. A thick succession of water-lain facies is succeeded by reddish-brown clayey soils, topped by a high-resolution loess–palaeosol sequence. These constitute one of the most complete recently discovered palaeoclimate archives in the Lower Danube Basin. The suggested stratigraphy is based on the position of the Matuyama–Brunhes boundary, rock magnetic, palaeopedological and sedimentological proxies, and it is confidently correlated with other loess records in the region (Roksolany and Kurortne), as well as with the marine isotope stratigraphy. The magnetic susceptibility records and palaeosol characteristics at Dolynske show an outstanding pattern that is transitional between eastern and south-eastern European loess records. Our data confirm that the well-developed S4 soil unit in Ukraine, and S5 units in Romania, Bulgaria and Serbia, correlate with the warm MIS 11. Furthermore, we suggest the correlation of rubified S6 palaeosols in Romania and Bulgaria and the V-S7–V-S8 double palaeosol in Serbia with S6 in Ukraine, a strong Mediterranean-type palaeosol which corresponds to MIS 15. Our new results do not support the hypothesis of a large magnetic lock-in depth like that previously interpreted for the Danube loess, and they prove that the Matuyama–Brunhes boundary is located within the palaeosol unit corresponding to MIS 19. The proposed stratigraphic correlation scheme may serve as a potential basis for further regional and global Pleistocene climatic reconstructions.

Keywords: Pleistocene; loess; magnetic stratigraphy; palaeoclimate; eastern Europe; regional stratigraphic correlation; Kurortne; Matuyama–Brunhes boundary

Citation: Hlavatskyi, D.; Bakhmutov, V. Early–Middle Pleistocene Magnetostratigraphic and Rock Magnetic Records of the Dolynske Section (Lower Danube, Ukraine) and Their Application to the Correlation of Loess–Palaeosol Sequences in Eastern and South-Eastern Europe. *Quaternary* **2021**, *4*, 43. https://doi.org/10.3390/quat4040043

Academic Editors: Dávid Molnár and Matthew Canti

Received: 29 August 2021
Accepted: 28 October 2021
Published: 2 December 2021

1. Introduction

Along with the well-known natural archives of ice cores, marine and lake sediments, which contain more complete records of environmental events, Quaternary climatic cycles are recorded in the most common subaerial deposits—loess–palaeosol sequences [1,2]. Loesses are relatively fresh aeolian deposits formed during colder climate periods (glaciations), whereas palaeosols develop on a loess layer by pedogenic processes during warmer and wetter conditions (interglaciations) [3]. In Eurasia they extend, approximately, in a belt running along the 40–50° N, from Belgium [4] and northern France [5] in the west, then eastward through the Danube River Basin [6–36], Poland [37–46], Ukraine [47–58], Belarus [59], Russia [60–70], Transcaucasia [71–73] and Central Asia [74–84] to the Chinese Loess Plateau (CLP) [85–99] in the east.

There has been significant focus on the implementation of new research methods within a multidisciplinary approach to search for new complete sections within the terrestrial archives, and to analyse the factors that have caused palaeoenvironmetal changes [100–119].

Rock magnetism (magnetic properties of rocks) and palaeomagnetic (magnetostratigraphy) methods, especially in combination with lithological–palaeopedological and palynological analyses, serve as a powerful tool in the reconstruction of palaeoenvironmental changes [120–122]. Magnetic susceptibility is a sensitive, fast and accurate technique to detect soil pedogenic processes and features and can improve the understanding of soil-forming and, correspondingly, palaeoclimate factors [86,123–140].

The accuracy of regional and, thus, global palaeoclimate reconstructions depends on the local chronostratigraphic interpretation of each studied stratigraphic sequence and its correlation with other land–sea records. Of the chronological approaches, magnetostratigraphic studies provide the key absolute time control for the loess–palaeosol deposits. The Matuyama–Brunhes boundary (MBB), the last geomagnetic field reversal, related to marine isotope stage (MIS) 19 and dated at ~780 ka [141,142] (or 773 ka according to recent data [143]), is one of the most frequently used time markers in the Quaternary stratigraphy [144–152]. The determination of the MBB allows for correlating even remote loess–palaesol sequences regardless of their lithostratigraphic subdivision.

Loess–palaeosol successions in Ukraine are unique in Europe in terms of their large distribution (479,000 km^2, 79% of Ukraine's territory), stratigraphic completeness and thickness, locally attaining up to 60 m in depth, e.g., Roksolany and Vyazivok sections [47,48,51,52,150,153–159]. The Ukrainian loess series were investigated by a multi-proxy approach in ~70 main profiles and at more than a thousand additional sites for the last hundred years [47,48,51,54,55,57,58,150,155,157,160–195], which allowed for constructing a detailed national stratigraphic framework [157,178,196–198]. The adjacent Lower Danube and Middle Danube Basins are also important loess regions, which have provided excellent archives for long-term high-resolution palaeoclimate studies [8,9,13–16,18,19,22,26–30,34,106,113,114,130,199–203]. A lack of reliable data from the Budzhak, southern Ukrainian region lying along the Black Sea between the Danube and Dniester rivers, which is exceptionally rich in most complete Quaternary sequences, reduces the quality of overall stratigraphic correlations [15,204–207] and palaeoclimatic reconstructions [102,110,208–212].

The aim of this paper is to derive new information on the late Early–Middle Pleistocene palaeoenvironmental dynamics and to establish regional chronostratigraphy from high-resolution rock magnetism and palaeomagnetic data at the Dolynske loess–palaeosol sequence. It is the last loess exposure along the left bank of the Danube River and the southernmost Ukrainian loess–palaeosol section studied. More importantly, it is located at the junction of East European and Danube loess domains. Consequently, pedostratigraphic and palaeoclimate interpretations of the magnetic data from the Dolynske section have important implications for the appropriate linking of Pleistocene climates and environments of other well-known eastern/south-eastern European terrestrial records.

2. Materials and Methods

2.1. Geological Setting

The Dolynske section (45°30′ N; 28°18′ E) is located between the village of Dolynske and the city of Reni, 4 km from the left bank of the Danube River, 220 km SW of Odesa (Figure 1). Previously, the Pleistocene subaerial deposits of the Danube terraces in this area were studied palaeomagnetically by Bakhmutov et al. [213]. Two famous loess sequences in Moldova, Etulia [214] and Etulia Nouă (also known as Novaya Etuliya) [215,216], which are located only 10 km NE from Dolynske, were studied using a multi-proxy approach (palaeopedology, magnetostratigraphy, rock magnetism) by different research teams [214–216]. However, their stratigraphic interpretations remained contradictory. Previous chronostratigraphic models of these sequences are shown in Table 1.

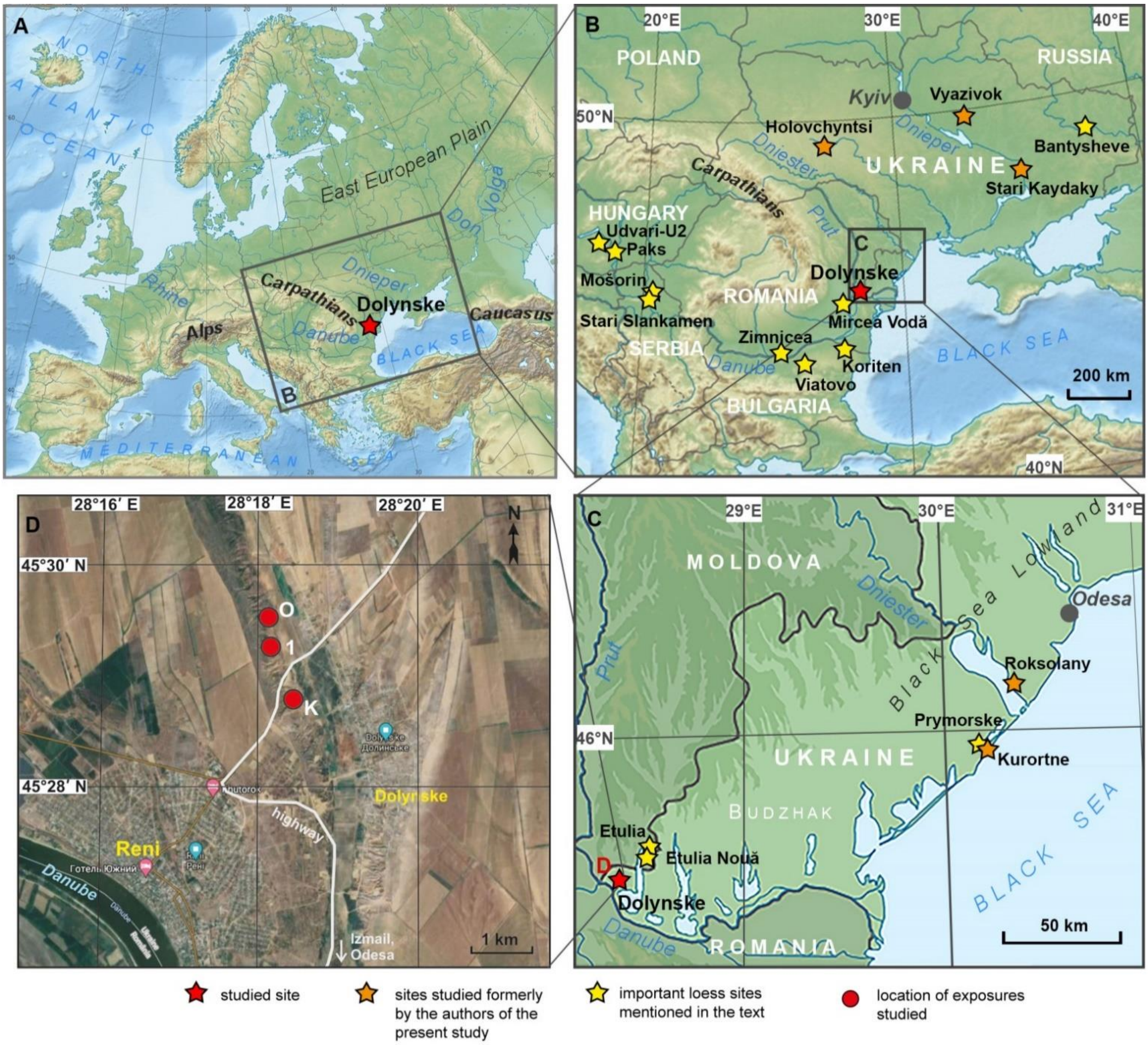

Figure 1. Location maps indicate the studied site: (**A**) Europe, (**B**) E-SE Europe, (**C**) Budzhak region, S Ukraine, and (**D**) exposures studied in the Dolynske area (adapted from: Wikimedia Commons and Google Maps).

The alluvial deposits and mammal fauna of the Dolynske area were studied extensively [217,218]. The so-called Porat Formation, a large sandy alluvial basin developed in different facies, is discerned as the Dolynske Member, which accumulated in the channel of a large river interpreted as the palaeo-Danube. According to mammal stratigraphy of the Porat Formation, this continental-scale river had reached the area by the Gelasian age to the early Calabrian age [218].

During a field reconnaissance of the Dolynske area (August 2020), the Early Pleistocene succession of water-lain (subaqual) facies (up to 17 m thick) overlain by reddish-brown soils was discovered in a newly opened quarry (section Dolynske-K; Figure 2E). These >8 m thick strong clayey and loamy soils, topped by 17 m thick loess–palaeosol succession of the Middle Pleistocene are best distinguished in two nearby exposures (Dolynske-O; Figure 2E, and Dolynske-1; Figure 2B–D). Currently, we have not reached any Late Pleistocene deposits at Dolynske.

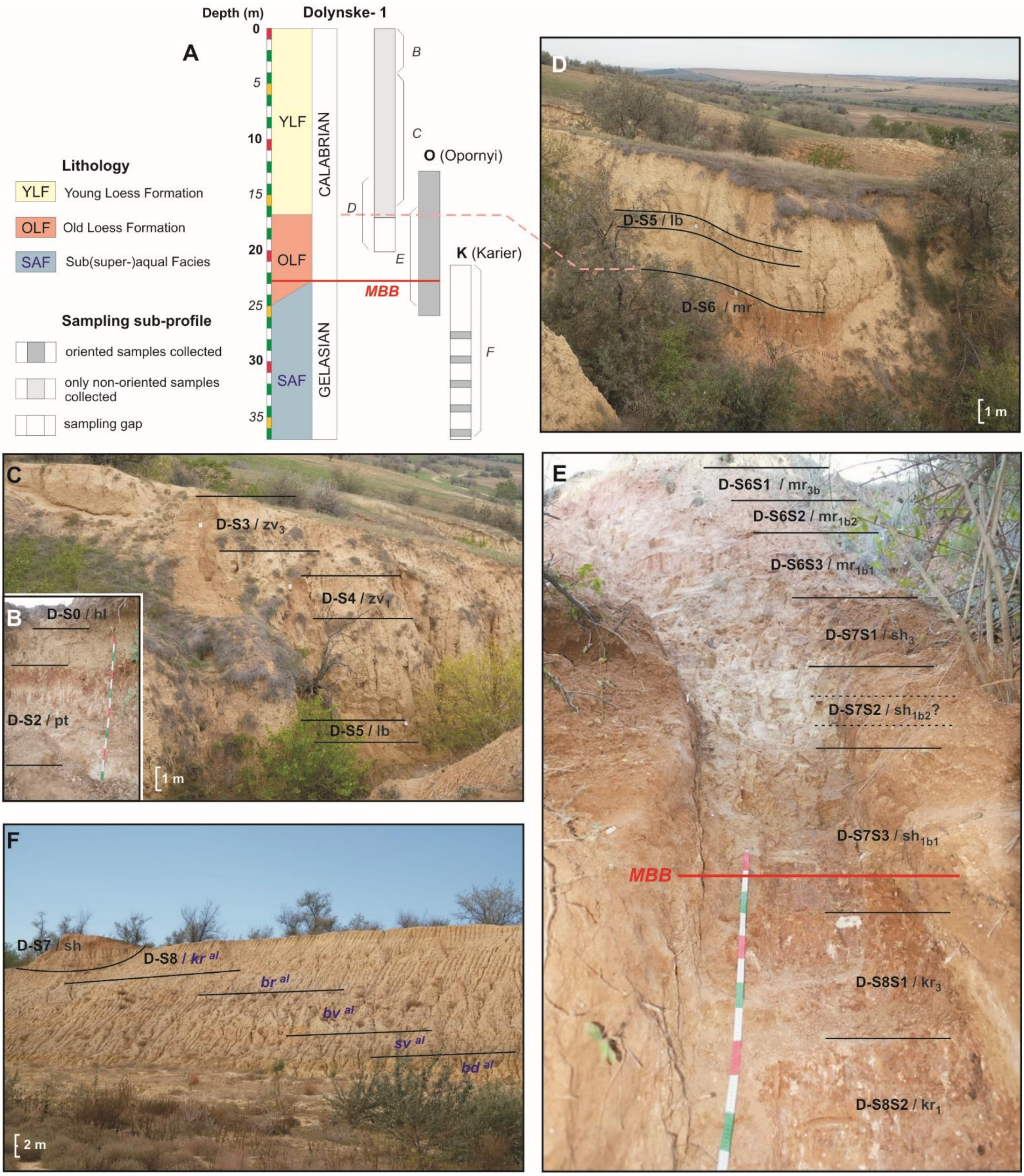

Figure 2. (**A**) Simplified geological section and sampling intervals of the named exposures (subprofiles) at the Dolynske site, accompanied by field photographs of (**B**) uppermost, (**C**) upper middle, (**D**) lower middle and (**E**) lowermost loess–palaeosol units and (**F**) alluvial deposits. For lithopedological description, see Section 3.1. The red line indicates the position of the detected Matuyama–Brunhes boundary (see Section 3.5).

Table 1. Chronostratigraphic models proposed for the Dolynske and nearby loess sections.

Etulia, after Veklich and Veklich [214]		Etulia Nouă, after Tsatskin et al. [215,216]		Dolynske (This Study)			
Palaeosol	**MIS**	**Palaeosol**	**MIS**	**Palaeosol**	**Index**	**Unit**	**MIS**
Vytachiv	5						
Pryluky	5	PK2	5				
Kaydaky	7	PK3	7–11				
Zavadivka	9–11	PK4	13–15	Potyagaylivka	pt	D-S2	7
Lubny 5	13	PK5	17	Upper Zavadivka	zv_{3c}	D-S3S1	9a
Lubny 3	15	PK6	19		zv_{3b1}	D-S3S3	9e
Lubny 1	17	PK7	21	Lower Zavadivka	zv_1	D-S4	11 [1]
Sula 2	18b–d	incipient soil	23	Lubny	lb	D-S5	13
Martonosha	19–23	PK8	25–27	Martonosha	mr	D-S6	15 [1]
Shyrokyne 3	25–?	PK9 + 10?	31–33?	Upper Shyrokyne	sh_3	D-S7S1	17
Shyrokyne 1		PK11 + 12?	35–?	Lower Shyrokyne	sh_{1b1}	D-S7S3	19c
Kryzhanivka		PK13?		Kryzhanivka	kr	D-S8	21

[1] Hereafter the MIS 11 and MIS 15 pedocomplexes are shown as marker horizons (indicated by warm colours).

For a representative interprofile correlation, neighbouring Roksolany and Kurortne loess sections were selected.

The Roksolany (formal name; in some papers known as Roxolany) section is a famous European loess profile extensively studied by numerous Ukrainian and international research teams [48,150,165,166,168–170,173,174,182,215,219–230]. Exposed in the left bank of the Dniester Estuary (46°11′ N; 30°26′ E; Figure 1C), it is quite thick (up to 55 m), probably the most complete loess sequence in the whole of southern Ukraine. The chronostratigraphy of the Roksolany section and the position of the MBB, until recently, have been a matter of concern, caused by a relative lack of pedostratigraphic basis and reliable chronological data, as well as by difficulties in determining the directions of the more stable (characteristic, ChRM) component of remanent magnetisation. Recently we have proposed a new chronostratigraphic model [150] (see Table 2), supported by established magnetostratigraphic markers, compiled existing radiocarbon and optically stimulated luminescence (OSL) dates, tephrostratigraphic, rock magnetism, palaeopedological and palaeoenvironmental proxies. This allowed for the preliminary correlation of the Ukrainian loess deposits with those in the Danube Basin and China, as well as with the marine isotope stratigraphy (further discussed in Sections 4.2 and 4.3 below).

In southern Ukraine, the closest loess section to Dolynske is the Kurortne section at the Black Sea shore (45°54′ N; 30°16′ E; Figure 1C), which is also comprehensively studied [48,171,231–233]. In some papers, it is known as Prymorske (or Primorskoje), named after another section near Kurortne, described by Veklich et al. [162]. The stratigraphy of Kurortne was further developed by Gozhik et al. [48], however, it was completely revised by Shovkoplyas et al. [232] (see Table 3). The later chronostratigraphic interpretation of the Late Pleistocene deposits [232] has recently been supported by OSL dating results [233]. The development of chronostratigraphic models for Roksolany and Kurortne/Prymorske is given in Tables 2 and 3, respectively.

Additionally, we compare our magnetostratigraphic and magnetic susceptibility records from Dolynske with those from well-known loess–palaeosol sequences in the Middle Dnieper area, at the Vyazivok and Stari Kaydaky sites, which we investigated formerly with a combined palaeomagnetic and rock magnetism approach [150,234,235].

In this study, we continue to follow the nomenclature of loess and palaeosol units used for Chinese loess stratigraphy [87,88,90], which designates loess/palaeosol layers as 'L'/'S', and the numbers of these layers are assigned in order of increasing age. We add a prefix indicating the section studied, e.g., 'D-' (Dolynske), 'R-' (Roksolany), 'K-' (Kurortne) etc. The prefix 'U-' is used for theoretical Ukrainian loess stratigraphy [150].

In parallel, we use the domestic loess stratigraphic system [157,178,183,196–198,236], in which warm stages/soil units are named by stratotype localities, and cold stages/loess units by the nearest rivers, lakes and seas. Each chronostratigraphic unit has its own index consisting of two letters (e.g., Shyrokyne—'sh'). Pedocomplexes include soils of the initial (designated by index 'a'), optimal ('b'), and final ('c') phases of pedogenesis. Usually, two middle 'b' soils (marked as 'b1' and 'b2') are well-defined and correspond to more pronounced climatic optimum. Soils of the initial and final phases, 'a' and 'c', show signs of development under cooler climates. Stages covering two–three climatic optima (usually, they correspond to interglacials *sensu stricto*) are designated by odd numbers, e.g., Lower Shyrokyne—'sh_1', Upper Shyrokyne—'sh_3'. Even numbers indicate cold stages (stadials and glacials), e.g., Middle Shyrokyne—'sh_2'.

Table 2. Chronostratigraphic models proposed for the Roksolany loess sequence.

Gozhik et al. [48,173,174], Bogucki et al. [182]		Tsatskin et al. [215]		Hlavatskyi and Bakhmutov [150]			Corrected Model Presented Here			
Palaeosol	**MIS**	**Palaeosol**	**MIS**	**Palaeosol**	**Unit**	**MIS**	**Palaeosol**	**Index**	**Unit**	**MIS**
Prychornomorya	2	PK2	5	Vytachiv	R-L1S1	3	Vytachiv	vt	R-L1S1	3
Dofinivka 1		PK3	7–11	Pryluky	R-S1S1	5a–c	Pryluky	pl	R-S1S1	5a–c
Dofinivka 2				Kaydaky	R-S1S2	5e	Kaydaky	kd	R-S1S2	5e
Vytachiv	3	PK4	13–15	Potyagaylivka	R-S2	7	Potyagaylivka	pt	R-S2	7
interstadial soil		PK5	17	Upper Zavadivka	R-S3S1	9a	Upper Zavadivka	zv_{3c}	R-S3S1	9a
Pryluky	5	PK6	19		R-S3S2 + 3	9c–e		zv_{3b}	R-S3S2 + 3	9c–e
Kaydaky	7	PK7	21	Lower Zavadivka	R-S4	11	Lower Zavadivka	zv_1	R-S4	11
Potyagaylivka	9	incipient soil	23	Lubny	R-S5	13–15	Lubny	lb	R-S5	13
Zavadivka 1	11	PK8	25–27	Upper Martonosha	R-S6S1	17a–c	Martonosha	mr	R-S6	15
Zavadivka 2–3	11	PK9	31	Lower Martonosha	R-S6S2	17e	Upper Shyrokyne	sh_3	R-S7S1	17
Lubny	13–15			Lower Shyrokyne	R-S7	19	Lower Shyrokyne	sh_1	R-S7S3	19c
Martonosha	17–19			Kryzhanivka	R-S8	21	Kryzhanivka	kr	R-S8	21
Shyrokyne	21			Middle Berezan	R-L9S1	23	Middle Berezan	br_2	R-L9S1	23

Table 3. Chronostratigraphic models proposed for the Kurortne/Prymorske loess sequence.

Prymorske, after Veklich et al. [162] and Gozhik et al. [48]		Kurortne, after Vozgrin [237,238] and Shovkoplyas et al. [232]		Kurortne, after Tecsa et al. [233]		Kurortne (Model Presented Here)			
Palaeosol	**MIS**	**Palaeosol**	**MIS**	**Palaeosol**	**MIS**	**Palaeosol**	**Index**	**Unit**	**MIS**
Prychornomorya		Vytachiv	3	Vytachiv	3	Vytachiv	vt	K-L1S1	3
Dofinivka 1		Pryluky	5a–c	Pryluky	5a–c	Pryluky	pl	K-S1S1	5a–c
Dofinivka 2	2	Kaydaky	5e	Kaydaky	5e	Kaydaky	kd	K-S1S2	5e
Vytachiv	3	Potyagaylivka	7			Potyagaylivka	pt	K-S2	7
Pryluky	5	Zavadivka	9			Upper Zavadivka	zv_{3c}	K-S3S1	9a
Kaydaky	7	Lubny	11				zv_{3b}	K-S3S2 + 3	9c–e
Zavadivka	9–11	Martonosha	?–19			Lower Zavadivka	zv_1	K-S4	11
Lubny [1]	13–15					Lubny	lb	K-S5	13
Martonosha	17–19					Martonosha	mr	K-S6	15

[1] Previously considered [208,236] as a correlative of MIS 13–17.

2.2. Sampling and Methods

A representative collection of samples at Dolynske was collected in October 2020 from three overlapping exposures (Figures 1D and 2A), designated as 'Dolynske-1', 'Dolynske-O' (Opornyi) and 'Dolynske-K' (Karier). The sampling subprofiles were overlapped by 3 m by tracing at least two characteristic soil layers. The distinct boundary between the older well-developed reddish-brown clayey palaeosols (from the D-S6 soil and lower) and the younger loess series, as well as a thin truncated greyish-brown soil, D-S5, served as useful correlation markers.

In total, 85 oriented block samples taken for magnetostratigraphic study and 296 non-oriented samples were extracted for rock magnetism measurements from the rest of the profile. Oriented samples were primarily collected around the expected position (based on the lithostratigraphic classification in the field) of the MBB (continuous sampling from a 13.62 to 24.38 m depth interval, 80 samples), and in the older alluvial deposits (five samples at a ~2.0 m interval). Rock magnetism and palaeomagnetic measurements were carried out in the laboratory of the Institute of Geophysics of the National Academy of Sciences of Ukraine (Kyiv).

To obtain a high-resolution magnetic susceptibility record of the loess–soil sequence, 537 specimens from the depth interval between 0.24 and 24.38 m were measured. Measurements of mass-specific susceptibility were carried out at the dual frequencies of 976 Hz (χ_{lf}) and 15616 Hz (χ_{hf}) using a MFK1-FB Kappabridge. The differences between the two susceptibilities provided the frequency-dependent magnetic susceptibility. Absolute (χ_{fd}) and its relative parameter ($\chi_{fd\%}$) were calculated as follows: $\chi_{fd} = \chi_{lf} - \chi_{hf}$; $\chi_{fd\%} = (\chi_{lf} - \chi_{hf})/\chi_{lf} \times 100$.

Isothermal remanent magnetisation (IRM) curves were obtained for 26 specimens from all stratigraphic units in magnetic fields from 0 to 1.0 T. Other rock magnetic parameters were measured for a pilot collection of 175 samples: (1) anhysteretic remanent magnetisation (ARM) produced along one spatial axis and induced with a 50 µT static field and 50 mT alternating field (AF) using an AMU-1A anhystereretic magnetizer; (2) saturation isothermal remanent magnetisation (SIRM) acquired under a magnetic field of 1.0 T field; (3) IRM_{-300mT} acquired under the opposite magnetic field of −300 mT. Combinations of these parameters were used for the determination of magnetic rock properties: granulometric indices ARM/SIRM, χ_{lf}/SIRM; indices of magnetic hardness S-ratio = IRM_{-300mT}/SIRM; HIRM = (SIRM + IRM_{-300mT})/2 [128,129].

For the magnetostratigraphic study, 249 standard oriented cubes (2.0 cm side) were cut (2–6 specimens from each sample). To avoid errors due to mechanical disturbances (caused by molehills, etc.), the anisotropy of magnetic susceptibility (AMS) was analyzed. Eventually, 113 specimens were selected for palaeomagnetic interpretation. Specimens were exposed in a magnetically-shielded room (a low-field cage, MMLFC) for at least one week before demagnetisation and remanence measuring to reduce the viscous magnetisation caused by the modern magnetic field.

A total of 95 specimens (including 8 specimens from alluvial deposits) were subjected to 5 steps of thermal demagnetisation from 150 °C to 295 °C at temperature intervals between 25 and 60 °C, using a MMTD 80 furnace with a residual field set at <10 nT. After each heating step, bulk susceptibility (κ) at room temperature was measured with a MFK1-FB Kappabridge to monitor possible mineralogical changes. Twelve duplicate specimens were subjected to AF demagnetisation from 3 to 80 mT at steps between 3 and 20 mT, using an LDA-3A demagnetizer. Then, they were heated to temperatures of 240 and 270 °C for cross-checking. An additional 6 samples were subjected to the hybrid demagnetisation process. This procedure involved one-time thermal demagnetisation up to 150 °C, then a standard stepwise AF demagnetisation from 3 to 80 mT at 3–20 mT intervals. The natural remanent magnetisation (NRM) of specimens was measured by a JR-6 spinner magnetometer.

Six samples collected from the K-S6 (Martonosha) alluvial soil unit at the Kurortne section were investigated by thermal demagnetisation.

Demagnetisation results were processed by multicomponent analysis of the demagnetisation path [239] using Remasoft 3.0 software [240]. Samples which failed to isolate the ChRM or had both anomalous AMS and anomalous ChRM directions were excluded from further interpretation. The magnetostratigraphic column was built with MPS software [241], which allows for the more accurate identification of zones of normal and reversed polarity.

Chronostratigraphic interpretation has been supported by a correlation between magnetic susceptibility stratigraphy and marine isotope stratigraphy [242,243].

3. Results

After the sampling of the Dolynske sequence, thorough field observations complemented by pedostratigraphic data (presented in Section 3.1) and magnetic susceptibility measurements (Section 3.2) enabled us to develop a new stratigraphy of the loess–palaeosol sequence for the interval of ~25 m. This was later corroborated by the magnetostratigraphic data presented in Section 3.5.

3.1. Pedostratigraphic Subdivision

In the subaerial part of the sequence, eight interglacial palaeosols could have been identified (Figures 2 and 3). Younger palaeosols are separated by thick loess units (D-L2 to D-L6). Loess layers inside older palaeosol series (between D-S6 and D-S8) have been reworked due to pedogenesis and replaced by carbonate horizons of the overlying soils.

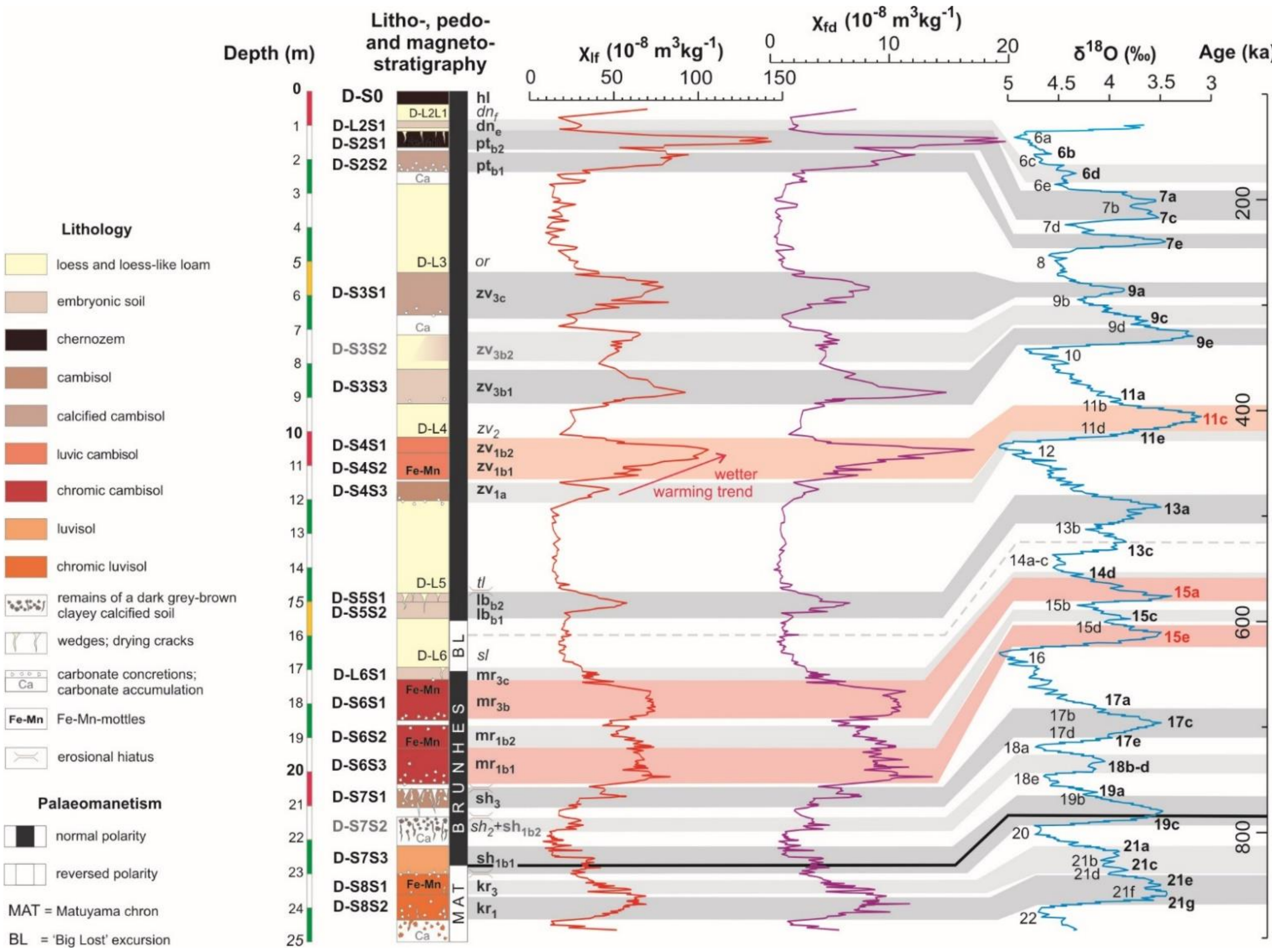

Figure 3. Low-field (χ_{lf}) and frequency dependence (χ_{fd}) magnetic susceptibility variations along lithological column of the Dolynske section, and proposed correlation with global marine isotope LR04 stack of Lisiecki and Raymo [242] (lettered substages adapted from Railsback et al. [243]. Magnetostratigraphic results are described in Section 3.5. Chronostratigraphic interpretation relative to marine isotope stratigraphy is given in Section 4.2.

The uppermost palaeosol, D-S2 (Potyagaylivka, abbreviated as 'pt') is a polygenetic soil, containing two well-developed soils separated by calcareous loam. The upper one, D-S2S1 (pt_{b2}), is a strong reddish-brown (7.5YR 4/6–6/6) soil, deformed by wedges of the overlying D-L2 (Dnipro, dn) loess. The lower soil, D-S2S1 (pt_{b1}), is thicker, has a yellowish brown colour (10YR 5/4), discoloured by carbonates in its lower part. An embryonic soil, D-L2S1 (dn_e), could have been found just above the D-S2S1 soil.

Below the D-S2 pedocomplex and underlying D-L3 (Oril, or) loess, the succession of peculiar Zavadivka (zv) cambisols D-S3S1 through D-S4 was exposed. The upper soil, D-S3S1 (zv_{3c}), is brown (10YR 4/3). A horizon is separated by a thick carbonate accumulation zone (Bk) and calcareous loess-like loam from the lower pedomember of weakly developed brown (10YR 5/3) D-S3S3 (zv_{3b1}) palaeosol. Yellowish brown (10YR 5/4) embryonic soil D-S3S2 (zv_{3b2}) occurs sometimes instead of the middle loessic layer. The A horizons are less developed than in the younger D-S2, presumably because of truncation or post-burial diagenesis.

The D-S4 (Lower Zavadivka, zv_1) soil unit is a relatively well-developed dark yellowish-brown (10YR 4/4–5/4) soil, but it has a weaker A horizon than the D-S2 pedocomplex. It is separated from the overlying pedocomplex by the loess layer, D-L4 (Middle Zavadivka, zv_2).

Overlain by thick D-L5 (Tyligul, tl) loess, the D-S5 (Lubny, lb) pedocomplex is partly eroded from the top. It is represented by two weakly developed brown (10YR 4/3–5/3) horizons. The upper soil is similar to brunizem, the lower soil is a cambisol.

The D-S5 palaeosol is overlying the D-L6 (Sula, sl) loess. In the lower part of D-L6, an embryonic soil, D-L6S1 (sl_2/mr_{3c}?), could have been observed. It is placed just above the D-S6 pedocomplex, the boundary between them is sharp.

The D-S6 (Martonosha, mr) unit consists of three thick well-developed soils. The upper palaeosol, D-S6S1 (mr_3), is reddish-brown (5YR 4/4) to yellowish-red (5YR 4/6) in colour, clayey–loamy, with a prismatic structure. The middle palaeosol, D-S6S2 (mr_{1b2}), is a strong brown (7.5YR 4/6–5/6) soil with a dark A horizon, with punctuated with manganese hydroxides and secondary carbonates and very clayey. The lower palaeosol, D-S6S3 (mr_{1b1}), is a thick strong brown (7.5YR 5/6) clayey soil, with abundant carbonates in its lower part. The upper soil of the D-S6 pedocomplex is remarkably similar to the Mediterranean red-brown soils, regarded as chromic cambisols, but in palaeodepressions they are much thicker than common cambisols. Two lower soils are transitional between cambisols and chromic cambisols, most enriched in clay fraction, similar to Shyrokyne (sh) soils in central Ukraine, but they are not dark enough in colour (like the sh_3 subunit), have a reddish hue (Figure 2E), they formed in warmer climatic conditions, and they do not have wedges or drying cracks indicating any succeeding glaciation.

On the contrary, the upper palaeosol (D-S7S1/Upper Shyrokyne, sh_3) of the underlying soil succession (D-S7) is deeply deformed, likely by the strong Pryazovya (pr) periglacial processes. D-S7S1 is a thin yellowish-brown (10YR 5/4) clayey soil, with abundant cracks filled by the material of carbonate horizon of the SK-S6S3 palaeosol. It has a high Bk horizon, with a relatively thick and firm underlying pale yellow (2.5Y 7/4) loess-like layer (aleurolite?) of the Middle Shyrokyne (?) subunit (sh_2?), indicating another glacial period. The latter contains remains of the dark greyish-brown soil, D-S7S2 (Lower Shyrokyne, sh_{1b2}), also with thick carbonate accumulation zone. The lowermost palaeosol in this soil succession, D-S7S3 (sh_{1b1}), is a brown (7.5YR 4/4) solid clayey forest soil formed in more humid climatic conditions. It does not have such a thick carbonate horizon like in the D-S7S1 and D-S7S2 soils, but it has abundant ferric–manganese punctuation. The sh_1 soils represent climatic optimum of the Shyrokyne pedogenesis period [52,155].

The lowermost studied subaerial unit at Dolynske, D-S8, is a yellowish-red (5YR 4/6–5/6) sandy soil, having a thick Bk horizon. The D-S8 palaeosol is very similar to chromic luvisols of the Kryzhanivka (kr) unit elsewhere in southern Ukraine [185].

In the quarry (Figure 2F), 1 km SE of the main exposure, a succession of water-lain Early Pleistocene deposits could have been observed below the D-S7 soil unit. They have been identified by Veklych [244] as correlatives of the warm Kryzhanivka (kr), cold Berezan (br), warm Beregove (bv), cold Siversk (sv) and warm Bogdanivka (bd) stages. Typically, both the Berezan and Beregove units contain three characteristic subunits (br_1, br_2, br_3; and bv_1, bv_2, bv_3), whereas the Bogdanivka unit consists of five subunits (bd_1–bd_5). The subaerial equivalents of Early Pleistocene units in Ukraine are best represented in stratotype sections within the Crimean Peninsula and Donbas [47,154,163,245].

3.2. Magnetic Susceptibility Values

Low-field magnetic susceptibility χ_{lf} ranges between 9 and 145 $\times$ 10^{-8} m^3kg^{-1} in the entire profile studied (Figure 3), with a mean of 42.6 $\times$ 10^{-8} m^3kg^{-1}, a median of 37 $\times$ 10^{-8} m^3kg^{-1}. χ_{lf} and χ_{fd} data, show the same trend with depth, with significantly lower χ_{fd} values (0.11–19.61 $\times$ 10^{-8} m^3kg^{-1}; Figure 3) with a mean of 4.62 $\times$ 10^{-8} m^3kg^{-1} and a median of 3.7 $\times$ 10^{-8} m^3kg^{-1}.

The alternation of loess and palaeosols is clearly expressed in the magnetic susceptibility record. The background χ_{lf} values are in a range from 10–15 $\times$ 10^{-8} m^3kg^{-1} in loess units. Maximum χ_{lf} values reach from 140–145 $\times$ 10^{-8} m^3kg^{-1} in the uppermost part of the D-S2 soil unit (Figure 3). χ_{lf} values of Zavadivka pedocomplexes (D-S3 and D-S4) are in a range from 80–110 $\times$ 10^{-8} m^3kg^{-1}, whereas χ_{lf} values of the D-S5 unit do not exceed 55 $\times$ 10^{-8} m^3kg^{-1}. χ_{lf} values of the D-S7 soil succession are much lower (20–40 $\times$ 10^{-8} m^3kg^{-1}) than in the overlying D-S6 pedocomplex (40–70 $\times$ 10^{-8} m^3kg^{-1}), probably due to the erosion of the former and intensive calcification processes. The lowermost D-S8 palaeosol has a distinct magnetic susceptibility peak up to 65 $\times$ 10^{-8} m^3kg^{-1} in its middle part.

The background χ_{lf} values at Dolynske are comparable with those in other Ukrainian sequences (5–10 $\times$ 10^{-8} m^3kg^{-1}) [150] as well as the nearby Danube loess archives (15–25 $\times$ 10^{-8} m^3kg^{-1}) [8,9,11,13–15,130]. Likely, the magnetic susceptibility measured at other southern Ukrainian, Danubian, Central Asian and Chinese loess profiles demonstrate a strong contrast between loess and palaeosol horizons as a result of the formation of small superparamagnetic (SP) particles yielding higher values for palaeosols compared to loess [86,89,124,246]. The magnetic susceptibility variations clearly suggest the development of palaeosols during warmer and wetter periods (interglacials) and loesses during colder and drier stages (glacials) and are widely used as proxy palaeoclimate changes [121].

Many previous investigations of loess–palaeosol sequences in Eurasia (e.g., [8,9,11,13–15,22,28,74,86,93,127]) used magnetic susceptibility peaks in soils as anchor points corresponding to warm MISs, and tentative correlations between Pleistocene climatic events recorded in the longest deep sea and terrestrial archives have been provided. At Dolynske, the magnetic susceptibility (both χ_{lf} and χ_{fd}) and marine oxygen isotope curves are strikingly similar (Figure 3), which greatly facilitates chronostratigraphic interpretation. Further correlation with marine isotope stratigraphy is discussed is Section 4.2.

The frequency dependence of magnetic susceptibility ($\chi_{fd\%}$) is a direct measure of the contribution of SP grains [247]. In general, $\chi_{fd\%}$ percentages greater than 6% indicate a considerable abundance of SP ferromagnetic particles, while maximum observed values of $\geq$15% indicate that susceptibility in these horizons is dominated by SP ferrimagnets [247]. At Dolynske, $\chi_{fd\%}$ ranges between 0.7 and $19_{\%}$, with a mean of 11% in palaeosols and of 6% in loesses (Figure 4A).

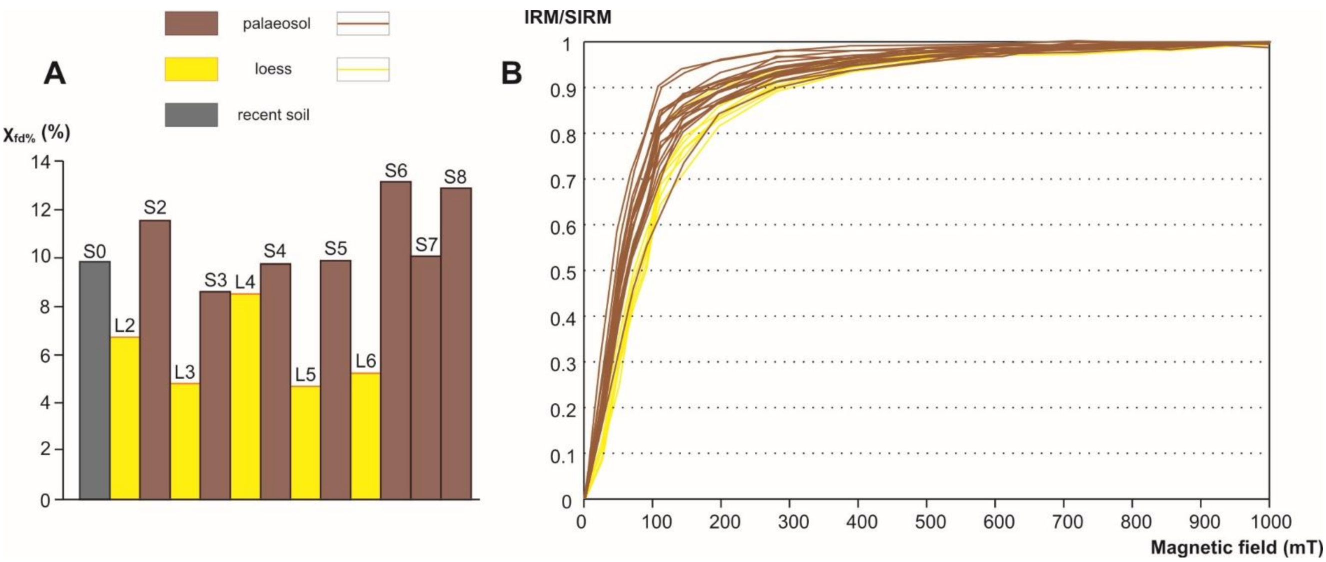

Figure 4. (**A**) Mean $\chi_{fd\%}$ values for each palaeosol and loess unit of the Dolynske section and (**B**) examples of isothermal remanent magnetisation acquisition curves of typical palaeosol and loess samples.

3.3. Selected Mineral Magnetic Properties

IRM acquisition curves for typical samples are displayed in Figure 4B. The curves get ~90% of the SIRM when the applied field is 200 mT for palaeosol samples and 300 mT for loess samples. Two palaeosol samples (from the D-S6S3 and D-S7S3 subunits) reach 90% of the SIRM in a field of 100 mT. This behaviour indicates the dominance of 'soft' magnetic minerals (like magnetite), especially in soils, while data from loess layers suggest a somewhat greater contribution of 'hard' magnetic minerals (like hematite).

ARM is sensitive to stable single-domain (SD) particles [124] due to the fact that multidomain (MD) grains generally have exceedingly low coercivities and are unable to retain any significant ARM. At Dolynske, ARM clearly increases in palaeosols compared to the loess (Figure 5), but, in our view, it depends more on the concentration of magnetic minerals rather than their domain state. SIRM is less dependent on grain size compared to ARM, but it is an excellent indicator of the concentration of magnetic minerals, and generally follows the magnetic susceptibility and ARM curves (not shown).

ARM/SIRM and χ_{lf}/SIRM ratios are widely employed as grain size indicators for magnetite [128]. Small particles yield higher values because they are more efficient at acquiring remanence, particularly ARM [248–250]. Palaeosol samples from Dolynske contain a higher fraction of SD particles yielding higher ARM/SIRM and χ_{lf}/SIRM ratios in contrast to the loesses (Figure 5).

The S-ratio is a common parameter that is used in environmental magnetism to quantify the proportion of 'hard' and 'soft' magnetic minerals [251,252]. The S-ratio is expressed as the ratio of an IRM acquired at some non-saturating backfield (often −300 mT) measured after the acquisition of an SIRM. Values close to unity indicate that the remanence is dominated by 'soft' ferrimagnets. The remanence held by 'hard' magnetic minerals within sediments is estimated by the 'hard' IRM or HIRM [253]. HIRM is typically defined as the difference between the SIRM and backfield IRM_{-300mT} divided by 2. The combination of these two parameters (S-Ratio and HIRM) provides a means of monitoring changes in magnetic mineralogy [128].

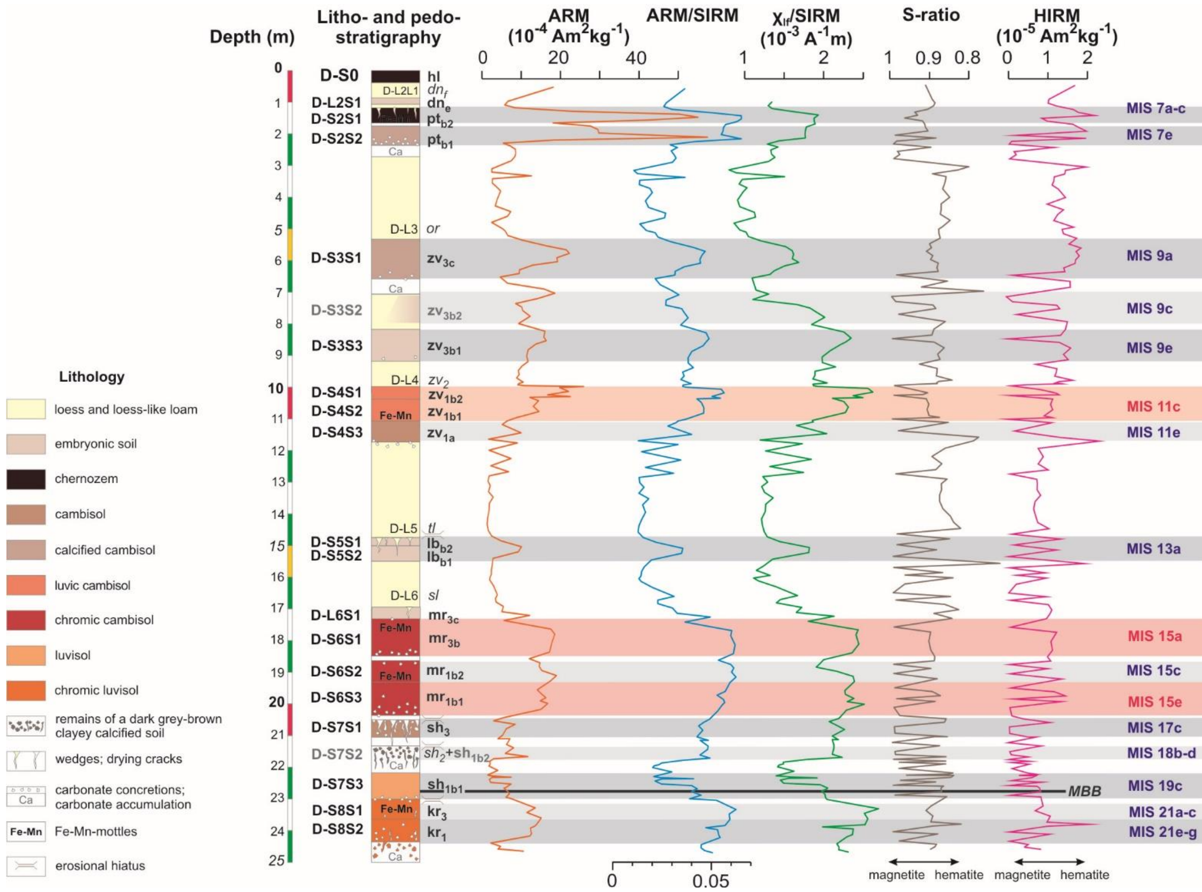

Figure 5. Variations of selected rock magnetic parameters of the Dolynske section (explanation in the text), and their relation to marine isotope stages (MIS).

The S-ratio in the Dolynske section weakly depends on lithology, but samples can be divided into two groups (Figure 5). The S-ratio of ~1/3 of specimens (mostly palaeosols) is close to 1, indicating a total dominance of magnetite, whereas the S-ratio of ~2/3 of samples (primarily, loess) fluctuates at approximately 0.9, suggesting a higher contribution of 'hard' magnetic minerals. Since the HIRM increases with the increasing fraction of magnetically 'hard' minerals, the S-ratio is linked with HIRM by negative correlation (Figure 5).

The magnetic susceptibility and ARM curves indicate the concentration of magnetic minerals, while the S-ratio and HIRM depends on the composition of a magnetic fraction. This feature reflects the difference in shape of the two types of curves (Figure 5).

Thus, rock magnetic results indicate the dominance of SP magnetite particles in palaeosols but suggest a higher contribution of 'hard' magnetic minerals (hematite) in loess.

3.4. Anisotropy of Magnetic Susceptibility

The magnetic texture of sediments reconstructed from ellipsoids of magnetic susceptibility anisotropy is closely associated with the deposition of magnetic grains with the subsequent transformation of the deposits. During diagenesis, the grains preserve their original orientation in the loess fabric. The preferred orientation of the crystallographic axis and grain elongation form magnetic fabric of the loess.

The magnetic fabric is reconstructed by the AMS analysis. The direction of palaeocurrents is reflected by the direction of maximum susceptibilities (K_{max}) [61,254,255]. The foliation plane (direction of minimum susceptibilities, K_{min}) mirrors the slope angle [256,257]. The position of the directions of the K_{max} and of the intermediate susceptibility (K_{int}) may indicate bioturbation or lamination [258–260].

The magnetic fabric of the loess and palaeosol specimens from Dolynske is mainly foliated (K_{min} axes are normal relative to the sedimentary plane; Figure S1). The maximum degree of AMS is revealed in the middle part of the section where it reaches Pj = 1.03 ÷ 1.04. In most loess–palaeosol sequences in Ukraine the degree of AMS does not exceed 1.08 [261,262], which is typical of autochthonous sedimentary deposits [59]. The degree of AMS of the loess–palaeosol deposits from the Black Sea region is lower (Pj $\leq$ 1.03) than noted in loesses and palaeosols of western and northern Ukraine (Pj $\leq$ 1.08).

The shape factor T in 97% of loess samples and in 69% of soil specimens is positive (from 0 to 1; Figure S1); samples with negative T-factor are less anisotropic (Pj $\leq$ 1.01). Thus, our results show that the AMS ellipsoids are mainly oblate in shape, and the mean inclinations of the maximum and minimum axes of susceptibility ellipsoids are generally horizontal and vertical, respectively. All this indicates a primary eolian magnetic fabric without significant disturbance which could potentially yield a reliable ChRM. All specimens with anomalous deviations from typical sedimentary texture have been excluded from further palaeomagnetic interpretation.

3.5. Magnetostratigraphy

The demagnetisation results of 87 specimens, treated by temperature, and 18 specimens, demagnetized by AF (including hybrid demagnetisation), from the depth interval of 13.78 to 24.38 m is shown in Figure 6.

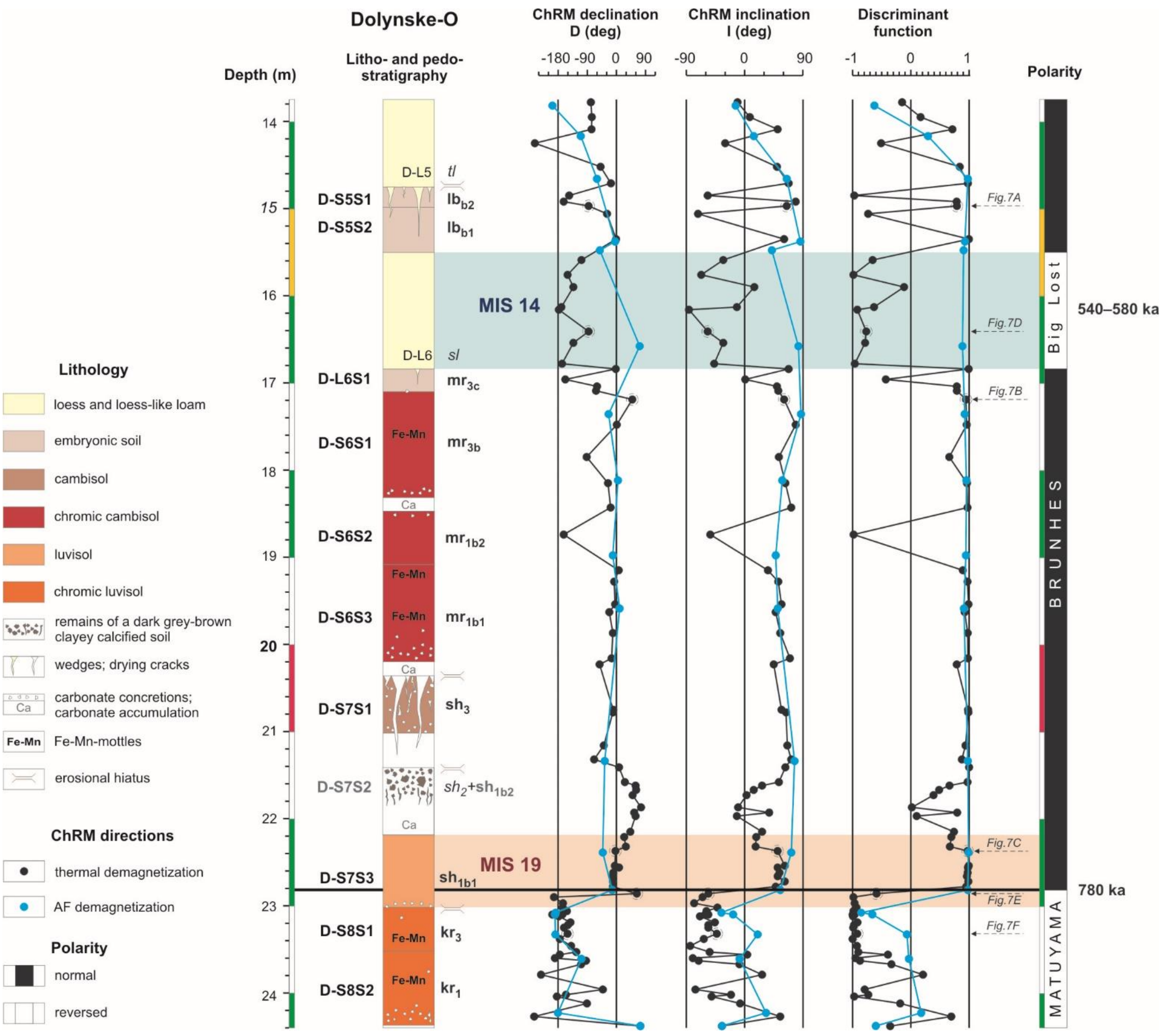

Figure 6. Results of palaeomagnetic study of the Dolynske-O subprofile. From the left—simplified lithostratigraphy, the directions of the ChRM components (expressed by declination D° and inclination I°), the discriminant function of these directions as a function of depth, and magnetostratigraphic chart. The arrows indicate the position of specimens for which the Zijderveld diagrams are shown in Figure 7.

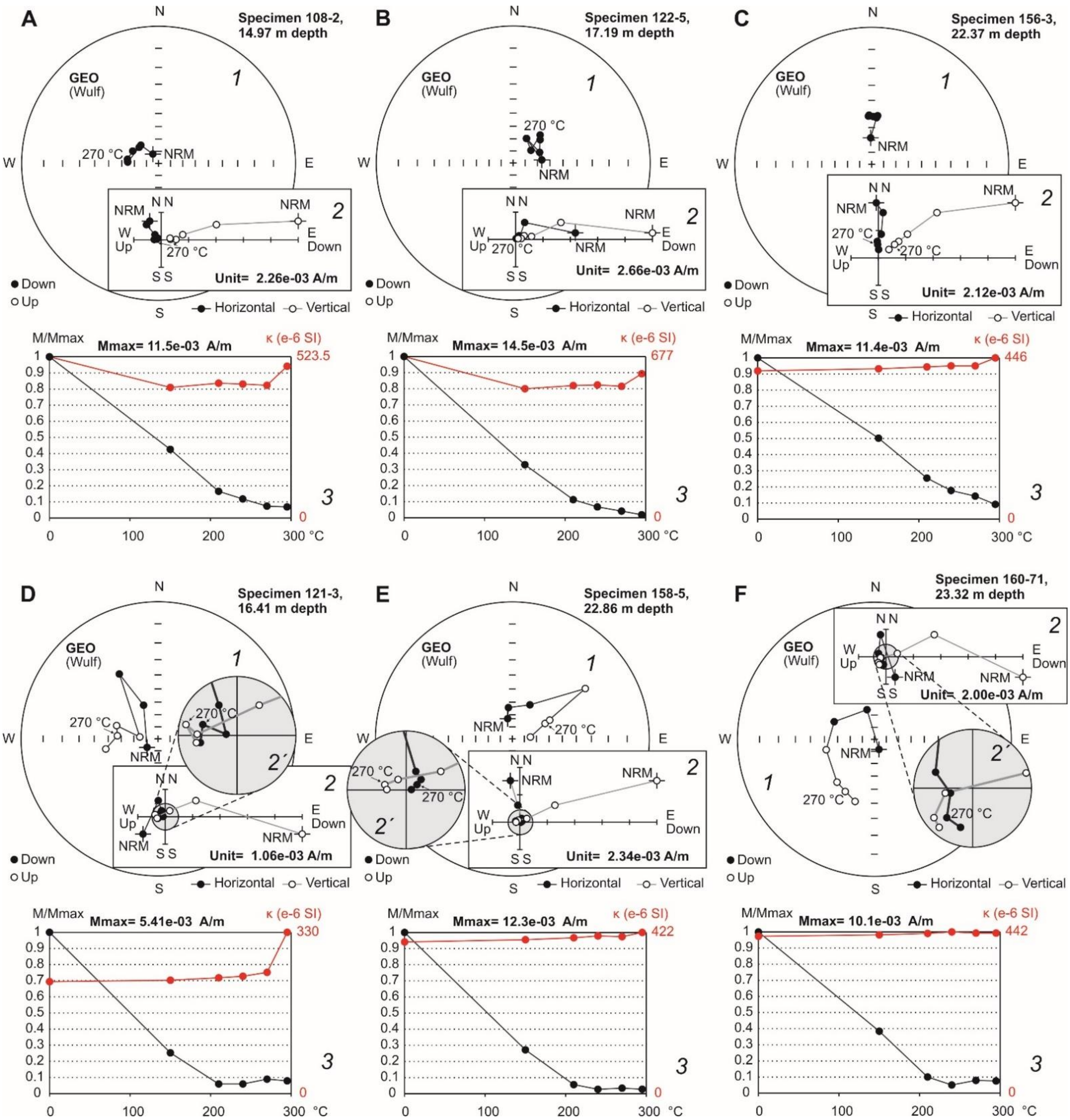

Figure 7. Examples of stepwise thermal demagnetisation of palaeosol specimens from (**A**) the D-S5S1 (lb_{b2}) subunit, (**B**) D-S6S1 (mr_3) subunit, (**C**) upper part of the D-S7S3 (sh_{1b1}) subunit, (**D**) loess specimen from the D-L6 (sl) unit, palaeosol specimens from (**E**) the lower part of the D-S7S3 (sh_{1b1}) subunit and (**F**) lower part of the D-S8S1 (kr_3) subunit. *1*—stereographic projections of demagnetisation directions (full and open circles represent projections in the lower and upper hemispheres, respectively); *2*—orthogonal demagnetisation paths (Zijderveld diagrams) on horizontal and vertical planes; *3*—NRM intensity decay curves of demagnetisation (M/M_{max}) and magnetic susceptibility (κ) variations after each demagnetisation step. Additional Zijderveld plots enlarged 5 times are shown in circular insets (*2′*).

As typical for southern Ukrainian loess [263], the data from thermal demagnetisation seem more informative: there is less scatter between demagnetisation steps, and conformity with the results of neihbouring specimens is observed. Multicomponent analysis of demagnetisation paths revealed that the NRM was composed of two components. The low stability component (viscous magnetisation parallel to the present-day field or acquired during storage) was erased in the temperature from 210 and 240 °C or by AF from 10–15 mT. The more stable (ChRM) component in many palaeosol and loess specimens was between <5 and 10% of the initial NRM (Figure 7).

The ChRM components for most samples separated between 240 °C and 295 °C, and 10–20 mT. In most specimens from the D-S5, D-S6 and D-S7 soil units these stable high temperature components decayed with increasing temperature towards the origin along nearly the same trajectory as the medium temperature components (e.g., Figure 7A–C) showing a normal polarity. In the remaining specimens from the D-L6 loess unit, the D-S8 soil unit and the very bottom of the D-S7S3 soil, a reversed polarity can be observed (Figure 7D–F). Statistical parameters of ChRM directions obtained by thermal and AF demagnetisation, namely: N—number of specimens; D—declination; I—inclination; R—length of the resultant vector; k—precision parameter; α95—the angle within which the unknown true mean lies at 95% confidence level [264], are given in Table 4.

Table 4. Group statistics of palaeomagnetic data from the Dolynske-O subprofile.

Depth Range (m)	Specimens	N	D (deg)	I (deg)	R	k	α95 (deg)
13.78 ÷ 15.21	101-5 ÷ 111-1	16	238.5	8.0	8.26	1.94	37.5
15.21 ÷ 16.81	111-6 ÷ 118A-4; 121-3	9	220.5	−31.7	6.28	2.94	36.5
16.81 ÷ 22.82	119-3 ÷ 158-1	46	346.4	67.4	25.41	2.19	19.2
22.82 ÷ 24.38	158-31 ÷ 168-1	34	197.9	−52.5	18.44	2.12	23.1
All specimens with normal polarity		54	342.2	70.8	36.09	2.96	13.8
All specimens with reversed polarity		51	211.1	−48.5	36.64	3.48	12.6

The discriminant function [241] was calculated using the ChRM directions to define the magnetostratigraphy of the composite section (Figure 6). With the intermediate directions omitted, opposite polarities of the successive specimens indicate borders between geomagnetic polarity zones. At the depth interval between 16.81 and 22.82 m, exclusively normal polarity is observed, corresponding to the Brunhes chron. At the interval between 13.78 and 15.45 m, the ChRM components are less stable, and some parallel samples yield contrasting results. The polarity of this part has been defined as normal according to the algorithm [241]. From 15.45 to 16.81 m and below 22.82 m in depth, two distinct reversed polarity zones have been identified, in our interpretation, corresponding to the Big Lost Excursion (~540–580 ka) [143,265,266] and Matuyama chron, respectively. Thus, the MBB has been defined at a depth of 22.82 m. Problems surrounding chronological assignment of the reversed polarity zone in the D-L6 loess at Dolynske, as well as the same excursion in the R-L6 loess at Roksolany, are to be discussed in Section 4.2 regarding regional stratigraphic correlation.

The final magnetostratigraphic chart does not include eight specimens from underlying alluvial deposits showing anomalous results, except for one specimen of stable reversed polarity from the Bogdanivka (bd) palaeosol unit, indicating its formation during the early Matuyama chron.

3.6. Additional Palaeomagnetic Study of the Lowermost Part of the Kurortne Section

In the previous palaeomagnetic study of the Kurortne section [171], the profile studied (from the Lubny/K-S5 unit to the top of the section) demonstrated entirely normal polarity. However, the Martonosha (K-S6) soil unit, i.e., the lowermost part of the section, was not sampled. In some earlier studies [48], the MBB was depicted in the upper part of the Martonosha soil based on stratigraphic schemes of the time.

Using a standard thermal demagnetisation procedure, we investigated six additional specimens from the very bottom of the sequence (the K-S6 palaeosol and underlying alluvium, Table 3). All specimens showed primary magnetic fabric (Figure S2) and stable palaeomagnetic results indicating completely normal polarity (Figure S3). Thus, our new palaeomagnetic data suggest that the entire loess–palaeosol sequence at Kurortne formed during the Brunhes chron.

4. Discussion

4.1. Magnetostratigraphy of Loess Sequences in the Western Black Sea Region

Previous palaeomagnetic data from two neighbouring sites (Etulia Nouă, Roksolany) have been used to establish a regional chronostratigraphic and pedostratigraphic scheme in the western Black Sea region for the past ca. 1.5 Ma [215]. The proposal was based on a position of the MBB in the upper part of pedocomplex PK7 (according to nomenclature of Tsatskin et al. [215,220]), i.e., S4, being correlated with MIS 21 (Tables 1 and 2, Figure 8). Additionally, the Jaramillo subchron in the PK8 pedocomplex (equivalent of S6) at Etulia Nouă has been reported. In our view, however, the accuracy of the stratigraphic system is based on the random interpretation of contradictory palaeomagnetic data. In [150,228,230] we have analysed, in detail, previous palaeomagnetic studies and have expressed concerns regarding methodological difficulties in the interpretation of NRM components in southern Ukrainian loesses and palaeosols. Our magnetostratigraphic data for the Roksolany section [150,226–228,230] differ from those obtained during previous investigations [215,220,221,224,225]. The reversed polarity interval between PK7 (i.e., R-S4) and PK9 (R-S7) palaeosols, which has been thought to be the Matuyama chron, was not confirmed by our results.

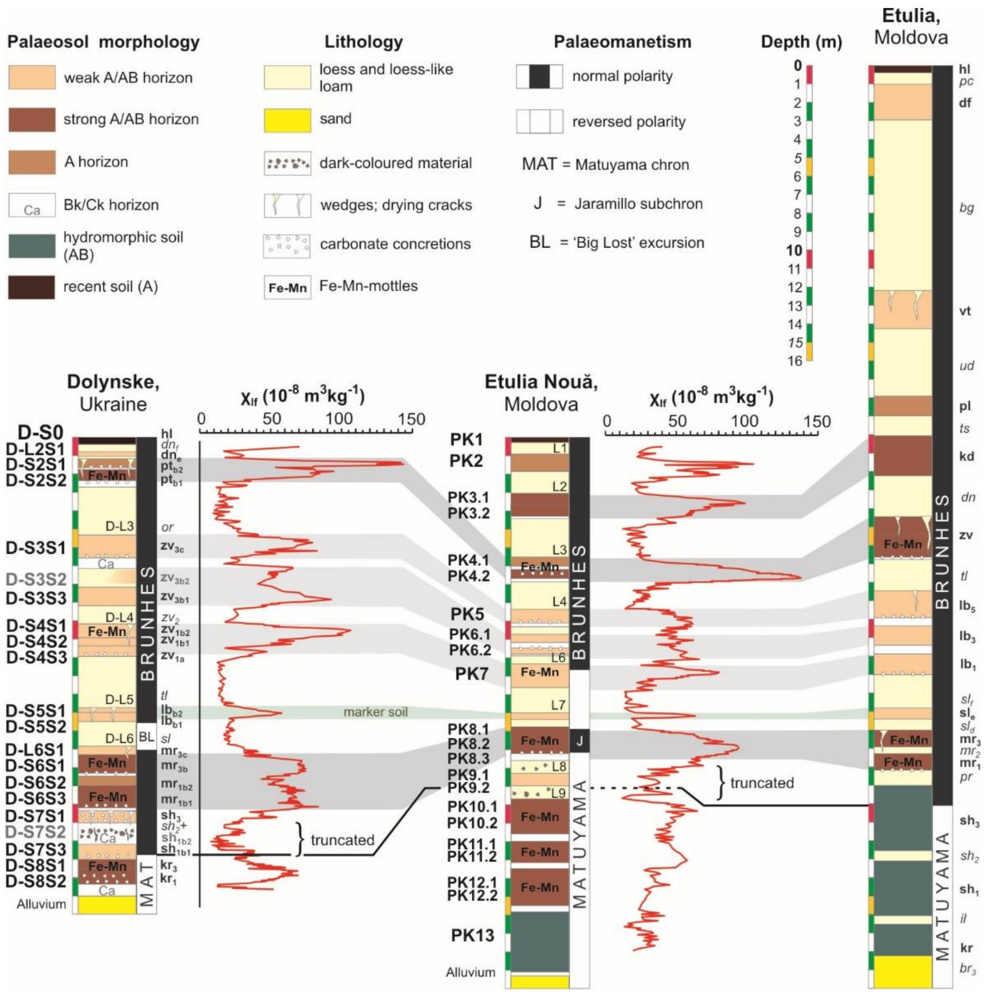

Figure 8. Correlation between loess–palaeosol sequences of Dolynske (this study), Etulia Nouă, adapted with permission from Tsatskin et al. [215], Elsevier, 2001, and Tsatskin et al. [216], Springer Nature, 2008, and Etulia, modified from Veklich and Veklich [214].

Our data reveal a lower position of the reversed polarity zone for the Dolynske section as well, which we correlate with the late Matuyama chron (Figures 6 and 8). Furthermore, the results are in good agreement with those obtained previously at Roksolany and Vyazivok. In all three sections, the MBB has been detected at the same pedostratigraphical level, in the lowermost part of the S7S3 (sh_{1b1}) soil complex, corresponding to MIS 19c [150].

Nonetheless, in most magnetostratigraphic records of Chinese loess–palaeosol profiles, the MBB is observed in the loess layer L8 [92,267–272]. These studies have revealed the problem of a climatostratigraphic inconsistency in the position of the Matuyama–Brunhes reversal in terrestrial and deep-sea records: the MBB is recorded in the loess unit (representing a cold period), but in MIS 19 in marine sediments (representing a warm period) [142].

Hyodo [273] and Hus and Han [274] pointed out that different post-depositional remanent magnetisation lock-in depths may explain the different stratigraphic positions of the MBB. Zhou and Shackleton [275] and Spassov et al. [269] proposed a large lock-in depth interval (~2–3 m) for the MBB in the Chinese loess. According to this interpretation, the inferred position of the MBB in loess sequences of the CLP was re-positioned higher within L8–S7 zone. The palaeosol unit S7 is correlated with MIS 19, and S8 with MIS 21 [269].

Some authors (e.g., Wang et al. [276], Jin and Liu [277] and Bolshakov [278]) have questioned the lock-in depth hypothesis. They consider the S8 palaeosol (instead of S7) as a correlative of MIS 19, proposing the correlation of S7 with MIS 18.2 interstadial [276] or singling out two palaeosol units corresponding to separate MIS 13 (S5) and MIS 15 (S6) [278,279]. This interpretation is supported by data from the Luochuan, Sunmenxia, Jixian and Baicaoyuan sections in the central and south-eastern part of the CLP [86,146,147,276,277,279,280] where the Matuyama–Brunhes reversal is fixed in the palaeosol S8 below L8. Thus, with the knowledge we have at present, the correlation with the loess–palaeosol sequences in the CLP is not straightforward.

Contradictions regarding the timing of palaeosol units around the detected MBB in Romania, Bulgaria and Serbia, as well as the D-S7S3 pedocomplex at Dolynske referred to, are to be discussed in the next section regarding further support for our correlation of the D-S7S3 palaeosol with MIS 19.

4.2. Land–Sea Correlations

A detailed description of stratigraphic units of the loess–palaeosol succession in Ukraine with lithopedological and magnetic properties, as well as their comparison to the Middle Danube Basin loess records has been given in Hlavatskyi and Bakhmutov [150]. Here, we focus on the further development of the regional stratigraphic correlation scheme in view of the new results obtained from the Dolynske section versus previous data from the Western Black Sea region and Lower Danube Basin loess sections.

4.2.1. Potyagaylivka Unit (MIS 7)

The double palaeosol D-S2 of Dolynske, in our interpretation, correlates with the welded pedocomplexes PK4 at Etulia Nouă [215,216] (Figure 8) and R-S2 at Roksolany [150] (Figure 9). The latter is strongly developed, although has lower χ_{lf} values (up to 82×10^{-8} m^{3}kg^{-1}). The corresponding unit at Kurortne (labelled in this study as K-S2) is likewise double, having maximum magnetic susceptibility enhancement up to 95×10^{-8} m^{3}kg^{-1} in its uppermost part [171]. It is interesting to note strikingly a similar magnetic susceptibility pattern of S2 at Dolynske, Roksolany and Kurortne (Figure 9) in Ukraine and that at the Lunca (after Necula, 2006 cited in [281]), Mostiștea [9] and Costinești [22] sections in Romania, having a characteristic double peak with a dominant upper peak. Based on the specific double peak in the benthic isotope record [141,242] in MIS 7, we correlate the D-S2 unit with the Danubian S2 unit and with MIS 7.

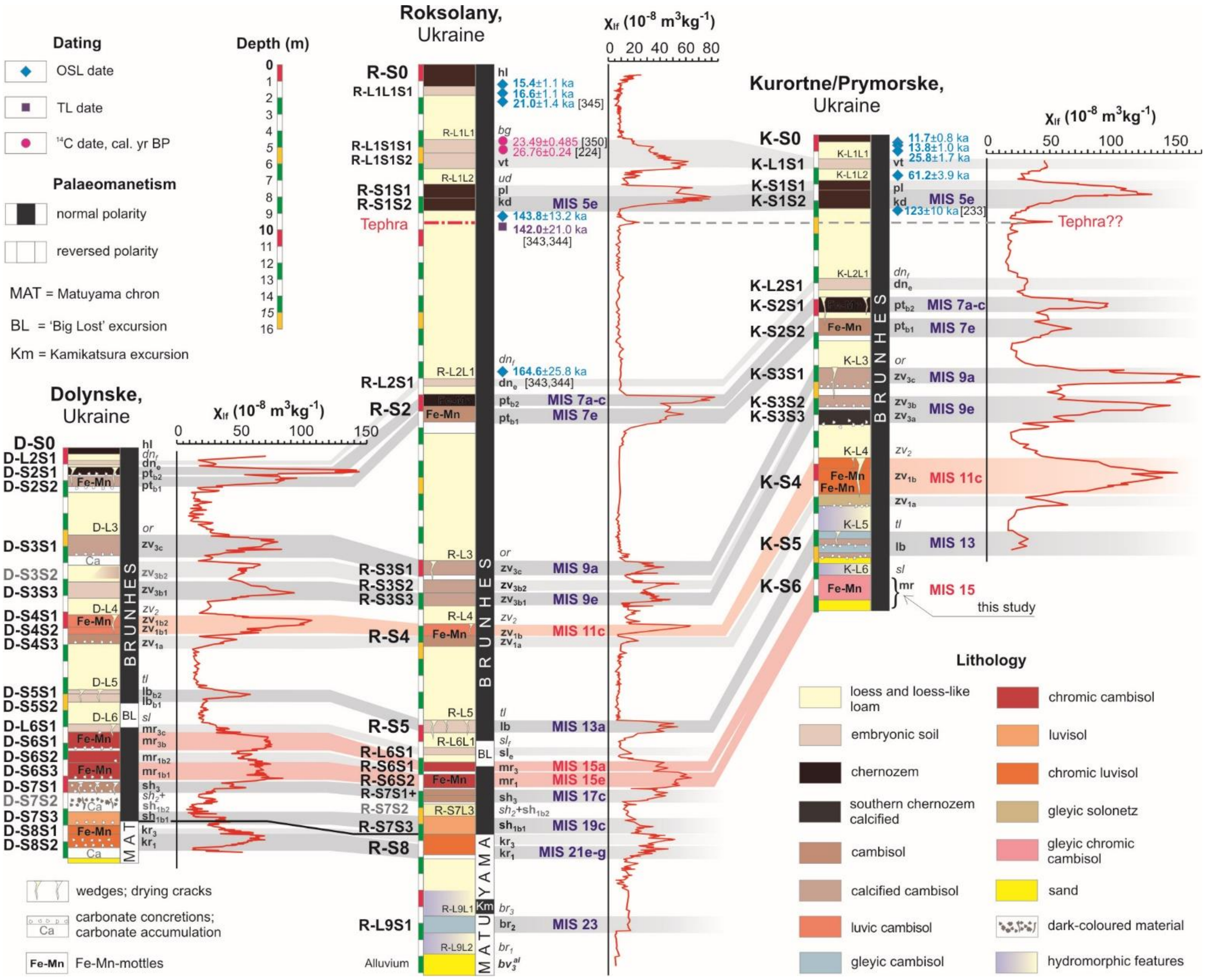

Figure 9. Correlation chart of the sequences studied at Dolynske, Roksolany and Kurortne (this study). The magnetic polarity zonation and magnetic susceptibility records of the Roksolany sequence are from Hlavatskyi and Bakhmutov [150], and Kurortne section adapted with permission from Nawrocki et al. [171], Elsevier, 1999 (units recalibrated by Stephens et al. [231]), accompanied by our additional palaeomagnetic measurements (see Section 3.6). Selected luminescence and radiocarbon dates (with references) for the Roksolany and Kurortne sections are shown.

In the lower part of the overlaying loess, L2, at Dolynske and Kurortne, an incipient palaeosol, L2S1, can be observed as a small peak in the magnetic susceptibility curves (Figure 9) corresponding to the interstadial marine isotope substage 6d (Figure 3). This pattern was described for several sections from the Lower Danube Basin: Lubenovo and Viatovo [130], Mostiștea [9], Koriten [8], Mircea Vodă [11,22] and Costinești [22].

4.2.2. Zavadivka Superunit (MIS 9–11)

Regarding palaeopedological features, D-S3S1, D-S3S2, D-S3S3 and D-S4 correlates with weakly developed soils PK5, PK6.1, PK6.2 and PK7 at Etulia Nouă (Figure 8). The corresponding units at Roksolany (R-S3S1, R-S3S2, R-S3S3 and R-S4) are more developed, have similar thickness (ca. 1–1.5 m each), lower χ_{lf} values (50–60 $\times$ 10^{-8} m^3kg^{-1}), but a remarkably identically shaped magnetic susceptibility curve (Figure 9). It is interesting to note three susceptibility peaks in the S3 pedocomplex of the Dolynske, Roksolany, Vyazivok [150] and Udvari-U2 (Hungary) [28] profiles, implying the presence of three interstadials within this interglacial recorded in the marine isotope curve as well (MIS 9a, 9c and 9e; Figures 3 and 9). A thick carbonate accumulation zone between S3S1 (corresponding to MIS 9a) and S3S2 (MIS 9c) soils is observed in all mentioned sections. In the Kurortne section, the K-S3 unit is composed of lower welded dark grey-brown soils (K-S3S2 and K-S3S3) and the upper reddish-brown calcareous soil (K-S3S1), again separated by a thick carbonate accumulation zone from the lower pedomember. However, at Kurortne, the K-S3 unit reveals only two pronounced magnetic susceptibility peaks similar to the susceptibility curves of MIS 9 soil units in the loess sections across the Danube Basin: Zimnicea in Romania, Viatovo and Koriten in Bulgaria, Stari Slankamen and Batajnica in Serbia [28], which may indicate a reduction in the MIS 9c interstadial soil at these sites (see Section 4.2.6).

It should be stressed that two different chronostratigraphic interpretations of S3 to S5 palaeosol units have been suggested for the Danube–Dnieper loess sequences. At Romanian, Bulgarian, Serbian and Ukrainian (i.e., Stari Kaydaky) sites the S3, S4 and S5 palaeosols were originally assigned to MIS 9, MIS 11 and MIS 13–15, respectively [8–11,13–15,18,22]. According to the modern pan-Eurasian stratigraphic scheme developed by Sümegi et al. [28], both S3 and S4 of the Serbian sites (e.g., Stari Slankamen, Batajnica), Bulgarian (Koriten, Viatovo) and some Romanian sites (e.g., Zimnicea) have been merged into a single pedocomplex representing MIS 9. Furthermore, well-developed rubified palaeosol S5 has been equated to S4 corresponding to the very warm interglacial MIS 11. Here, we have adopted the latter suggestion [28] because it is consistent with magnetic susceptibility patterns of the Ukrainian MIS 9–11 soils and corresponds more closely with the general palaeoclimatic reconstructions obtained from the central Ukrainian loess–palaeosol sequences [47,52,150,155,235]. Furthermore, based on our record for MIS 9 and MIS 11 from Roksolany and Vyazivok [150], and the similar palaeosol succession patterns, the former SK-S4 soil unit at Stari Kaydaky [10,11] has been recently reinterpreted as a lower member of the SK-S3 pedocomplex, whereas the well-developed rubified palaeosol SK-S5 below has been renamed as SK-S4 and correlated with MIS 11 [235].

The thick, dark yellowish-brown D-S4 soil at Dolynske with a characteristic magnetic susceptibility pattern and stratigraphic position is clearly correlated with the strongly developed dark reddish-brown R-S4 soil at Roksolany (Figure 9), and, therefore, with MIS 11. Correlation with one of the best developed and longest interglacials of the past 800 ka, MIS 11 [28,242,282,283], better explains the higher degree of pedogenesis in the case of these pedocomplexes. The best expression of intensely warm and humid climatic conditions of MIS 11 is given by the strongest chromic palaeosol at Kurortne, the K-S4. Large thickness (>3 m), brick-red colour and abundant Fe–Mn mottles are characteristic of the pedocompex. Increasing hydromorphic influence is noted downwards from the top of the K-S4 pedocomplex with higher intensities of gleyic features below the referred palaeosol. Similar features are observed in lower parts of the MIS 11 pedocomplex and the underlying MIS 12 loess at the Vyazivok [150,156,162], Udvari-U2, Paks and Batajnica sections [28]. High χ_{lf} values (~150 $\times$ 10^{-8} m^3kg^{-1}), a specific shape of the magnetic susceptibility curve, similarity with chromic luvisols and large thickness corresponds well to coeval features in the MIS 11 pedocomplexes within the Danubian loess–palaeosol sequences [28].

4.2.3. Lubny Unit (MIS 13)

The next weak greyish-brown chernozem-like soil, D-S5, of Dolynske, in our view, corresponds to the incipient soil at Etulia Nouă (Figure 8) and truncated R-S5 pedocomplex at Roksolany (Figure 9). The corresponding unit K-S5 at Kurortne/Prymorske has a more complex structure. It contains two middle dark-brown chernozem-like soils, with an underlying sandy layer, and an overlying reddish-brown sandy gleyed soil [162]. We correlate D-S5 (like we did previously at Roksolany) with the Lubny unit corresponding to MIS 13 [235]. Although the referred pedocomplex is well-developed in loess records from northern and central Ukraine, the climate of the Lubny warm stage (represented by chernozems, meadow brown, grey forest and, in lower parts, gleyed soils), is commonly characterized as less warm than that of the Early Zavadivka (expressed by strong rubified brown forest soils) [47,52,55,155,183,284] related to MIS 11 [179]. The Tyligul cold stage in-between, reflected in the first glacier appearance in Ukraine, is correlated with the very extensive glaciation of MIS 12, associated with the advance of large ice sheets in the temperate belt [209,242]. The correlation is based on a number of other indicators: relatively significant magnetic susceptibility peaks in S5 at Roksolany and Dolynske, not typical for embryonic soils [150]; the thin S5 soil is a nice lithostratigraphic marker placed just above the double red-brown pedocomplex S6, which is another stratigraphic marker across loess sequences in Ukraine; equal thicknesses of the thin underlying (Sula/L6) and thick overlying (Tyligul/L5) loess units at Vyazivok [162], Roksolany [150], Gayvoron [285] and Dolynske sections. The K-S5 pedocomplex at Kurortne/Prymorske has been correctly correlated with the Lubny unit previously [48,162] (Table 3). In global reference curves [141,242,286], the MIS 13 interglacial is colder than MIS 15 and especially MIS 11, which better explains the weaker development and relatively colder climate of the Lubny stage, in comparison with the preceding Martonosha period and succeeding Early Zavadivka period [235].

In Chinese loess–palaeosol sequences, a well-expressed MIS 13 interglacial is hallmarked by a well-developed S5S1 pedocomplex [287,288] because of an enhanced East-Asian Summer Monsoon bringing more precipitation [289–291]. In Europe, in contrast to eastern Asia, the higher degree of pedogenesis development and, particularly, rubification is recorded in MIS 11 pedocomplexes [28,210]. Moreover, the regional diversity in the intensity of the S5S1 soil formation also exists in China. For instance, in contrast to the central and eastern CLP, the S5S1 palaeosol is weakly developed in the western CLP, whereas the S4 palaeosol (formed during MIS 11) is the best developed soil in the Quaternary loess–palaeosol sequences [287,288].

4.2.4. Martonosha Unit (MIS 15)

At Dolynske, the old palaeosol series (D-S6 to D-S8) demonstrate a higher degree of pedogenesis compared to that in the younger palaeosols, supported by higher χ_{fd} values relative to χ_{lf} (Figure S4) and the highest mean $\chi_{fd\%}$ values in the section up to 14% (Figure 4A). The D-S6 (Martonosha) pedocomplex seems to show a strong similarity to the rubified palaeosols V-S6 at Vyazivok, SK-S6 at Stari Kaydaky, and R-S6 at Roksolany both in terms of pedological characteristics and large thickness (>2–3 m). Moreover, the magnetic susceptibility pattern of D-S6 at Dolynske is very similar to that of the Martonosha soils at the Bantysheve site in Donbas [175] (Figure 10).

Based on the position of the MBB in the underlying Shyrokyne unit and the general assumption about the presence of a single MIS 13–15 pedocomplex in Eurasia [292], in Ukraine in particular, the S6 unit at Roksolany and Vyazivok has been previously correlated with MIS 17 [150]. However, recently at Stari Kaydaky [235], we have preliminarily correlated the Martonosha (SK-S6) unit with MIS 15. In contrast to MIS 15, MIS 17 was a relatively cold interglacial as was recorded by global reference curves [141,242,286]. Pedostratigraphically, the Martonosha (S6) soils at Vyazivok, Roksolany, Stari Kaydaky and at Dolynske as well, are well-developed, clayey, rubified forest soils, transitional to subtropical ones, representing a more intense, warmer interglacial period, unlike the preceding Late Shyrokyne stage and succeeding Lubny stage. Furthermore, the cold event corresponding to MIS 14 is reflected in Lake Baikal, Antarctica, and stacked $\delta^{18}O$ LR04 palaeoclimatic records. The absolute values of $\delta^{18}O$ for MIS 14 are commensurate with similar quantities for MIS 4, MIS 8, MIS 34 and MIS 36 treated as glaciations in the LR04-stack [141,242,278].

In addition, the magnetic susceptibility curve of D-S6 is strikingly similar to the shape of the marine isotope curve at the ODP 677 site [141] of MIS 15 (Figure 10). Two pronounced peaks in D-S6S1 and D-S6S3 soils correspond to MIS 15a and 15e, respectively, whereas the middle weaker peak in the D-S6S2 subunit correlates with MIS 15c. The marine substages 15a and 15c–e in the benthic record are separated in the same way as the magnetic susceptibility peak of the upper soil, D-S6S1, (mr_3) is offset from the bimodal peak (with a dominant lower peak) of the lower palaeosol, D-S6S2–D-S6S3 (mr$_1$). Furthermore, the characteristic susceptibility pattern of the D-S6 soil succession of Dolynske replicates that of the lower part of the S5 pedocomplex at Darai Kalon in Tajikistan [76,78] (Figure 10) which is correlated with MIS 15.

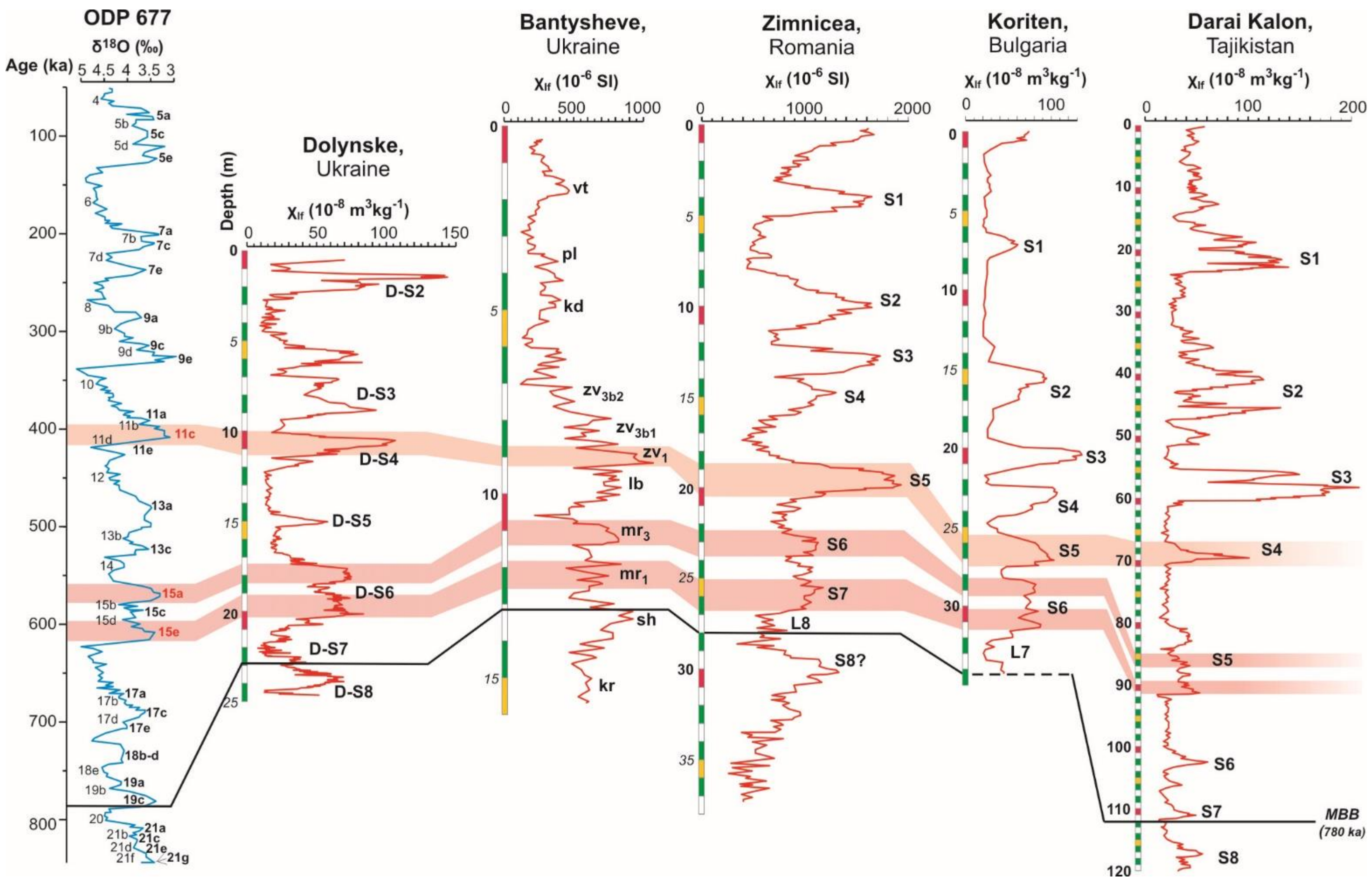

Figure 10. Correlation between marine isotope record from ODP site 677 [141] and selected loess–palaeosol sections from Ukraine [175], Lower Danube Basin [8,19] and Central Asia [78] resulting from magnetic susceptibility records and the positions of the Matuyama–Brunhes boundary (MBB).

Finally, the Martonosha (S6), Shyrokyne (S7) and Kryzhanivka (S8) soil units in Ukraine have the typical palaeopedological and pollen features of their counterparts in the central regions of the East European Plain and have been correlated by Bolikhovskaya and Molodkov [64] with the Muchkap/Vorona (MIS 15), Il'inka/Rzhaksa (MIS 17–19) and Petropavlovka/Balashov (MIS 21) interglacials, respectively. Similar to Martonosha stage, the Muchkap interglacial had two main climatic optima, which we correlate with MIS 15a and MIS 15e. The correlation between the Martonosha pedocomplex and MIS 15 is also shared by Gerasimenko [235,238].

This implies that the reversed polarity zone in the L6 loess between S5 and S6 pedocomplexes at Dolynske and Roksolany is supposed to correspond to the time equivalent of MIS 14. At Roksolany, this event was considered first as the Emperor/Big Lost Excursion [228], which corresponds exactly to MIS 14 [143,242,265,266], but later it was reassigned [150] as the Stage 17 excursion (at 670 ka) based on the coeval zone of reversed polarity in the Stari Slankamen and Udvari-U2A loess records [28]. The Big Lost Excursion (at ~540–580 ka) is a well-documented geomagnetic reversal in many terrestrial and marine records all over the world [143,265,266] and, thus, more likely corresponds to the established geomagnetic reversal at Dolynske and Roksolany.

4.2.5. Shyrokyne Superunit (MIS 17–19)

The older Shyrokyne stage of soil development of the Ukrainian loess–palaeosol sequences contains two interglacials, early sh_1 (warmer and damper stage represented by succession of reddish-brown clayey forest soils), and late sh_3 (relatively colder and drier stage represented by dark brown clayey steppe and forest–steppe soils) [52,55,154,155,183,293]. The Shyrokyne soils commonly are separated by loess-like loam (sh_2) reflecting nearly periglacial conditions. The lowermost soil, S7S3/sh_1b_1, is a light-brown clayey forest soil (luvisol). The climate during the sh_{1b1} period was wetter and cooler than that during the Kryzhanivka period [52,55,155]. The upper pedomember of Lower Shyrokyne unit (S7S2/sh_{1b2}) has a darker greyish-brown colour, is always carbonated, and often deformed by drying cracks filled with the material of the loessic layer sh_2. The uppermost soil (S7S1/sh_3) is similar to brunizems, and it was formed in more temperate climatic conditions than the sh_1 soils. It is also strongly deformed by Pryazovya cryogenic processes; this feature may indicate harsh climatic conditions during the succeeding glacial [47]. In central and eastern Ukraine, the Shyrokyne pedocomplex is commonly well-developed (up to between 3 and 8 m thick) [163,294]. The climatic optimum of the Shyrokyne stage corresponds to the early sh_{1b1} substage (S7S3).

Additional field observations made at Roksolany (June 2021) revealed that the former R-S6S2 soil subunit, by palaeopedological characteristics, belongs to the Shyrokyne unit and, thus, has been renamed as 'R-S7S1'. This subunit is correlated with the D-S7S1 (sh_3) soil at Dolynske and likely with MIS 17. The original R-S7 palaeosol corresponding to MIS 19 [150] has been preliminarily marked as the 'R-S7S3' subunit and correlated with our D-S7S3 (sh_{1b1}) soil of Dolynske (Figure 9). Remarkably, the MBB is related to the same lithostratigraphical level in both sections, the lowermost part of the S7S3 subunit. Thus, the Martonosha (S6) palaeosol at Roksolany is twice thinner than that of Dolynske, but it is similarily composed of two main subunits. Shyrokyne (S7) soils both at Dolynske and Roksolany are truncated, likely deformed during the strong Pryazovya glaciation (MIS 16?) and succeeding extensive Martonosha pedogenesis. Both D-S7 and R-S7 have relatively low magnetic susceptibility values because of the development of thick carbonate accumulation horizons having lower magnetic enhancement.

4.2.6. Correlation with the Romanian, Bulgarian and Serbian Loess Sequences

At the Viatovo site in Bulgaria, the MBB has been detected slightly below the pedocomplex S6 in clayey loess L7 [130]. At the Koriten site, the MBB has not been defined by palaeomagnetic studies, but its position was expected to be below the S6 pedocompex [8]. Thus, Jordanova et al. [130] correlated the welded S6 pedocomplex with MIS 17–19. At the site of Mircea Vodă (Romania), Buggle et al. [11] similarly subdivided the S6 pedocomplex into S6S1, S6L1 and S6S2 indicating that S6S1 is an equivalent of MIS 17. Rădan [19] reported the position of the MBB in the Zimnicea borehole in Romania within the loess layer L8, which corresponds to the L7 unit at Viatovo and Koriten (Figure 10). He labelled the overlying palaeosols as S6 and S7 corresponding to MIS 17 and MIS 19, respectively [19].

The correlation of the S6 pedocomplex at the referred Ukrainian sites with MIS 15 depicted in Figures 3, 9 and 10 has an important influence on the formerly proposed chronostratigraphic position of the S6 pedocomplex in the Lower Danube Basin. The MIS 17 age of S6 was determined on a pedostratigraphic conception implying the correlation of the overlying well-developed rubified pedocomplex S5 with MIS 13–15 in most of the Romanian, Bulgarian and Serbian sites, in the lack of reliable chronological data [28]. This assumption was based on the generally well-developed nature of S5, similar to its Chinese counterpart in addition to the highly similar magnetic susceptibility patterns. As shown in the recent stratigraphic scheme developed by Sümegi et al. [28], the S5 palaeosol unit at these sites should be correlated with MIS 11 instead of MIS 13–15.

The upper soil of the underlying welded palaeosol S6 in Romanian and Bulgarian loess records is, likewise, a well-developed clayey rubified forest soil, indicating its formation in nearly subtropical conditions [10,11,103]. Therefore, it is unlikely that it corresponds to colder MIS 17 as proposed in the previous studies. Consequently, the S6 double palaeosol at Koriten, Viatovo, Mircea Vodă and the S6–S7 pedocomplex at Zimnicea, like the D-S6 unit of Dolynske, should be correlated with MIS 15. Our interpretation is in line with very similar magnetic susceptibility patterns in all mentioned sites and almost identical with the marine isotope record for MIS 15 (Figure 10).

It is obvious from the positions of the MBB and similar magnetic susceptibility patterns that the D-S7 soil succession of Dolynske corresponds to the Romanian L8 (at Zimnicea) and Bulgarian L7 loess-like clays. At Stari Slankamen in Vojvodina, Marković et al. [15] have correlated the lowermost thick loess unit V-L9 with L8 in Romania, L7 in Bulgaria and with the glacial MIS 22. The correlation was made based on the apparent similarity between Serbian and Chinese magnetic susceptibility records, despite a position of the MBB in the middle of fossil soil V-S9 below loess V-L9 according to AF demagnetisation results [13–15]. Marković et al. [14,15] explained that the primary remanence between V-S7 and V-S9 units is heavily masked or even destroyed by deep rooting and related pedogenic processes and correlated the V-S9 unit with MIS 23. The overlying double rubified pedocomplex composed of V-S7 and V-S8 soils has been equated with MIS 19–21, weak palaeosol V-L7S1 with interstadial substage 18.2, and V-S6 cambisol with temperate MIS 17. Based on similar magnetic susceptibility curves, the Romanian and Bulgarian pedocomplex S6 has been linked to the V-S6 to V-S8 palaeosol succession of Vojvodina and, thus, correlated with MIS 17–21 [15].

In the most recent palaeomagnetic study of the composite Mošorin/Stari Slankamen profile conducted by Song et al. [295], using thermal and hybrid demagnetisation procedures, the MBB has been detected again in palaeosol V-S9 (considered as a correlative of Chinese soil L9SS1; Figure 11). The distance between the detected position of the MBB in V-S9 (at ~52.2 m; Figure 8 in [295]) and inferred position in the bottom of the V-S7 soil (regarded as MIS 19 equivalent; ~49.7 m) reaches, however, 2.5 m, which has been interpreted as the possible impact of lock-in depth and soil forming processes. Nevertheless, if the primary magnetisation was destroyed, it could equally likely be of normal or reversed polarity.

Furthermore, in the Chinese loess profiles, the MBB has never been detected so deeply in the loess unit L9 (MIS 22–24). We should consider that loess sediments are affected by soil formation processes less than soils are [278]. The overprinting effect of chemical magnetisation in loess is less significant and loess itself is not susceptible to the large lock-in depth effect. Thus, if the Matuyama–Brunhes reversal is synchronous with the formation of a part of a soil layer, the palaeomagnetic record of the reversal in general cannot be displaced appreciably below the boundary between the soil and underlying loess [278]. At Stari Slankamen, two loess units (V-L8 and V-L9) and one more palaeosol (V-S8) between V-S7 and V-S9 have normal polarity, which does not indicate secondary processes overprinting the palaeomagnetic record in the V-S9 soil. Therefore, the V-S9 soil unit at Stari Slankamen should be related to MIS 19 (Figure 11, Table 5).

Based on identical shape of magnetic susceptibility curves in MIS 11 pedocomplexes at the Dolynske, Roksolany (Figure 9), Vyazivok, Stari Kaydaky, and Stari Slankamen (Figure 11) and Batajnica sites, in accordance with the recent stratigraphic scheme of Sümegi et al. [28], the strong rubified palaeosol unit V-S5 in Serbia is safely correlated with MIS 11. The underlying embryonic soil V-L6S1 was linked to MIS 13–15 [28] based on the position of a possible Stage 17 excursion (at 670 ka) in the bottom of the underlying V-L6L2 loess unit of Stari Slankamen [13,15,296]. Nevertheless, this interpretation was taken in line with the former stratigraphic subdivision [13–15] of the lowermost units (from V-S6 to V-S9). While in the previous stratigraphic model, the lock-in depth for the MBB record at Stari Slankamen was applied, the consequences of applying the lock-in depth hypothesis for geomagnetic excursions in loess have not been clarified. Moreover, the reversed polarity zone at this level has not been confirmed by the succeeding palaeomagnetic study of Song et al. [295].

Addressing the question of timing of the V-S6 to V-S8 palaeosols at Stari Slankamen, the only reliable information that we have is that they are older than MIS 11, but definitely younger than MIS 19. At a first glance, the shape of the magnetic susceptibility curve of V-S6 to V-S8 soils seems to be similar to that in the Romanian and Bulgarian pedocomplex S6, as well as in the D-S6 soil of Dolynske. However, the V-S6 soil unit has much lower χ_{lf} values (50–60 $\times$ 10^{-8} m^3kg^{-1}) as compared to those in V-S7 and V-S8 (up to 100 $\times$ 10^{-8} m^3kg^{-1}; Figures 10 and 11). In contrast, the Lower Danube pedocomplex S6 shows two equivalent peaks. Similar to the S6 double palaeosol at the referred Ukrainian, Romanian and Bulgarian loess sites, V-S7 and V-S8 at Stari Slankamen have formed a double soil complex showing a distinct bimodal magnetic susceptibility peak with the same susceptibility values in each soil subunit.

Table 5. The proposed correlation between national loess stratigraphies in eastern and south-eastern Europe (since the Middle Pleistocene), its relation to marine isotope stages and Geomagnetic Polarity Time Scale.

Age (ka)	GPTS	MIS	Ukraine [157,178,183,196–198], Moldova [214]		Ukraine [150]	Romania [9,22]	Bulgaria [8,130]	Serbia [13–15]
			Unit (Stratotype)	Index				
0		1	Holocene	hl	U-S0	S0	S0	V-S0
		2	Bug	bg	U-L1L1	L1L1	L1LL1	V-L1S1
		3	Vytachiv	vt	U-L1S1	L1S1	L1SS1	V-L1S1
		4	Uday	ud	U-L1L2	L1L2	L1LL2	V-L1L2
		5	Pryluky + Kaydaky	pl + kd	U-S1	S1	S1	V-S1
		6	Dnipro	dn	U-L2	L2	L2	V-L2
		7	Potyagaylivka	pt	U-S2	S2	S2	V-S2
		8	Oril	or	U-L3	L3	L3	V-L3
		9	Upper Zavadivka	zv_3	U-S3	S3 + S4	S3 + S4	V-S3 + V-S4
		10	Middle Zavadivka	zv_2	U-L4	L5	L5	V-L5
		11	Lower Zavadivka	zv_1	U-S4	S5	S5	V-S5
		12	Tyligul	tl	U-L5	L6	L6	V-L6
		13	Lubny	lb	U-S5			V-S6 + V-L7S1
		14	Sula	sl	U-L6			V-L7L2
		15	Martonosha	mr	U-S6	S6 + S7 [1]/S6 [2]	S6	V-S7 + V-S8
		16	Pryazovya	pr	U-L7	L8	L7	V-L9 (L9LL1)
		17	Upper Shyrokyne	sh_3	U-S7S1			
		18	Middle Shyrokyne	sh_2	U-S7L1			
780	B	19	Lower Shyrokyne	sh_1	U-S7S2 + 3			V-S9 (L9SS1)
	M	20	Illichivsk	il	U-L8			V-L10 (L9LL2)
		21?	Kryzhanivka	kr	U-S8?	S8?	Red clay	Basal complex

[1] At Zimnicea; [2] Mircea Voda.

According to the palaeopedological description, V-S6 soil in Serbia, on the one hand, and the upper soil S6S1 in Ukrainian, Romanian and Bulgarian loess sequences, on the other hand, are related to completely different types of palaeosols. The V-S6 soil at Stari Slankamen is a cambisol, and at Batajnica it is a cambisol highly disturbed by hydromorphic features [14]. In contrast to the Serbian V-S6, the upper soil of the S6 pedocomplex in the Lower Danube and Ukrainian loess sequences is a well-developed clayey rubified palaeosol, regarded as a chromic cambisol [10,11,235]. Hence, the climate during the formation of S6 was of a more intense Mediterranean character in the Lower Danube Basin and Ukraine, in contrast to the one with lower temperatures in the Middle Danube basin reconstructed from the weaker V-S6 palaeosol [103]. In our view, palaeopedological features and shapes of magnetic susceptibility curves of the S6 pedocomplex in Ukraine, Romania and Bulgaria match better with those in the double V-S7–V-S8 palaeosol of Serbia alone. Using this logic, the welded V-S7–V-S8 chromic cambisol pedocomplex in Vojvodina should be related to the warm MIS 15. Consequently, the Serbian cambisol V-S6 naturally correlates with typical S5 cambisols and hydromorphic soils in the Ukrainian loess–palaeosol sequences, formed during colder MIS 13 (Table 5). It is interesting to note that the shape of the magnetic susceptibility curve between V-S5 and V-S8 at Stari Slankamen is similar to the one measured at Stari Kaydaky [235], where the minor peak in the V-L7S1 cambisol could have been assigned to sandy and clayey gleyed palaeosol SK-S5S3 (lb_1) corresponding to MIS 13c (Figure 11). At Roksolany, we have found a tiny embryonic soil above the R-S6 unit expressed by a weak susceptibility peak ('R-L6S1' in Figure 9) which may correspond to Serbian V-L7S1.

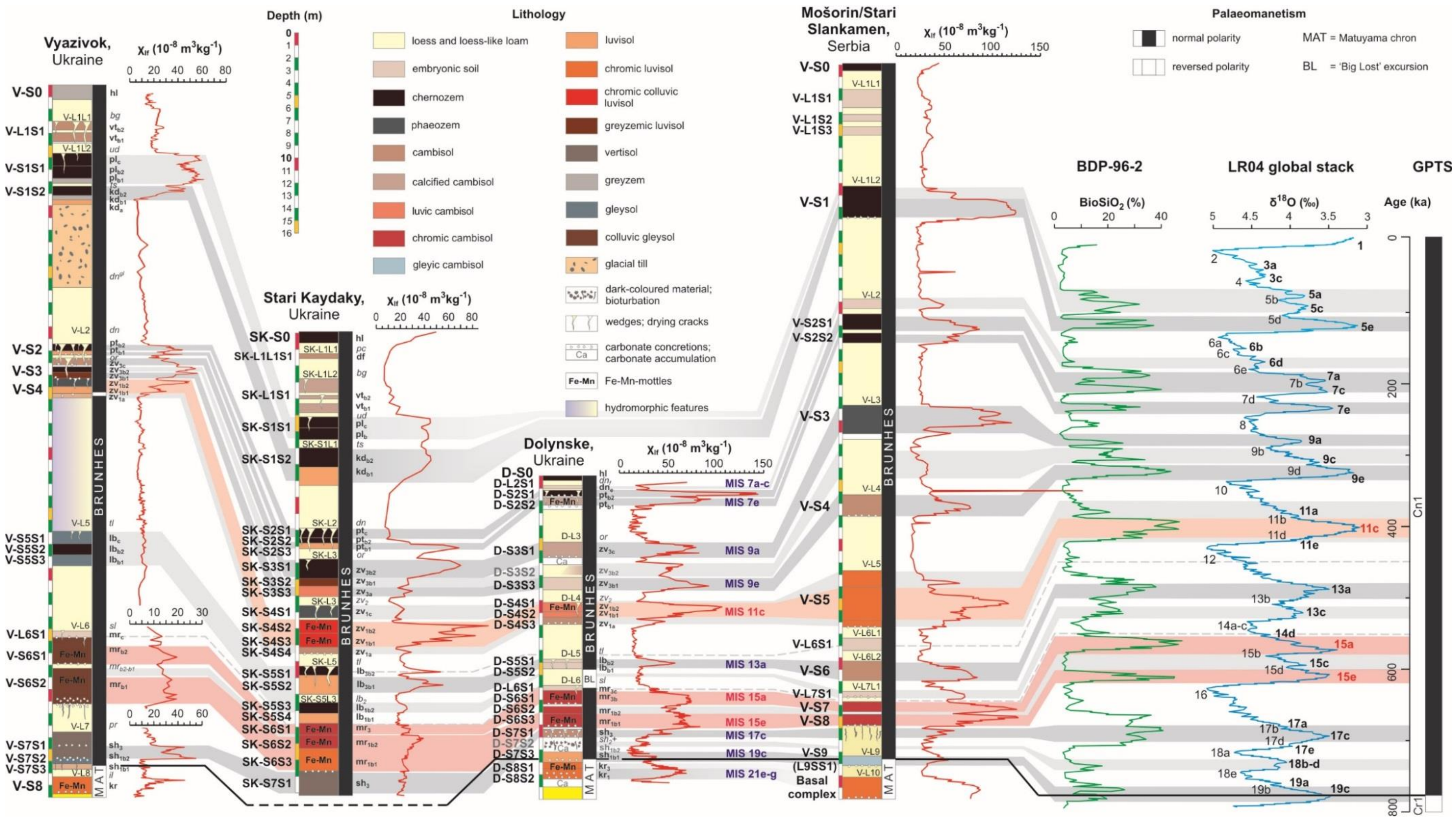

Figure 11. Correlation chart of the sequences studied at Vyazivok [150], Stari Kaydaky [235] and Dolynske (this study), Serbian reference sequence of Mošorin/Stari Slankamen, adapted with permission from Marković et al. [15], Elsevier, 2015, palaeoclimatic record of biogenic silica (%) from Lake Baikal, adapted with permission from Williams et al. [297], The American Association for the Advancement of Science, 1997, marine oxygen isotope stack LR04 [242] and Geomagnetic Polarity Time Scale. Magnetic susceptibility curve of the upper 17 m of the Stari Kaydaky section adapted with permission from Buggle et al. [11], Elsevier, 2015. Correlation of the V-S5 soil unit of Stari Slankamen with MIS 11 has been suggested by Sümegi et al. [28]. Correlation of V-S6 to V-S9 units with MIS 13–19 is proposed by this study.

In addition, the shape of the magnetic susceptibility curve at Stari Slankamen for V-S5 to V-S8 completely duplicates variations in the global benthic $\delta^{18}O$ stack [242] and climatic record of Lake Baikal [297] through MIS 11–15 (Figure 11). This implies that the magnetic susceptibility record of Stari Slankamen, like the typical Ukrainian loess–palaeosol sequences, reflects almost all the interstadials recorded in this archive during MIS 11–15 reported in the global palaeoclimate curves.

The MIS 17 soil has likely been reworked by pedogenic processes of the overlying V-S8 soil, but the former may be identified by a small susceptibility peak similar to a weak peak in the D-S7S1 palaeosol at Dolynske (Figure 11). Unlike the truncated Danube MIS 17 soil, the Upper Shyrokyne (S7S1/sh_3) palaeosol unit in central and eastern loess–palaeosol sequences in Ukraine is represented by well-developed vertisols and brunizems, formed in a warm–temperate climate. The coeval MIS 17 Upper Il'inka (Semiluky) soil complex formed in temperate climatic conditions is well-described in loess sequences of the Don and Kuma River Basins in Russia [298].

In the Stari Kaydaky and Holovchyntsi sections, the S7S1 soil is not less than 2 m thick and has normal polarity [235,299]. At Vyazivok, the palaeosol is equally 2 m thick, showing a specific double magnetic susceptibility peak in its lower part, somewhat similar to the Lake Baikal climate record for two early MIS substages 17c–e (Figure 11). The soil is overlying by the 0.8–2 m thick Pryazovya (V-L7) loess unit (now estimated as a correlative of MIS 16) and topped by well-developed double dark-cinnamonic gleyic palaeosol S6 with a very similar susceptibility pattern of the MIS 15 records (Figure 11). At Vyazivok, the distance between the Lower Shyrokyne unit (sh1b1/V-S7S3) with the detected MBB and the Upper Martonosha unit (mrb2/V-S6S1, equivalent to V-S7 soil at Stari Slankamen) reaches almost 9 m, which definitively excludes the possibility of applying the lock-in hypothesis.

Returning to the lowermost part of Stari Slankamen, based on similar stratigraphic position and magnetic susceptibility curves, the lowermost ('basal') clay complex can be reasonably correlated with the Kryzhanivka (S8) pedocomplex (MIS 21?) at Dolynske, Roksolany, Vyazivok [150] and Zimnicea [19] (Table 5). It is noteworthy that in the initial pedostratigraphic scheme of Stari Slankamen, Marković et al. [300] labelled the basal complex as 'SL S8' and preliminarily correlated it with MIS 21. Furthemore, in the publication referred to, two overlying soils (designated later as 'V-S7–V-S8') were accurately considered as a single pedocomplex 'SL S7', which is in line with our interpretation in which we suggest the correlation of the double pedocomplex with only one interglacial, MIS 15. It may also be worth considering the previous correlation model of the loess–palaeosol sequences in the Middle and Lower Danube Basins made by Fitzsimmons et al. [18], in which the basal complex in Serbia and Bulgaria has been correlated with the Hungarian soil PD2 related to MIS 21 [28,286].

Therefore, eight global glacial–interglacial cycles identified in the Brunhes chron from the deep-sea oxygen isotope records are recorded in the Ukrainian loess–palaeosol sequence as well. The discrepancies in the number of glacial–interglacial cycles determined from the deep-water and terrestrial palaeoclimatic records largely come from the loess sequences of different regions [301]. Incomplete geological record, inaccurate local or regional stratigraphic model, the uncertain position of the Matuyama–Brunhes geomagnetic reversal in the geological sequence, and incorrect identification of the climatic rank of the corresponding warmings and coolings are the most probable sources of this inconsistency [302]. A consistent systematic approach applied in the integrated investigations of the more complete eastern European loess–soil sequences is likely to yield the solution to these problems. We suggest focusing on the accurate identification of the position of the MBB as a major chronological benchmark in the Pleistocene loess–palaeosol sequences. Furthermore, the loess–palaeosol cycles identified using rock magnetic proxies should be confirmed by a comprehensive lithological, palaeopedological, sedimentological and palynological study to support the proposed correlation.

4.3. Promising Geochronometric Tools for Further Development of a Unified Ukrainian–Danube Loess Stratigraphic Model

To build a consistent chronostratigraphic framework, it is common practice to investigate loess–palaeosol deposits with a multidisciplinary approach. In addition to magnetostratigraphy, a reliable geochronology, biostratigraphy and tephrochronology are mandatory to interpret the results of such investigations [28,303–306].

Early developments in thermoluminescence (TL) dating and new luminescence methodologies such as optically stimulated luminescence dating (OSL) and infrared stimulated luminescence dating (IRSL) have a distinct advantage because of the possibility for absolute dating. However, these methods are not without limitations. Luminescence dating of loessic quartz is generally acknowledged to have an upper age limit ranging from 50 to 100 ka [307–312]. The IRSL technique, partially developed on European loess, extends the dating range beyond that of quartz, potentially up to 300 ka [313,314]. These protocols have been successfully applied to a number of Danube, Polish, Ukrainian and southern Russian sites, and confirm or extend existing chronostratigraphic models [15,34,36,303,313,315–342].

In southern Ukraine, two loess sections have been studied by luminescence dating methods in the last decade. Fedorowicz et al. [343,344] obtained coupled TL and OSL dating results from loess unit R-L2 at the Roksolany site yielding ages from 97 to 165 ka (Figure 9), which support our suggestion of a penultimate glacial age for the unit [150]. Recent luminescence data from last glacial loess unit R-L1L1 yield ages from approximately 15 to 21 ka [345]. The ages are in good agreement with the palaeomagnetic time-depth model and assign R-L1L1, R-L1L2 and R-L2L1 to MIS 2, MIS 4 and MIS 6, respectively [150].

At Kurortne, similar OSL dates have been obtained for the coeval K-L1L1 (12 to 26 ka), K-L1L2 (61 ka) and K-L2L1 (123 ka) loess units [233] (Figure 9). These results are consistent with the previous TL dating and stratigraphic classification of the Kurortne loess sequence [232], in which the uppermost three loess units have been assigned to the Bug (i.e., MIS 2), Uday (MIS 4) and Dnipro (MIS 6) units. In light of these successful results, further luminescence dating of the Dolynske section and nearby Ukrainian and Moldovian loess sites are crucial for developing a reliable regional stratigraphic model.

The alluvial deposits within the Lower Prut River Basin and northern Dolynske area contain famous and extensively studied biostratigraphical records of Khaprov and Taman faunal complexes [217] correlated with the early and late Matuyama chron, respectively [174,224,346–348]. However, their precise stratigraphic position relative to our section is not clear and needs to be refined. The Taman fauna has been found in the bottom of the Roksolany section (below the R-S7 soil unit), as well as in numerous loess sites across the Black Sea northern coast.

Of additional interest is the observation of a possible tephra layer in the upper part of the loess unit K-L2 at Kurortne shown by an expressive magnetic susceptibility peak (Figure 9). A tephra layer at a similar stratigraphic position to the hypothesised K-L2 tephra is well-documented in the R-L2 loess at the Roksolany section and appears to have a luminescence age of ~144 kyr [343,344]. The most probable tephrostarigraphic equivalent of the Roksolany tephra is the L2 tephra of the same age [150] described from several exposures in the Danube Basin (e.g., [15,316,336,349]). These widespread tephra layers most likely originated in the southern Italian area [349].

From the other point of view, the Roksolany tephra was derived from the Ciomadul volcano in Romania approximately 29 kyr ago [350], based on controversial ^{14}C ages of soil samples without organic matter [351]. Ciomadul explosive volcanic products have a typical phenocryst assemblage containing plagioclase, amphibole (hornblende and pargasite) and biotite [352,353]. The Roksolany tephra differs significantly from Ciomadul, as it contains clinopyroxene [350] instead of amphibole, and, thus, is unlikely to be derived from Ciomadul [354].

5. Conclusions

The magnetostratigraphic and enviromagnetic study of the Quaternary loess record in the valley of the Danube at Dolynske has been conducted in combination with the reinvestigation of two key nearby localities, Roksolany and Kurortne, on the western shore of the Black Sea. The MBB has been detected at the base of the Shyrokyne (S7) palaeosol complex in the Dolynske and Roksolany sections, providing an excellent chronological benchmark for regional correlation. Palaeopedological features combined with magnetic susceptibility profiles have provided additional control for stratigraphic classification.

The results presented here reveal that the southern Ukrainian loess–palaeosol sequences are of essential importance in the stratigraphic and palaeoclimatic interpretation of the Middle Pleistocene in Europe. High-resolution magnetic susceptibility and palaeopedological data demonstrate details in the interglacials, interstadials and stadials which are clearly comparable to marine oxygen isotope variations down to the substage level. A distinct pattern of the proxy records has been used to correlate the Lower Danube loess succession to other key sites in Ukraine, Moldova and the Middle Danube loess regions.

The suggested correlation scheme indicates that the conventional stratigraphic models for the Danube loess [8–11,13–15,18,19,22,130,295] have a systematic bias towards older ages resulted from the misinterpretation of the magnetostratigraphic data. In our conception, the Matuyama–Brunhes reversal remains a key chronological benchmark in the loess–palaeosol sequences across eastern and south-eastern Europe, within a palaeosol unit formed during MIS 19.

Furthermore, unlike the more complete Pleistocene terrestrial records in eastern Europe, the longest loess sequences in south-eastern Europe do not have continuous records. In our interpretation, the deposits of at least three separate temperate climatic episodes (MIS 9c, MIS 13, MIS 17) are well-developed within the loess–palaeosol sequence of the central part of eastern Europe, whereas they are truncated in southern Ukraine and Moldova, and absent in the Romanian and Bulgarian successions. In Serbia, MIS 9c and MIS 17 soils have been eroded or replaced by loessic layers, whereas the MIS 13 pedocomplex is represented by cambisols. Alongside the position of the MBB, we propose using the well-developed rubified palaeosols of MIS 11 and MIS 15, formed in climates close to subtropical, as reliable markers for regional stratigraphic correlation.

Supplementary Materials: The following are available online at https://www.mdpi.com/article/10.3390/quat4040043/s1, Figure S1: Magnetic fabric data based on anisotropy of magnetic susceptibility parameters from (A) loess specimens; (B) palaeosol specimens above the MBB; (C) palaeosol specimens below the MBB at the Dolynske section. Directions of the maximum principal axes (K_{max}) and minimum principal axes K_{min} are shown on stereographic projections by squares and circles, respectively; N—number of specimens; T (shape parameter) versus Pj (degree of anisotropy). Figure S2: Magnetic fabric data based on anisotropy of magnetic susceptibility parameters from palaeosols of the K-S6 unit at the Kurortne section. Directions of the maximum principal axes (K_{max}), intermediate principal axes (K_{int}) and minimum principal axes K_{min} are shown on stereographic projections by squares, triangles and circles, respectively; N—number of specimens; T (shape parameter) versus Pj (degree of anisotropy) [240]. Figure S3: Stereographic projections of ChRM directions calculated after thermal demagnetisation of soil specimens from the K-S6 unit at the Kurortne section. Full and open circles represent projections in the lower and upper hemispheres, respectively. Average values for vectors projections were calculated: N—quantity of specimens; D—declination; I—inclination; R—resultant vector; k—precision parameter; a95—confidence limit [264]. Figure S4: Low-frequency susceptibility (χ_{lf}) plotted against frequency dependence susceptibility (χ_{fd}) of soil (circles) and loess (squares) specimens as a characteristic of magnetic enhancement for the Dolynske loess–palaeosol sequence.

Author Contributions: Conceptualization, D.H.; methodology, D.H. and V.B.; software, D.H. and V.B.; validation, V.B.; formal analysis, D.H.; investigation, D.H. and V.B.; resources, V.B.; data curation, D.H.; writing—original draft preparation, D.H.; writing—review and editing, D.H. and V.B.; visualization, D.H.; supervision, V.B.; project administration, V.B.; funding acquisition, D.H. and V.B. All authors have read and agreed to the published version of the manuscript.

Funding: This research was funded by the National Research Foundation of Ukraine, grant number 2020.02/0406.

Institutional Review Board Statement: Not applicable.

Informed Consent Statement: Not applicable.

Data Availability Statement: The data presented in this study are available upon request from the corresponding author.

Acknowledgments: We wish to thank Y. Veklych for his assistance during the field work and help in the stratigraphic classification of alluvial deposits. We thank V. Shpyra and V. Voronov for collecting and preparing block samples. We also thank T. Skarboviychuk, L. Dyachuk and S. Cherkes for their help with the rock magnetic measurements. We would like to extend sincere thanks to four anonymous reviewers for their constructive reviews and useful comments which improved the quality of the manuscript.

Conflicts of Interest: The authors declare no conflict of interest.

References

1. Lowe, J.J.; Walker, M. *Reconstructing Quaternary Environments*, 3rd ed.; Routledge: London, UK, 2014; 538p. [CrossRef]
2. Li, Y.; Shi, W.; Aydin, A.; Beroya-Eitner, M.A.; Gao, G. Loess Genesis and Worldwide Distribution. *Earth-Sci. Rev.* **2020**, *201*, 102947. [CrossRef]
3. Pecsi, M. Loess stratigraphy and Quaternary climatic change. *Loess inForm* **1995**, *3*, 23–30.
4. Haesaerts, P.; Damblon, F.; Gerasimenko, N.; Spagna, P.; Pirson, S. The Late Pleistocene Loess-Palaeosol Sequence of Middle Belgium. *Quat. Int.* **2016**, *411*, 25–43. [CrossRef]
5. Antoine, P.; Coutard, S.; Bahain, J.-J.; Locht, J.-L.; Hérisson, D.; Goval, E. The Last 750 Ka in Loess–Palaeosol Sequences from Northern France: Environmental Background and Dating of the Western European Palaeolithic. *J. Quat. Sci.* **2021**, in press. [CrossRef]
6. Smalley, I.J.; Leach, J.A. The Origin and Distribution of the Loess in the Danube Basin and Associated Regions of East-Central Europe—A Review. *Sediment. Geol.* **1978**, *21*, 1–26. [CrossRef]
7. Forster, T.; Heller, F.; Evans, M.E.; Havliček, P. Loess in the Czech Republic: Magnetic Properties and Paleoclimate. *Stud. Geophys. Geod.* **1996**, *40*, 243–261. [CrossRef]
8. Jordanova, D.; Petersen, N. Palaeoclimatic Record from a Loess-Soil Profile in Northeastern Bulgaria—II. Correlation with Global Climatic Events during the Pleistocene. *Geophys. J. Int.* **1999**, *138*, 533–540. [CrossRef]
9. Panaiotu, C.G.; Panaiotu, E.C.; Grama, A.; Necula, C. Paleoclimatic Record from a Loess-Paleosol Profile in Southeastern Romania. *Phys. Chem. Earth Part A Solid Earth Geod.* **2001**, *26*, 893–898. [CrossRef]
10. Buggle, B.; Glaser, B.; Zöller, L.; Hambach, U.; Marković, S.; Glaser, I.; Gerasimenko, N. Geochemical Characterization and Origin of Southeastern and Eastern European Loesses (Serbia, Romania, Ukraine). *Quat. Sci. Rev.* **2008**, *27*, 1058–1075. [CrossRef]
11. Buggle, B.; Hambach, U.; Glaser, B.; Gerasimenko, N.; Marković, S.; Glaser, I.; Zöller, L. Stratigraphy, and Spatial and Temporal Paleoclimatic Trends in Southeastern/Eastern European Loess–Paleosol Sequences. *Quat. Int.* **2009**, *196*, 86–106. [CrossRef]
12. Kovács, J.; Fábián, S.Á.; Varga, G.; Újvári, G.; Varga, G.; Dezső, J. Plio-Pleistocene Red Clay Deposits in the Pannonian Basin: A Review. *Quat. Int.* **2011**, *240*, 35–43. [CrossRef]
13. Marković, S.B.; Hambach, U.; Stevens, T.; Kukla, G.J.; Heller, F.; McCoy, W.D.; Oches, E.A.; Buggle, B.; Zöller, L. The Last Million Years Recorded at the Stari Slankamen (Northern Serbia) Loess-Palaeosol Sequence: Revised Chronostratigraphy and Long-Term Environmental Trends. *Quat. Sci. Rev.* **2011**, *30*, 1142–1154. [CrossRef]
14. Marković, S.B.; Hambach, U.; Stevens, T.; Jovanović, M.; O'Hara-Dhand, K.; Basarin, B.; Lu, H.; Smalley, I.; Buggle, B.; Zech, M.; et al. Loess in the Vojvodina Region (Northern Serbia): An Essential Link between European and Asian Pleistocene Environments. *Neth. J. Geosci.* **2013**, *91*, 173–188. [CrossRef]
15. Marković, S.B.; Stevens, T.; Kukla, G.J.; Hambach, U.; Fitzsimmons, K.E.; Gibbard, P.; Buggle, B.; Zech, M.; Guo, Z.; Hao, Q.; et al. Danube Loess Stratigraphy–Towards a Pan-European Loess Stratigraphic Model. *Earth-Sci. Rev.* **2015**, *148*, 228–258. [CrossRef]
16. Marković, S.B.; Sümegi, P.; Stevens, T.; Schaetzl, R.J.; Obreht, I.; Chu, W.; Buggle, B.; Zech, M.; Zech, R.; Zeeden, C.; et al. The Crvenka Loess-Paleosol Sequence: A Record of Continuous Grassland Domination in the Southern Carpathian Basin during the Late Pleistocene. *Palaeogeogr. Palaeoclim. Palaeoecol.* **2018**, *509*, 33–46. [CrossRef]
17. Varga, G. Similarities among the Plio–Pleistocene Terrestrial Aeolian Dust Deposits in the World and in Hungary. *Quat. Int.* **2011**, *234*, 98–108. [CrossRef]
18. Fitzsimmons, K.E.; Marković, S.B.; Hambach, U. Pleistocene Environmental Dynamics Recorded in the Loess of the Middle and Lower Danube Basin. *Quat. Sci. Rev.* **2012**, *41*, 104–118. [CrossRef]
19. Rădan, S.-C. Towards a Synopsis of Dating the Loess from the Romanian Plain and Dobrogea: Authors and Methods through Time. *Geo-Eco-Marina* **2012**, *18*, 153–172. [CrossRef]

20. Újvári, G.; Varga, A.; Raucsik, B.; Kovács, J. The Paks Loess-Paleosol Sequence: A Record of Chemical Weathering and Provenance for the Last 800ka in the Mid-Carpathian Basin. *Quat. Int.* **2014**, *319*, 22–37. [CrossRef]
21. Hošek, J.; Hambach, U.; Lisá, L.; Grygar, T.M.; Horáček, I.; Meszner, S.; Knésl, I. An Integrated Rock-Magnetic and Geochemical Approach to Loess/Paleosol Sequences from Bohemia and Moravia (Czech Republic): Implications for the Upper Pleistocene Paleoenvironment in Central Europe. *Palaeogeogr. Palaeoclim. Palaeoecol.* **2015**, *418*, 344–358. [CrossRef]
22. Necula, C.; Dimofte, D.; Panaiotu, C. Rock Magnetism of a Loess-Palaeosol Sequence from the Western Black Sea Shore (Romania). *Geophys. J. Int.* **2015**, *202*, 1733–1748. [CrossRef]
23. Terhorst, B.; Sedov, S.; Sprafke, T.; Peticzka, R.; Meyer-Heintze, S.; Kühn, P.; Solleiro Rebolledo, E. Austrian MIS 3/2 Loess–Palaeosol Records—Key Sites along a West–East Transect. *Palaeogeogr. Palaeoclim. Palaeoecol.* **2015**, *418*, 43–56. [CrossRef]
24. Lehmkuhl, F.; Zens, J.; Krauß, L.; Schulte, P.; Kels, H. Loess-Paleosol Sequences at the Northern European Loess Belt in Germany: Distribution, Geomorphology and Stratigraphy. *Quat. Sci. Rev.* **2016**, *153*, 11–30. [CrossRef]
25. Sauer, D.; Kadereit, A.; Kühn, P.; Kösel, M.; Miller, C.E.; Shinonaga, T.; Kreutzer, S.; Herrmann, L.; Fleck, W.; Starkovich, B.M.; et al. The Loess-Palaeosol Sequence of Datthausen, SW Germany: Characteristics, Chronology, and Implications for the Use of the Lohne Soil as a Marker Soil. *Catena* **2016**, *146*, 10–29. [CrossRef]
26. Sümegi, P.; Náfrádi, K.; Molnár, D.; Sávai, S. Results of Paleoecological Studies in the Loess Region of Szeged-Öthalom (SE Hungary). *Quat. Int.* **2015**, *372*, 66–78. [CrossRef]
27. Sümegi, P.; Marković, S.B.; Molnár, D.; Sávai, S.; Náfrádi, K.; Szelepcsényi, Z.; Novák, Z. Črvenka Loess-Paleosol Sequence Revisited: Local and Regional Quaternary Biogeographical Inferences of the Southern Carpathian Basin. *Open Geosci.* **2016**, *8*, 390–404. [CrossRef]
28. Sümegi, P.; Gulyás, S.; Molnár, D.; Sümegi, B.P.; Almond, P.C.; Vandenberghe, J.; Zhou, L.; Pál-Molnár, E.; Törőcsik, T.; Hao, Q.; et al. New Chronology of the Best Developed Loess/Paleosol Sequence of Hungary Capturing the Past 1.1 Ma: Implications for Correlation and Proposed Pan-Eurasian Stratigraphic Schemes. *Quat. Sci. Rev.* **2018**, *191*, 144–166. [CrossRef]
29. Sümegi, P.; Gulyás, S.; Molnár, D.; Sümegi, B.P.; Törőcsik, T.; Almond, P.C.; Smalley, I.; Zhou, L.; Galovic, L.; Pál-Molnár, E.; et al. Periodicities of Paleoclimate Variations in the First High-Resolution Non-Orbitally Tuned Grain Size Record of the Past 1 Ma from SW Hungary and Regional, Global Correlations. *Aeolian Res.* **2019**, *40*, 74–90. [CrossRef]
30. Zeeden, C.; Kels, H.; Hambach, U.; Schulte, P.; Protze, J.; Eckmeier, E.; Marković, S.B.; Klasen, N.; Lehmkuhl, F. Three Climatic Cycles Recorded in a Loess-Palaeosol Sequence at Semlac (Romania)–Implications for Dust Accumulation in South-Eastern Europe. *Quat. Sci. Rev.* **2016**, *154*, 130–142. [CrossRef]
31. Bösken, J.; Obreht, I.; Zeeden, C.; Klasen, N.; Hambach, U.; Sümegi, P.; Lehmkuhl, F. High-Resolution Paleoclimatic Proxy Data from the MIS3/2 Transition Recorded in Northeastern Hungarian Loess. *Quat. Int.* **2019**, *502*, 95–107. [CrossRef]
32. Banak, A.; Mandic, O.; Pavelić, D.; Kovačić, M.; Lirer, F. Pleistocene Climate Change in Central Europe. In *Pleistocene Archaeology–Migration, Technology, and Adaptation*; Ono, R., Ed.; IntechOpen: London, UK, 2020.
33. Flašarová, K.; Strouhalová, B.; Šefrna, L.; Verrecchia, E.; Lauer, T.; Juřičková, L.; Kolařík, P.; Ložek, V. Multiproxy Evidence of Middle and Late Pleistocene Environmental Changes in the Loess-Paleosol Sequence of Bůhzdař (Czech Republic). *Quat. Int.* **2020**, *552*, 4–14. [CrossRef]
34. Novothny, Á.; Barta, G.; Végh, T.; Bradák, B.; Surányi, G.; Horváth, E. Correlation of Drilling Cores and the Paks Brickyard Key Section at the Area of Paks, Hungary. *Quat. Int.* **2020**, *552*, 50–61. [CrossRef]
35. Sprafke, T.; Schulte, P.; Meyer-Heintze, S.; Händel, M.; Einwögerer, T.; Simon, U.; Peticzka, R.; Schäfer, C.; Lehmkuhl, F.; Terhorst, B. Paleoenvironments from Robust Loess Stratigraphy Using High-Resolution Color and Grain-Size Data of the Last Glacial Krems-Wachtberg Record (NE Austria). *Quat. Sci. Rev.* **2020**, *248*, 106602. [CrossRef]
36. Wacha, L.; Laag, C.; Grizelj, A.; Tsukamoto, S.; Zeeden, C.; Ivanišević, D.; Rolf, C.; Banak, A.; Frechen, M. High-Resolution Palaeoenvironmental Reconstruction at Zmajevac (Croatia) over the Last Three Glacial/Interglacial Cycles. *Palaeogeogr. Palaeoclim. Palaeoecol.* **2021**, *576*, 110504. [CrossRef]
37. Issmer, K. Vistulian Loess Deposits in Western Poland and Their Palaeoenvironmental Implications. *Quat. Int.* **2001**, *76–77*, 129–139. [CrossRef]
38. Lindner, L.; Gozhik, P.; Marciniak, B.; Marks, L.; Yelovicheva, Y. Main climatic changes in the Quaternary of Poland, Belarus and Ukraine. *Geol. Q.* **2004**, *48*, 97–114.
39. Lindner, L.; Bogutsky, A.; Gozhik, P.; Marks, L.; Łanczont, M.; Wojtanowicz, J. Correlation of Pleistocene deposits in the area between the Baltic and Black Sea, Central Europe. *Geol. Q.* **2006**, *50*, 195–210.
40. Lindner, L.; Marks, L. Pleistocene Stratigraphy of Poland and Its Correlation with Stratotype Sections in the Volhynian Upland (Ukraine). *Geochronometria* **2008**, *31*, 31–37. [CrossRef]
41. Badura, J.; Jary, Z.; Smalley, I. Sources of Loess Material for Deposits in Poland and Parts of Central Europe: The Lost Big River. *Quat. Int.* **2013**, *296*, 15–22. [CrossRef]
42. Krawczyk, M.; Ryzner, K.; Skurzyński, J.; Jary, Z. Lithological Indicators of Loess Sedimentation of SW Poland. Contemp. *Trends Geosci.* **2017**, *6*, 94–111. [CrossRef]
43. Chmielowska, D.; Woronko, B. A Source of Loess-like Deposits and Their Attendant Palaeoenvironment–Orava Basin, Western Carpathian Mountains, S Poland. *Aeolian Res.* **2019**, *38*, 60–76. [CrossRef]
44. Marks, L.; Bińka, K.; Woronko, B.; Majecka, A.; Teodorski, A. Revision of the Late Middle Pleistocene Stratigraphy and Palaeoclimate in Poland. *Quat. Int.* **2019**, *534*, 5–17. [CrossRef]

45. Dzierżek, J.; Lindner, L. Stratigraphy and conditions of accumulation of the Younger Loesses (Vistulian) in the Holy Cross Mountains area, Poland. *Stud. Quat.* **2020**, *37*, 109–120. [CrossRef]
46. Dzierżek, J.; Lindner, L.; Nawrocki, J. The Loess Section in Wąchock as the Key Site of Vistulian Loesses and Palaeosols in the Holy Cross Mountains (Poland). *Geol. Q.* **2020**, *64*, 252–262. [CrossRef]
47. Veklich, M.F. *Stratigraphy of the Loess Formation of Ukraine and Adjacent Countries*; Naukova Dumka: Kiev, Ukraine, 1968; 201p. (In Russian)
48. Gozhik, P.; Shelkoplyas, V.; Khristoforova, T. Development stages of loessial and glacial formations in Ukraine (Stratigraphy of loesses in Ukraine). *Ann. UMCS Sect. B* **1995**, *50*, 65–74.
49. Rousseau, D.-D.; Gerasimenko, N.; Matviischina, Z.; Kukla, G. Late Pleistocene Environments of the Central Ukraine. *Quat. Res.* **2001**, *56*, 349–356. [CrossRef]
50. Rousseau, D.-D.; Antoine, P.; Gerasimenko, N.; Sima, A.; Fuchs, M.; Hatté, C.; Moine, O.; Zoeller, L. North Atlantic Abrupt Climatic Events of the Last Glacial Period Recorded in Ukrainian Loess Deposits. *Clim. Past* **2011**, *7*, 221–234. [CrossRef]
51. Gerasimenko, N. Upper Pleistocene Loess–Palaeosol and Vegetational Successions in the Middle Dnieper Area, Ukraine. *Quat. Int.* **2006**, *149*, 55–66. [CrossRef]
52. Gozhik, P.F.; Gerasimenko, N.P. The Lower and Middle Pleistocene of Ukraine. In *Quaternary Studies in Ukraine, Proceedings of the XVIII Congress of the International Assosiation on the Study of the Quaternary period (INQUA), Bern, Switzerland, 21–27 July 2011*; Gerasimenko, N.P., Gozhik, P.F., Dykan, N.I., Matviishyna, Z.M., Shelkoplyas, V.M., Vozgrin, B.D., Eds.; Institute of Geological Sciences NASU: Kyiv, Ukraine, 2011; pp. 9–26.
53. Łanczont, M.; Bogucki, A.; Yatsyshyn, A.; Terpiłowski, S.; Mroczek, P.; Orłowska, A.; Hołub, B.; Zieliński, P.; Komar, M.; Woronko, B.; et al. Stratigraphy and Chronology of the Periphery of the Scandinavian Ice Sheet at the Foot of the Ukrainian Carpathians. *Palaeogeogr. Palaeoclim. Palaeoecol.* **2019**, *530*, 59–77. [CrossRef]
54. Matviishyna, Z.M.; Doroshkevych, S.P. Micromorphological Peculiarities of the Pleistocene Soils in the Middle Pobuzhzhya (Ukraine) and Their Significance for Paleogeographic Reconstructions. *J. Geol. Geogr. Geoecol.* **2019**, *28*, 327–347. [CrossRef]
55. Sirenko, O.A. Changes in Pleistocene Vegetation and Climate of Ukraine in the Range of 1.8–0.4 Million Years. *J. Geol. Geogr. Geoecol.* **2019**, *28*, 355–366. [CrossRef]
56. Sirenko, O. Palaeoenvironmental Conditions of the Formation of Sediments of the Early Pliocene of Ukrainian Plain and the Vegetation Cover Dynamics. *Geol. J.* **2021**, *56*, 839–850. [CrossRef]
57. Bonchkovskyi, O.S. Changes in Pedogenic Processes during Pryluky Times (Late Pleistocene) in the Central Part of the Volyn Upland. *J. Geol. Geogr. Geoecol.* **2019**, *28*, 230–240. [CrossRef]
58. Bonchkovskyi, O. The Loess-Palaeosol Sequence of Novyi Tik: A New Middle and Upper Pleistocene Record for Volyn' Upland (North-West Ukraine). *Quaternaire* **2020**, *31*, 281–308. [CrossRef]
59. Marks, L.; Woronko, B.; Majecka, A.; Rylova, T.; Orłowska, A.; Hrachanik, M.; Rychel, J.; Zbucki, Ł.; Bahdasarau, M.; Hradunova, A.; et al. Middle Pleistocene Deposits at Rechitsa, Western Belarus, and Their Input to MIS 12-6 Stratigraphy in Central Europe. *Quat. Int.* **2020**, *553*, 34–52. [CrossRef]
60. Velichko, A.A. Loess-paleosol formation on the Russian Plain. *Quat. Int.* **1990**, *7–8*, 103–114. [CrossRef]
61. Matasova, G.; Petrovský, E.; Jordanova, N.; Zykina, V.; Kapička, A. Magnetic Study of Late Pleistocene Loess/Palaeosol Sections from Siberia: Palaeoenvironmental Implications. *Geophys. J. Int.* **2001**, *147*, 367–380. [CrossRef]
62. Matasova, G.G.; Kazansky, A.Y.; Shchetnikov, A.A.; Erbajeva, M.A.; Filinov, I.A. New Rock- and Paleomagnetic Data on Quaternary Deposits of the Tologoi Key Section, Western Transbaikalia, and Their Paleoclimatic Implications. *Izv. Phys. Solid Earth* **2020**, *56*, 392–412. [CrossRef]
63. Chlachula, J.; Evans, M.E.; Rutter, N.W. A Magnetic Investigation of a Late Quaternary Loess/Palaeosol Record in Siberia. *Geophys. J. Int.* **2002**, *132*, 128–132. [CrossRef]
64. Bolikhovskaya, N.S.; Molodkov, A.N. East European Loess–Palaeosol Sequences: Palynology, Stratigraphy and Correlation. *Quat. Int.* **2006**, *149*, 24–36. [CrossRef]
65. Konstantinov, E.A.; Velichko, A.A.; Kurbanov, R.N.; Zakharov, A.L. Middle to Late Pleistocene Topography Evolution of the North-Eastern Azov Region. *Quat. Int.* **2018**, *465*, 72–84. [CrossRef]
66. Panin, P.G.; Timireva, S.N.; Morozova, T.D.; Kononov, Y.M.; Velichko, A.A. Morphology and Micromorphology of the Loess-Paleosol Sequences in the South of the East European Plain (MIS 1–MIS 17). *Catena* **2018**, *168*, 79–101. [CrossRef]
67. Zastrozhnov, A.; Danukalova, G.; Shick, S.; van Kolfshoten, T. State of Stratigraphic Knowledge of Quaternary Deposits in European Russia: Unresolved Issues and Challenges for Further Research. *Quat. Int.* **2018**, *478*, 4–26. [CrossRef]
68. Költringer, C.; Stevens, T.; Bradák, B.; Almqvist, B.; Kurbanov, R.; Snowball, I.; Yarovaya, S. Enviromagnetic Study of Late Quaternary Environmental Evolution in Lower Volga Loess Sequences, Russia. *Quat. Res.* **2020**, 1–25. [CrossRef]
69. Sycheva, S.; Frechen, M.; Terhorst, B.; Sedov, S.; Khokhlova, O. Pedostratigraphy and Chronology of the Late Pleistocene for the Extra Glacial Area in the Central Russian Upland (Reference Section Aleksandrov Quarry). *Catena* **2020**, *194*, 104689. [CrossRef]
70. Zykina, V.S.; Zykin, V.S.; Volvakh, A.O.; Radaković, M.G.; Gavrilov, M.B.; Marković, S.B. Late Pleistocene Loess-Paleosol Sequence at the Belovo Section, South of Western Siberia, Russia: Preliminary Results. *Quat. Int.* **2020**. [CrossRef]
71. Wolf, D.; Baumgart, P.; Meszner, S.; Fülling, A.; Haubold, F.; Sahakyan, L.; Meliksetian, K.; Faust, D. Loess in Armenia–Stratigraphic Findings and Palaeoenvironmental Indications. *Proc. Geol. Assoc.* **2016**, *127*, 29–39. [CrossRef]

72. Richter, C.; Wolf, D.; Walther, F.; Meng, S.; Sahakyan, L.; Hovakimyan, H.; Wolpert, T.; Fuchs, M.; Faust, D. New Insights into Southern Caucasian Glacial–Interglacial Climate Conditions Inferred from Quaternary Gastropod Fauna. *J. Quat. Sci.* **2020**, *35*, 634–649. [CrossRef]
73. Mazneva, E.; Konstantinov, E.; Zakharov, A.; Sychev, N.; Tkach, N.; Kurbanov, R.; Sedaeva, K.; Murray, A. Middle and Late Pleistocene Loess of the Western Ciscaucasia: Stratigraphy, Lithology and Composition. *Quat. Int.* **2021**, *590*, 146–163. [CrossRef]
74. Forster, T.; Heller, F. Loess Deposits from the Tajik Depression (Central Asia): Magnetic Properties and Paleoclimate. *Earth Planet. Sci. Lett.* **1994**, *128*, 501–512. [CrossRef]
75. Ding, Z.L.; Ranov, V.; Yang, S.L.; Finaev, A.; Han, J.M.; Wang, G.A. The Loess Record in Southern Tajikistan and Correlation with Chinese Loess. *Earth Planet. Sci. Lett.* **2002**, *200*, 387–400. [CrossRef]
76. Dodonov, A.E.; Sadchikova, T.A.; Sedov, S.N.; Simakova, A.N.; Zhou, L.P. Multidisciplinary Approach for Paleoenvironmental Reconstruction in Loess-Paleosol Studies of the Darai Kalon Section, Southern Tajikistan. *Quat. Int.* **2006**, *152–153*, 48–58. [CrossRef]
77. Wang, X.; Wei, H.; Taheri, M.; Khormali, F.; Danukalova, G.; Chen, F. Early Pleistocene Climate in Western Arid Central Asia Inferred from Loess-Palaeosol Sequences. *Sci. Rep.* **2016**, *6*, 20560. [CrossRef]
78. Jia, J.; Lu, H.; Wang, Y.; Xia, D. Variations in the Iron Mineralogy of a Loess Section in Tajikistan During the Mid-Pleistocene and Late Pleistocene: Implications for the Climatic Evolution in Central Asia. *Geochem. Geophys.* **2018**, *19*, 1244–1258. [CrossRef]
79. Sprafke, T.; Fitzsimmons, K.E.; Grützner, C.; Elliot, A.; Marquer, L.; Nigmatova, S. Reevaluation of Late Pleistocene Loess Profiles at Remizovka (Kazakhstan) Indicates the Significance of Topography in Evaluating Terrestrial Paleoclimate Records. *Quat. Res.* **2018**, *89*, 674–690. [CrossRef]
80. Vlaminck, S.; Kehl, M.; Rolf, C.; Franz, S.O.; Lauer, T.; Lehndorff, E.; Frechen, M.; Khormali, F. Late Pleistocene Dust Dynamics and Pedogenesis in Southern Eurasia–Detailed Insights from the Loess Profile Toshan (NE Iran). *Quat. Sci. Rev.* **2018**, *180*, 75–95. [CrossRef]
81. Dar, R.A.; Zeeden, C. Loess-Palaeosol Sequences in the Kashmir Valley, NW Himalayas: A Review. *Front. Earth Sci.* **2020**, *8*, 113. [CrossRef]
82. Li, Y.; Song, Y.; Fitzsimmons, K.E.; Chen, X.; Prud'homme, C.; Zong, X. Origin of Loess Deposits in the North Tian Shan Piedmont, Central Asia. *Palaeogeogr. Palaeoclim. Palaeoecol.* **2020**, *559*, 109972. [CrossRef]
83. Zhang, J.; Zhou, X.; Long, H. Late Quaternary Loess Accumulation at the Rudak Section in Uzbekistan, Central Asia: Chronology and Palaeoclimate Implications. *Palaeogeogr. Palaeoclim. Palaeoecol.* **2020**, *547*, 109695. [CrossRef]
84. Kehl, M.; Vlaminck, S.; Köhler, T.; Laag, C.; Rolf, C.; Tsukamoto, S.; Frechen, M.; Sumita, M.; Schmincke, H.-U.; Khormali, F. Pleistocene Dynamics of Dust Accumulation and Soil Formation in the Southern Caspian Lowlands–New Insights from the Loess-Paleosol Sequence at Neka-Abelou, Northern Iran. *Quat. Sci. Rev.* **2021**, *253*, 106774. [CrossRef]
85. Heller, F.; Liu, T.-S. Magnetostratigraphical Dating of Loess Deposits in China. *Nature* **1982**, *300*, 431–433. [CrossRef]
86. Heller, F.; Liu, T.-S. Magnetism of Chinese Loess Deposits. *Geophys. J. Int.* **1984**, *77*, 125–141. [CrossRef]
87. Liu, T.-S. *Loess and Environment*; China Ocean Press: Beijing, China, 1985; pp. 31–67.
88. Kukla, G.J. Loess stratigraphy in Central China. *Quat. Sci. Rev.* **1987**, *6*, 191–219. [CrossRef]
89. Kukla, G.; Heller, F.; Ming, L.X.; Chun, X.T.; Sheng, L.T.; Sheng, A.Z. Pleistocene Climates in China Dated by Magnetic Susceptibility. *Geology* **1988**, *16*, 811–814. [CrossRef]
90. Kukla, G.; An, Z. Loess Stratigraphy in Central China. *Palaeogeogr. Palaeoclim. Palaeoecol.* **1989**, *72*, 203–225. [CrossRef]
91. Ding, Z.; Yu, Z.; Rutter, N.W.; Liu, T. Towards an Orbital Time Scale for Chinese Loess Deposits. *Quat. Sci. Rev.* **1994**, *13*, 39–70. [CrossRef]
92. Ding, Z.L.; Derbyshire, E.; Yang, S.L.; Yu, Z.W.; Xiong, S.F.; Liu, T.S. Stacked 2.6-Ma Grain Size Record from the Chinese Loess Based on Five Sections and Correlation with the Deep-Sea δ^{18}O Record. *Paleoceanography* **2002**, *17*, 5-1–5-21. [CrossRef]
93. Evans, M.E.; Heller, F. Magnetic Enhancement and Palaeoclimate: Study of A Loess/Palaeosol Couplet Across the Loess Plateau of China. *Geophys. J. Int.* **1994**, *117*, 257–264. [CrossRef]
94. Bloemendal, J.; Liu, X.M.; Rolph, T.C. Correlation of the Magnetic Susceptibility Stratigraphy of Chinese Loess and the Marine Oxygen Isotope Record: Chronological and Palaeoclimatic Implications. *Earth Planet. Sci. Lett.* **1995**, *131*, 371–380. [CrossRef]
95. Vandenberghe, J.; Zhisheng, A.; Nugteren, G.; Huayu, L.; Huissteden, K.V. New Absolute Time Scale for the Quaternary Climate in the Chinese Loess Region by Grain-Size Analysis. *Geology* **1997**, *25*, 35–38. [CrossRef]
96. Sun, D.; Shaw, J.; An, Z.; Cheng, M.; Yue, L. Magnetostratigraphy and Paleoclimatic Interpretation of a Continuous 7.2 Ma Late Cenozoic Eolian Sediments from the Chinese Loess Plateau. *Geophys. Res. Lett.* **1998**, *25*, 85–88. [CrossRef]
97. Lu, H.; Liu, X.; Zhang, F.; An, Z.; Dodson, J. Astronomical Calibration of Loess-Paleosol Deposits at Luochuan, Central Chinese Loess Plateau. *Palaeogeogr. Palaeoclim. Palaeoecol.* **1999**, *154*, 237–246. [CrossRef]
98. Heslop, D.; Langereis, C.G.; Dekkers, M.J. A New Astronomical Timescale for the Loess Deposits of Northern China. *Earth Planet. Sci. Lett.* **2000**, *184*, 125–139. [CrossRef]
99. Nugteren, G.; Vandenberghe, J.; van Huissteden, J.K.; Zhisheng, A. A Quaternary Climate Record Based on Grain Size Analysis from the Luochuan Loess Section on the Central Loess Plateau, China. *Glob. Planet. Chang.* **2004**, *41*, 167–183. [CrossRef]
100. Vandenberghe, J.; Nugteren, G. Rapid Climatic Changes Recorded in Loess Successions. *Glob. Planet. Chang.* **2001**, *28*, 1–9. [CrossRef]

101. Bokhorst, M.P.; Beets, C.J.; Marković, S.B.; Gerasimenko, N.P.; Matviishina, Z.N.; Frechen, M. Pedo-Chemical Climate Proxies in Late Pleistocene Serbian–Ukranian Loess Sequences. *Quat. Int.* **2009**, *198*, 113–123. [CrossRef]
102. Buggle, B.; Hambach, U.; Kehl, M.; Marković, S.B.; Zöller, L.; Glaser, B. The Progressive Evolution of a Continental Climate in Southeast-Central European Lowlands during the Middle Pleistocene Recorded in Loess Paleosol Sequences. *Geology* **2013**, *41*, 771–774. [CrossRef]
103. Buggle, B.; Hambach, U.; Müller, K.; Zöller, L.; Marković, S.B.; Glaser, B. Iron Mineralogical Proxies and Quaternary Climate Change in SE-European Loess–Paleosol Sequences. *Catena* **2014**, *117*, 4–22. [CrossRef]
104. Galović, L.; Peh, Z. Mineralogical Discrimination of the Pleistocene Loess/Paleosol Sections in Srijem and Baranja, Croatia. *Aeolian Res.* **2016**, *21*, 151–162. [CrossRef]
105. Hošek, J.; Lisá, L.; Hambach, U.; Petr, L.; Vejrostová, L.; Bajer, A.; Grygar, T.M.; Moska, P.; Gottvald, Z.; Horsák, M. Middle Pleniglacial Pedogenesis on the Northwestern Edge of the Carpathian Basin: A Multidisciplinary Investigation of the Bíňa Pedo-Sedimentary Section, SW Slovakia. *Palaeogeogr. Palaeoclim. Palaeoecol.* **2017**, *487*, 321–339. [CrossRef]
106. Bösken, J.; Sümegi, P.; Zeeden, C.; Klasen, N.; Gulyás, S.; Lehmkuhl, F. Investigating the Last Glacial Gravettian Site 'Ságvár Lyukas Hill' (Hungary) and Its Paleoenvironmental and Geochronological Context Using a Multi-Proxy Approach. *Palaeogeogr. Palaeoclim. Palaeoecol.* **2018**, *509*, 77–90. [CrossRef]
107. Rousseau, D.-D.; Derbyshire, E.; Antoine, P.; Hatté, C. European Loess Records. In *Reference Module in Earth Systems and Environmental Sciences*; Elsevier: Amsterdam, The Netherlands, 2018.
108. Schaetzl, R.J.; Bettis, E.A.; Crouvi, O.; Fitzsimmons, K.E.; Grimley, D.A.; Hambach, U.; Lehmkuhl, F.; Marković, S.B.; Mason, J.A.; Owczarek, P.; et al. Approaches and Challenges to the Study of Loess—Introduction to the LoessFest Special Issue. *Quat. Res.* **2018**, *89*, 563–618. [CrossRef]
109. Wacha, L.; Rolf, C.; Hambach, U.; Frechen, M.; Galović, L.; Duchoslav, M. The Last Glacial Aeolian Record of the Island of Susak (Croatia) as Seen from a High-Resolution Grain–Size and Rock Magnetic Analysis. *Quat. Int.* **2018**, *494*, 211–224. [CrossRef]
110. Zeeden, C.; Hambach, U.; Obreht, I.; Hao, Q.; Abels, H.A.; Veres, D.; Lehmkuhl, F.; Gavrilov, M.B.; Marković, S.B. Patterns and Timing of Loess-Paleosol Transitions in Eurasia: Constraints for Paleoclimate Studies. *Glob. Planet. Chang.* **2018**, *162*, 1–7. [CrossRef]
111. Zhao, J.-B.; Ma, Y.-D.; Lui, R.; Luo, X.-Q.; Shao, T.-J. Palaeoclimatic and Hydrological Environments Inferred by Moisture Indexes from the S4 Palaeosol Section in the Xi'an Region, China. *Quat. Int.* **2018**, *493*, 127–136. [CrossRef]
112. Molnár, D.; Makó, L.; Sümegi, P.; Sümegi, B.P.; Törőcsik, T. Revisiting the Palaeolithic site at Szeged-Öthalom: Attempt for appoint the Palaeolithic horizon. *Stud. Quat.* **2019**, *36*, 45–53. [CrossRef]
113. Molnár, D.; Sümegi, P.; Fekete, I.; Makó, L.; Sümegi, B.P. Radiocarbon Dated Malacological Records of Two Late Pleistocene Loess-Paleosol Sequences from SW-Hungary: Paleoecological Inferences. *Quat. Int.* **2019**, *504*, 108–117. [CrossRef]
114. Molnár, D.; Makó, L.; Cseh, P.; Sümegi, P.; Fekete, I.; Galović, L. Middle and Late Pleistocene loess-palaeosol archives in East Croatia: Multi-proxy palaeoecological studies on Zmajevac and Šarengrad II sequences. *Stud. Quat.* **2021**, *38*, 3–17. [CrossRef]
115. Varga, G.; Újvári, G.; Kovács, J. Interpretation of Sedimentary (Sub)Populations Extracted from Grain Size Distributions of Central European Loess-Paleosol Series. *Quat. Int.* **2019**, *502*, 60–70. [CrossRef]
116. Csonka, D.; Bradák, B.; Barta, G.; Szeberényi, J.; Novothny, Á.; Végh, T.; Süle, G.T.; Horváth, E. A Multi-Proxy Study on Polygenetic Middle-to Late Pleistocene Paleosols in the Hévízgyörk Loess-Paleosol Sequence (Hungary). *Quat. Int.* **2020**, *552*, 25–35. [CrossRef]
117. Krauss, L.; Klasen, N.; Schulte, P.; Lehmkuhl, F. New Results Concerning the Pedo- and Chronostratigraphy of the Loess–Palaeosol Sequence Attenfeld (Bavaria, Germany) Derived from a Multi-Methodological Approach. *J. Quat. Sci.* **2021**, in press. [CrossRef]
118. Laag, C.; Hambach, U.; Zeeden, C.; Lagroix, F.; Guyodo, Y.; Veres, D.; Jovanović, M.; Marković, S.B. A Detailed Paleoclimate Proxy Record for the Middle Danube Basin Over the Last 430 Kyr: A Rock Magnetic and Colorimetric Study of the Zemun Loess-Paleosol Sequence. *Front. Earth Sci.* **2021**, *9*, 1–24. [CrossRef]
119. Scheidt, S.; Berg, S.; Hambach, U.; Klasen, N.; Pötter, S.; Stolz, A.; Veres, D.; Zeeden, C.; Brill, D.; Brückner, H.; et al. Chronological Assessment of the Balta Alba Kurgan Loess-Paleosol Section (Romania)—A Comparative Study on Different Dating Methods for a Robust and Precise Age Model. *Front. Earth Sci.* **2021**, *8*, 1–23. [CrossRef]
120. Meng, X.; Derbyshire, E.; Kemp, R.A. Origin of the Magnetic Susceptibility Signal in Chinese Loess. *Quat. Sci. Rev.* **1997**, *16*, 833–839. [CrossRef]
121. Hambach, U.; Rolf, C.; Schnepp, E. Magnetic Dating of Quaternary Sediments, Volcanites and Archaeological Materials: An Overview. *E&G Quat. Sci. J.* **2008**, *57*, 25–51. [CrossRef]
122. Cervi, E.C.; Maher, B.; Poliseli, P.C.; de Souza Junior, I.G.; da Costa, A.C.S. Magnetic Susceptibility as a Pedogenic Proxy for Grouping of Geochemical Transects in Landscapes. *J. Appl. Geophys.* **2019**, *169*, 109–117. [CrossRef]
123. Nawrocki, J.; Wøjcik, A.; Bogucki, A. The Magnetic Susceptibility Record in the Polish and Western Ukrainian Loess-Palaeosol Sequences Conditioned by Palaeoclimate. *Boreas* **1996**, *25*, 161–169. [CrossRef]
124. Maher, B.A. Magnetic Properties of Modern Soils and Quaternary Loessic Paleosols: Paleoclimatic Implications. *Palaeogeogr. Palaeoclim. Palaeoecol.* **1998**, *137*, 25–54. [CrossRef]
125. Maher, B.A. The Magnetic Properties of Quaternary Aeolian Dusts and Sediments, and Their Palaeoclimatic Significance. *Aeolian Res.* **2011**, *3*, 87–144. [CrossRef]

126. Maher, B.A. Palaeoclimatic Records of the Loess/Palaeosol Sequences of the Chinese Loess Plateau. *Quat. Sci. Rev.* **2016**, *154*, 23–84. [CrossRef]
127. Evans, M.; Heller, F. Magnetism of loess/palaeosoil sequences: Recent development. *Earth-Sci. Rev.* **2001**, *54*, 129–144. [CrossRef]
128. Evans, M.E.; Heller, F. *Environmental Magnetism. Principles and Applications of Enviromagnetics*; Academic Press: San Diego, CA, USA, 2003; pp. 9–29.
129. Matasova, G.G.; Kazansky, A.Y. Magnetic properties and magnetic fabrics of Pleistocene loess/palaeosol deposits along west-central Siberian transect and their palaeoclimatic implications. *Geol. Soc. Spec. Publ.* **2004**, *238*, 145. [CrossRef]
130. Jordanova, D.; Hus, J.; Geeraerts, R. Palaeoclimatic Implications of the Magnetic Record from Loess/Palaeosol Sequence Viatovo (NE Bulgaria). *Geophys. J. Int.* **2007**, *171*, 1036–1047. [CrossRef]
131. Maxbauer, D.P.; Feinberg, J.M.; Fox, D.L. Magnetic Mineral Assemblages in Soils and Paleosols as the Basis for Paleoprecipitation Proxies: A Review of Magnetic Methods and Challenges. *Earth-Sci. Rev.* **2016**, *155*, 28–48. [CrossRef]
132. Menshov, O.; Sukhorada, A. Basic theory and methodology of soil geophysics: The first results of application. *Visnyk Taras Shevchenko Natl. Univ. Kyiv Geol.* **2017**, *79*, 35–39. [CrossRef]
133. Radaković, M.G.; Gavrilov, M.B.; Hambach, U.; Schaetzl, R.J.; Tošić, I.; Ninkov, J.; Vasin, J.; Marković, S.B. Quantitative Relationships between Climate and Magnetic Susceptibility of Soils on the Bačka Loess Plateau (Vojvodina, Serbia). *Quat. Int.* **2019**, *502*, 85–94. [CrossRef]
134. Bradák, B.; Seto, Y.; Chadima, M.; Kovács, J.; Tanos, P.; Újvári, G.; Hyodo, M. Magnetic Fabric of Loess and Its Significance in Pleistocene Environment Reconstructions. *Earth-Sci. Rev.* **2020**, *210*, 103385. [CrossRef]
135. Bradák, B.; Seto, Y.; Stevens, T.; Újvári, G.; Fehér, K.; Költringer, C. Magnetic Susceptibility in the European Loess Belt: New and Existing Models of Magnetic Enhancement in Loess. *Palaeogeogr. Palaeoclim. Palaeoecol.* **2021**, *569*, 110329. [CrossRef]
136. Ghafarpour, A.; Khormali, F.; Balsam, W.; Forman, S.L.; Cheng, L.; Song, Y. The Formation of Iron Oxides and Magnetic Enhancement Mechanisms in Northern Iranian Loess-Paleosol Sequences: Evidence from Diffuse Reflectance Spectrophotometry and Temperature Dependence of Magnetic Susceptibility. *Quat. Int.* **2021**, *589*, 68–82. [CrossRef]
137. Jordanova, D.; Jordanova, N. Updating the Significance and Paleoclimate Implications of Magnetic Susceptibility of Holocene Loessic Soils. *Geoderma* **2021**, *391*, 114982. [CrossRef]
138. Költringer, C.; Bradák, B.; Stevens, T.; Almqvist, B.; Banak, A.; Lindner, M.; Kurbanov, R.; Snowball, I. Palaeoenvironmental Implications from Lower Volga Loess–Joint Magnetic Fabric and Multi-Proxy Analyses. *Quat. Sci. Rev.* **2021**, *267*, 107057. [CrossRef]
139. Namier, N.; Gao, X.; Hao, Q.; Marković, S.B.; Fu, Y.; Song, Y.; Zhang, H.; Wu, X.; Deng, C.; Gavrilov, M.B.; et al. Mineral Magnetic Properties of Loess–Paleosol Couplets of Northern Serbia over the Last 1.0 Ma. *Quat. Res.* **2021**, *103*, 35–48. [CrossRef]
140. Zeeden, C.; Hambach, U. Magnetic Susceptibility Properties of Loess from the Willendorf Archaeological Site: Implications for the Syn/Post-Depositional Interpretation of Magnetic Fabric. *Front. Earth Sci.* **2021**, *8*, 599491. [CrossRef]
141. Shackleton, N.J.; Berger, A.; Peltier, W.R. An Alternative Astronomical Calibration of the Lower Pleistocene Timescale Based on ODP Site 677. *Earth Environ. Sci. Trans. R. Soc. Edinb.* **1990**, *81*, 251–261. [CrossRef]
142. Tauxe, L.; Herbert, T.; Shackleton, N.J.; Kok, Y.S. Astronomical Calibration of the Matuyama-Brunhes Boundary: Consequences for Magnetic Remanence Acquisition in Marine Carbonates and the Asian Loess Sequences. *Earth Planet. Sci. Lett.* **1996**, *140*, 133–146. [CrossRef]
143. Ogg, J.G. Chapter 5–Geomagnetic Polarity Time Scale. In *Geologic Time Scale 2020*; Gradstein, F.M., Ogg, J.G., Schmitz, M.D., Ogg, G.M., Eds.; Elsevier: Amsterdam, The Netherlands, 2020; pp. 159–192.
144. Nawrocki, J.; Bogucki, A.; Łanczont, M.; Nowaczyk, N.R. The Matuyama–Brunhes Boundary and the Nature of Magnetic Remanence Acquisition in the Loess–Palaeosol Sequence from the Western Part of the East European Loess Province. *Palaeogeogr. Palaeoclim. Palaeoecol.* **2002**, *188*, 39–50. [CrossRef]
145. Singer, B.S.; Hoffman, K.A.; Coe, R.S.; Brown, L.L.; Jicha, B.R.; Pringle, M.S.; Chauvin, A. Structural and Temporal Requirements for Geomagnetic Field Reversal Deduced from Lava Flows. *Nature* **2005**, *434*, 633–636. [CrossRef]
146. Liu, Q.; Roberts, A.P.; Rohling, E.J.; Zhu, R.; Sun, Y. Post-Depositional Remanent Magnetization Lock-in and the Location of the Matuyama–Brunhes Geomagnetic Reversal Boundary in Marine and Chinese Loess Sequences. *Earth Planet. Sci. Lett.* **2008**, *275*, 102–110. [CrossRef]
147. Liu, Q.; Jin, C.; Hu, P.; Jiang, Z.; Ge, K.; Roberts, A.P. Magnetostratigraphy of Chinese Loess–Paleosol Sequences. *Earth-Sci. Rev.* **2015**, *150*, 139–167. [CrossRef]
148. Wu, Y.; Zhu, Z.; Qiu, S.; Han, Y.; Cai, J.; Rao, Z. Magnetic Stratigraphy Constraints on the Matuyama–Brunhes Boundary Recorded in a Loess Section at the Southern Margin of Chinese Loess Plateau. *Geophys. J. Int.* **2016**, *204*, 1072–1085. [CrossRef]
149. Samus, M.L.G.; Rico, Y.; Bidegain, J.C. Magnetostratigraphy and Magnetic Parameters in Quaternary Sequences of Balcarce, Argentina. A Contribution to Understand the Magnetic Behaviour in Cenozoic Sediments of South America. *GeoResJ* **2017**, *13*, 66–82. [CrossRef]
150. Hlavatskyi, D.V.; Bakhmutov, V.G. Magnetostratigraphy and Magnetic Susceptibility of the Best Developed Pleistocene Loess-Palaeosol Sequences of Ukraine: Implications for Correlation and Proposed Chronostratigraphic Models. *Geol. Q.* **2020**, *64*, 723–753. [CrossRef]
151. Ricci, J.; Carlut, J.; Marques, F.O.; Hildenbrand, A.; Valet, J.-P. Volcanic Record of the Last Geomagnetic Reversal in a Lava Flow Sequence from the Azores. *Front. Earth Sci.* **2020**, *8*, 1–13. [CrossRef]

152. Soler-Arechalde, A.M.; Goguitchaichvili, A.; Carrancho, Á.; Sedov, S.; Caballero-Miranda, C.I.; Ortega, B.; Solis, B.; Contreras, J.J.M.; Urrutia-Fucugauchi, J.; Bautista, F. A Detailed Paleomagnetic and Rock-Magnetic Investigation of the Matuyama-Brunhes Geomagnetic Reversal Recorded in the Tephra-Paleosol Sequence of Tlaxcala (Central Mexico). *Front. Earth Sci.* **2015**, *3*, 1–12. [CrossRef]
153. Veklich, M.F. Pleistocene loesses and fossil soils of the Ukraine. *Acta Geol. Acad. Scient. Hung.* **1979**, *22*, 35–62.
154. Veklich, M.F. *Stages and Stratotypes of the Soil Formations of Ukraine in the Upper Cenozoic*; Naukova Dumka: Kiev, Ukraine, 1982; 208p. (In Russian)
155. Sirenko, N.A.; Turlo, S.I. *Successions of Soils and Vegetation of Ukraine during the Pliocene and Pleistocene*; Naukova Dumka: Kiev, Ukraine, 1986; 488p. (In Russian)
156. Gozhik, P.; Gerasimenko, N.; Matviishina, Z.; Palienko, V.; Korniets, N.; Komar, M.; Mel'michuk, I.; Perederiy, V.; Shelkoplyas, V.; Rousseau, D.-D.; et al. *The Ukraine Quaternary Explored: The Middle and Upper Pleistocene of the Middle Dnieper Area and Its Importance for the East-West Correlation. Excursion Guide*; Institute of Geological Sciences NASU: Kyiv, Ukraine, 2001; 64p.
157. Gerasimenko, N.P. *Quaternary Evolution of Zonal Paleoecosystems in Ukraine*; Institute of Geography NASU: Kyiv, Ukraine, 2004. (In Ukrainian)
158. Haase, D.; Fink, J.; Haase, G.; Ruske, R.; Pécsi, M.; Richter, H.; Altermann, M.; Jäger, K.-D. Loess in Europe—Its Spatial Distribution Based on a European Loess Map, Scale 1:2,500,000. *Quat. Sci. Rev.* **2007**, *26*, 1301–1312. [CrossRef]
159. Lehmkuhl, F.; Nett, J.J.; Pötter, S.; Schulte, P.; Sprafke, T.; Jary, Z.; Antoine, P.; Wacha, L.; Wolf, D.; Zerboni, A.; et al. Loess Landscapes of Europe–Mapping, Geomorphology, and Zonal Differentiation. *Earth-Sci. Rev.* **2020**, 103496. [CrossRef]
160. Krokos, V.I. Short description of the Quaternary deposits of Ukraine. *Bull. MOIP Sect. Geol.* **1926**, *4*, 214–264. (In Russian)
161. Krokos, V.I. Short description of the Quaternary deposits of Ukraine. *Chetvertynnyi Period* **1932**, *3*, 17–55. (In Russian)
162. Veklich, M.F.; Artyushenko, A.T.; Sirenko, N.A.; Dubnyak, V.A.; Mel'nichuk, I.V.; Parishkura, S.I. *Key Sections of the Anthropogene of Ukraine*; Naukova Dumka: Kiev, Ukraine, 1967; pp. 13–50. (In Russian)
163. Veklich, M.F.; Sirenko, N.A. *Key Sections of the Anthropogene of Ukraine. Part III.*; Naukova Dumka: Kiev, Ukraine, 1972; 225p. (In Russian)
164. Tretyak, A.N.; Volok, Z.E. *Paleomagnetic Stratigraphy of Pliocene and Quaternary Sediments in Ukraine*; Naukova Dumka: Kiev, Ukraine, 1976; 88p. (In Russian)
165. Tretyak, A.N. Regim of the Pleistocene geomagnetic field and structure of the Brunhes geomagnetic epoch. *Geofiz. Zhurnal* **1980**, *5*, 75–87. (In Russian)
166. Tretyak, A.N. *Natural Remnant Magnetization and Problem of Sediments Paleomagnetic Stratification*; Naukova Dumka: Kiev, Ukraine, 1983; 256p. (In Russian)
167. Bogucki, A. Quaternary cover sediments in Volyn-Podillia. In *Quaternary Deposits of Ukraine*; Makarenko, D.E., Ed.; Naukova Dumka: Kiev, Ukraine, 1986. (In Russian)
168. Tretyak, A.N.; Shevchenko, A.I.; Dudkin, V.P.; Vigilyanskaya, L.I. *Paleomagnetic Stratigraphy of Key Late Cenozoic Sections of the South of Ukraine*; Institute of Geological Sciences AS USSR: Kiev, Ukraine, 1987; 50p. (In Russian)
169. Tretyak, A.N.; Vigilyanskaya, L.I.; Makarenko, V.N.; Dudkin, V.P. *Thin Structure of Geomagnetic Field in Late Cenozoic*; Naukova Dumka: Kiev, Ukraine, 1989; 156p. (In Russian)
170. Tretyak, A.N.; Vigilyanskaya, L.I. Magnetostratigraphic scale of Pleistocene of Ukraine. *Geofiz. Zhurnal* **1994**, *16*, 3–14. (In Russian)
171. Nawrocki, J.; Bakhmutov, V.; Bogucki, A.; Dolecki, L. The Paleo- and Petromagnetic Record in the Polish and Ukrainian Loess-Paleosol Sequences. *Phys. Chem. Earth Part A Solid Earth Geod.* **1999**, *24*, 773–777. [CrossRef]
172. Nawrocki, J.; Łanczont, M.; Bogutsky, A. Palaeomagnetic studies of the loess-palaeosol sequence from the Kolodiiv section (East Carpathian Foreland, Ukraine). *Geol. Q.* **2007**, *51*, 161–166.
173. Gozhik, P.F.; Shelkoplyas, V.N.; Komar, M.S.; Matviishyna, Z.M.; Perederiy, V.I. *Guide X of the Polish-Ukrainian Seminar "Correlation of Loesses and Ice deposits"*; Institute of Geological Sciences NASU: Kyiv, Ukraine, 2000. (In Ukrainian)
174. Gozhik, P.; Komar, M.; Krokhmal, O.; Shovkoplias, V.; Khrystoforova, T.; Dykan, N.; Prylypko, S. The key section of Neopleistocene subaerial deposits near Roxolany village (Odessa region). In *Problems of the Middle Pleistocene Interglacial*; Vydavnychyi tsentr LNU imeni Ivana Franka: Lviv, Ukraine, 2007; pp. 109–128. (In Ukrainian)
175. Vigilyanskaya, L.I.; Tretyak, A.N. Palaeomagnetism of key Pliocene-Pleistocene sections in North-Western W Donbass. *Geofiz. Zhurnal* **2000**, *22*, 96–104. (In Russian)
176. Vigilyanskaya, L.I.; Tretyak, A.N. Palaeomagnetic studies of Pliocene-Pleistocene deposits of loess-palaeosol stratum in Middle Dnieper region. *Geofiz. Zhurnal* **2002**, *24*, 36–42. (In Russian)
177. Gerasimenko, N. Late Pleistocene vegetational and soil evolution at the Kiev loess plain as recorded in the Stari Bezradychy section, Ukraine. *Stud. Quat.* **2000**, *17*, 19–28.
178. Gerasimenko, N.P. *Quaternary Palaeogeography of Ukraine (Palaeolandscapes)*; Print-Service: Kyiv, Ukraine, 2020. (In Ukrainian)
179. Gerasimenko, N.; Matvijishyna, Z. The problems of Zavadiv "great interglacial". In *Problems of Middle Pleistocene Interglacial, Proceedings of the XIV Ukrainian-Polish Workshop, Lutsk, Ukraine, 12–16 September 2007*; Bogucki, A., Gozhik, P., Łanczont, M., Lindner, L., Yelovicheva, J., Eds.; Vydavnychyi tsentr LNU imeni Ivana Franka: Lviv, Ukraine, 2007; pp. 194–206. (In Ukrainian)
180. Łanczont, M.; Bogutsky, A. High-resolution terrestrial archive of climatic oscillations during Oxygen Isotope Stages 5-2 in the loess-palaeosol sequence at Kolodiiv (East Carpathian Foreland, Ukraine). *Geol. Q.* **2007**, *51*, 105–126.

181. Boguckyj, A.B.; Łanczont, M.; Łącka, B.; Madeyska, T.; Nawrocki, J. Quaternary Sediment Sequence at Skala Podil'ska, Dniester River Basin (Ukraine): Preliminary Results of Multi-Proxy Analyses. *Quat. Int.* **2009**, *198*, 173–194. [CrossRef]
182. Bogucki, A.; Łanczont, M.; Gozhik, P.; Komar, M. Roksolany loess section: Location, research history and characteristics of deposits. In *Loess Cover of the North Black Sea Region, Proceedings of the XVIII Ukrainian-Polish Workshop, Roksolany, Ukraine, 8–13 September 2013*; Bogucki, A., Gozhik, P., Łanczont, M., Madejska, T., Yeovicheva, J., Eds.; KARTPOL S. C. Lublin: Lublin, Poland, 2013; pp. 34–58. (In Ukrainian)
183. Matviishyna, Z.M.; Gerasimenko, N.P.; Perederyi, V.I.; Bragin, A.M.; Ivchenko, A.S.; Karmazinenko, S.P.; Nagirnyi, V.M.; Parkhomenko, O.G. *Spatio-Temporal Correlation of Quaternary Palaeogeographic Conditions on the Territory of Ukraine*; Naukova Dumka: Kyiv, Ukraine, 2010; 191p. (In Ukrainian)
184. Sirenko, O. *Palynostratigraphy of Continental Upper Pliocene—Lower Neopleistocene Deposits of Southern Part of the East European Platform*; Naukova Dumka: Kyiv, Ukraine, 2017; 165p. (In Russian)
185. Sirenko, O.A. Palynological Data on the Description of the Gelasian and Calabriane Analogues in the Strato- Type Section of the Kuyalnik Deposits near Kryzhanivka Village (Odessa Region). *J. Geol. Geogr. Geoecol.* **2019**, *28*, 727–737. [CrossRef]
186. Doroshkevych, S.P. *Pleistocene palaeoenvironment in Middle Pobuzhzhia: According to the study of buried soils*; Naukova Dumka: Kyiv, Ukraine, 2018; 176p. (In Ukrainia)
187. Komar, M.; Łanczont, M.; Fedorowicz, S.; Gozhik, P.; Mroczek, P.; Bogucki, A. Stratigraphic Interpretation of Loess in the Marginal Zone of the Dnieper I Ice Sheet and the Evolution of Its Landscape after Deglaciation (Dnieper Upland, Ukraine). *Geol. Q.* **2018**, *62*, 536–552. [CrossRef]
188. Gerasimenko, N.P.; Koval'chuk, I.P. The Late Pleistocene Soils as Indicators of the Impact of Environmental Changes on Development of Pedogenic Processes (the Study Case from the Kryva Luka Site, Donetsk Area). *J. Geol. Geogr. Geoecol.* **2019**, *28*, 262–274. [CrossRef]
189. Gozhik, P.F. On the Lower Boundary of the Quaternary System in the Azov-Black Sea Basin. *J. Geol. Geogr. Geoecol.* **2019**, *28*, 292–300. [CrossRef]
190. Karmazinenko, S.P. Pleistocene Soils of the Azov Lowland, Ukraine. *J. Geol. Geogr. Geoecol.* **2019**, *28*, 313–326. [CrossRef]
191. Veklych, Y. Map of Quaternary Formations of Ukraine in Scale 1:2,500,000. *J. Geol. Geogr. Geoecol.* **2019**, *28*, 367–376. [CrossRef]
192. Bondar, K.; Ridush, B.; Baryshnikova, M.; Popiuk, Y. On Palaeomagnetic Dating of Fluvial Deposits in the Section of Neporotove Gravel Quarry on the Middle Dniester. *J. Geol. Geogr. Geoecol.* **2019**, *28*, 241–249. [CrossRef]
193. Haesaerts, P.; Gerasimenko, N.; Damblon, F.; Yurchenko, T.; Kulakovska, L.; Usik, V.; Ridush, B. The Upper Palaeolithic Site Doroshivtsi III: A New Chronostratigraphic and Environmental Record of the Late Pleniglacial in the Regional Context of the Middle Dniester-Prut Loess Domain (Western Ukraine). *Quat. Int.* **2020**, *546*, 196–215. [CrossRef]
194. Manyuk, V.V. New Data on Geology of the Rybalsky Quarry, Unique Object of Geological Heritage of Global Significance. *J. Geol. Geogr. Geoecol.* **2021**, *30*, 100–121. [CrossRef]
195. Popiuk, Y.; Ridush, B.; Solovey, T. Middle and Late Pleistocene terrestrial snails from the Middle Dniester area, Ukraine (based on Mykola Kunytsia's collections). *Geol. Q.* **2021**, *65*, 1–12. [CrossRef]
196. Veklich, M.F.; Sirenko, N.A.; Matviishyna, Z.N.; Melnychuk, I.V.; Perederyi, V.I.; Turlo, S.I.; Vozgrin, B.D. *Palaeogeographical Succession and Detailed Stratigraphic Division of the Pleistocene of Ukraine (Methodological Developments)*; Naukova Dumka: Kiev, Ukrainie, 1984; 32p. (In Russian)
197. Veklich, M.F.; Sirenko, N.A.; Matviishyna, Z.N.; Gerasimenko, N.P.; Perederiy, V.I.; Turlo, S.I. The Pleistocene Stratigraphical Framework of the Ukraine. In *Stratigraphic Schemes of Fanerozoic and Precambrian of Ukraine*; State Committee of Geology of Ukraine: Kiev, Ukrainie, 1993. (In Russian)
198. Gozhik, P.F. (Ed.) *Stratigraphic Code of Ukraine*; National Stratigraphic Committee of Ukraine: Kyiv, Ukraine, 2012; p. 64. (In Ukrainian)
199. Antoine, P.; Rousseau, D.-D.; Fuchs, M.; Hatté, C.; Gauthier, C.; Marković, S.B.; Jovanović, M.; Gaudenyi, T.; Moine, O.; Rossignol, J. High-Resolution Record of the Last Climatic Cycle in the Southern Carpathian Basin (Surduk, Vojvodina, Serbia). *Quat. Int.* **2009**, *198*, 19–36. [CrossRef]
200. Antoine, P.; Lagroix, F.; Jordanova, D.; Jordanova, N.; Lomax, J.; Fuchs, M.; Debret, M.; Rousseau, D.-D.; Hatté, C.; Gauthier, C.; et al. A Remarkable Late Saalian (MIS 6) Loess (Dust) Accumulation in the Lower Danube at Harletz (Bulgaria). *Quat. Sci. Rev.* **2019**, *207*, 80–100. [CrossRef]
201. Galović, L. Geochemical Archive in the Three Loess/Paleosol Sections in the Eastern Croatia: Zmajevac I, Zmajevac and Erdut. *Aeolian Res.* **2014**, *15*, 113–132. [CrossRef]
202. Jipa, D.C. The Loess-like Deposits in the Lower Danube Basin. Genetic Significance. *Geo-Eco-Marina* **2014**, *20*, 7–18. [CrossRef]
203. Makó, L.; Molnár, D.; Runa, B.; Bozsó, G.; Cseh, P.; Nagy, B.; Sümegi, P. Selected Grain-Size and Geochemical Analyses of the Loess-Paleosol Sequence of Pécel (Northern Hungary): An Attempt to Determine Sediment Accumulation Conditions and the Source Area Location. *Quaternary* **2021**, *4*, 17. [CrossRef]
204. Bronger, A. Correlation of Loess–Paleosol Sequences in East and Central Asia with SE Central Europe: Towards a Continental Quaternary Pedostratigraphy and Paleoclimatic History. *Quat. Int.* **2003**, *106–107*, 11–31. [CrossRef]
205. Zoeller, L. New Approaches to European Loess: A Stratigraphic and Methodical Review of the Past Decade. *Open Geosci.* **2010**, *2*, 19–31. [CrossRef]

206. Bronger, A.; Smolíková, L. Quaternary Loess-Paleosol Sequences in East and Central Asia in Comparison with Central Europe–Micromorphological and Paleoclimatological Conclusions. *Bol. Soc. Geol. Mex.* **2019**, *71*, 65–92. [CrossRef]
207. Gibbard, P.L.; Hughes, P.D. Terrestrial Stratigraphical Division in the Quaternary and Its Correlation. *J. Geol. Soc.* **2021**, *178*, jgs2020-134. [CrossRef]
208. Veklich, M.F. *Problems of Palaeoclimatology*; Naukova Dumka: Kiev, Ukrainie, 1987; 190p. (In Russian)
209. Head, M.J.; Gibbard, P.L. Early–Middle Pleistocene Transitions: Linking Terrestrial and Marine Realms. *Quat. Int.* **2015**, *389*, 7–46. [CrossRef]
210. Bradák, B.; Seto, Y.; Nawrocki, J. Significant Pedogenic and Palaeoenvironmental Changes during the Early Middle Pleistocene in Central Europe. *Palaeogeogr. Palaeoclim. Palaeoecol.* **2019**, *534*, 109335. [CrossRef]
211. Obreht, I.; Zeeden, C.; Hambach, U.; Veres, D.; Marković, S.B.; Bösken, J.; Svirčev, Z.; Bačević, N.; Gavrilov, M.B.; Lehmkuhl, F. Tracing the Influence of Mediterranean Climate on Southeastern Europe during the Past 350,000 Years. *Sci. Rep.* **2016**, *6*, 36334. [CrossRef]
212. Obreht, I.; Zeeden, C.; Hambach, U.; Veres, D.; Marković, S.B.; Lehmkuhl, F. A Critical Reevaluation of Palaeoclimate Proxy Records from Loess in the Carpathian Basin. *Earth-Sci. Rev.* **2019**, *190*, 498–520. [CrossRef]
213. Bakhmutov, V.G.; Mokriak, I.N.; Skarboviychuk, T.V.; Yakukhno, V.I. Results of palaeomagnetic studies of Danube terraces sections and problems of Pleistocene magnetostratigraphy of the west Black Sea region. *Geofiz. Zhurnal* **2005**, *25*, 980–991. (In Russian)
214. Veklich, M.F.; Veklich, Y.M. *Stage and Stratoregion of the Estuary-Marine Pleistocene of the Azov–Black Sea Basin*; Institute of Geography, NASU: Kyiv, Ukraine, 1993; 186p. (In Russian)
215. Tsatskin, A.; Heller, F.; Gendler, T.S.; Virina, E.I.; Spassov, S.; Du Pasquier, J.; Hus, J.; Hailwood, E.A.; Bagin, V.I.; Faustov, S.S. A New Scheme of Terrestrial Paleoclimate Evolution during the Last 1.5 Ma in the Western Black Sea Region: Integration of Soil Studies and Loess Magmatism. *Phys. Chem. Earth Part A Solid Earth Geod.* **2001**, *26*, 911–916. [CrossRef]
216. Tsatskin, A.; Gendler, T.S.; Heller, F. Improved Paleopedological Reconstruction of Vertic Paleosols at Novaya Etuliya, Moldova via Integration of Soil Micromorphology and Environmental Magnetism. In *New Trends in Soil Micromorphology*; Kapur, S., Mermut, A., Stoops, G., Eds.; Springer: Berlin/Heidelberg, Germany, 2008; pp. 91–110. [CrossRef]
217. Konstantinova, N.A. *Antropogene of the Southern Moldaviia and South-Western Ukraine*; Nauka: Moscow, Russia, 1967; Volume 173, pp. 1–138. (In Russian)
218. Matoshko, A.; Matoshko, A.; de Leeuw, A. The Plio–Pleistocene Demise of the East Carpathian Foreland Fluvial System and Arrival of the Paleo-Danube to The Black Sea. *Geol. Carpath.* **2019**, *70*, 91–112. [CrossRef]
219. Gozhik, P.F. *Guidebook of VIII International Sympozium on Loess Deposits*; Gozhik, P.F., Chugunnyi, Y.G., Melnik, V.I., Eds.; Naukova Dumka: Kiev, Ukraine, 1976; 71p. (In Russian)
220. Tsatskin, A.; Heller, F.; Hailwood, E.A.; Gendler, T.S.; Hus, J.; Montgomery, P.; Sartori, M.; Virina, E.I. Pedosedimentary Division, Rock Magnetism and Chronology of the Loess/Palaeosol Sequence at Roxolany (Ukraine). *Palaeogeogr. Palaeoclim. Palaeoecol.* **1998**, *143*, 111–133. [CrossRef]
221. Sartori, M. The Quaternary Climate in Loess Sediments: Evidence from Rock and Mineral Magnetic and Geochemical Analysis. Ph.D. Thesis, Swiss Federal Institute of Technology, Zurich, Switzerland, 2000; 231p.
222. Sharonova, Z.V.; Pilipenko, O.V.; Trubikhin, V.M.; Didenko, A.N.; Feyn, A.G. Restoration of geomagnetic field according to paleomagnetic records in loess-soil section Roxolany (Dnestr river, Ukraine) for last 75 000 years. *Fizika Zemli* **2004**, *1*, 4–13. (In Russian)
223. Pilipenko, O.V.; Sharonova, Z.V.; Trubikhin, V.M.; Didenko, A.N. Thin structure and evolution of geomagnetic field 75–10 kyr ago on the example of the loess-palaeosol section Roksolany (Ukraine). *Fizika Zemli* **2005**, *1*, 66–73. (In Russian)
224. Dodonov, A.E.; Zhou, L.P.; Markova, A.K.; Tchepalyga, A.L.; Trubikhin, V.M.; Aleksandrovski, A.L.; Simakova, A.N. Middle–Upper Pleistocene Bio-Climatic and Magnetic Records of the Northern Black Sea Coastal Area. *Quat. Int.* **2006**, *149*, 44–54. [CrossRef]
225. Gendler, T.S.; Heller, F.; Tsatskin, A.; Spassov, S.; Du Pasquier, J.; Faustov, S.S. Roxolany and Novaya Etuliya—Key Sections in the Western Black Sea Loess Area: Magnetostratigraphy, Rock Magnetism, and Paleopedology. *Quat. Int.* **2006**, *152–153*, 78–93. [CrossRef]
226. Bakhmutov, V.G.; Hlavatskyi, D.V. New data about Matuyama—Brunhes boundary in Roxolany section. *Geol. Zhurnal* **2014**, *347*, 73–84. [CrossRef]
227. Bakhmutov, V.G.; Hlavatskyi, D.V. Identification of the Matuyama-Brunhes Boundary by Paleomagnetic Studies of the Roxolany Profile (Western Black Sea Region). *Dopov. Nac. Akad. Nauk Ukr.* **2014**, *10*, 92–98. [CrossRef]
228. Bakhmutov, V.G.; Kazanskii, A.Y.; Matasova, G.G.; Glavatskii, D.V. Rock Magnetism and Magnetostratigraphy of the Loess-Sol Series of Ukraine (Roksolany, Boyanychi, and Korshev Sections). *Izv. Phys. Solid Earth* **2017**, *53*, 864–884. [CrossRef]
229. Nawrocki, J.; Gozhik, P.; Łanczont, M.; Pańczyk, M.; Komar, M.; Bogucki, A.; Williams, I.S.; Czupyt, Z. Palaeowind Directions and Sources of Detrital Material Archived in the Roxolany Loess Section (Southern Ukraine). *Palaeogeogr. Palaeoclim. Palaeoecol.* **2018**, *496*, 121–135. [CrossRef]

230. Hlavatskyi, D.V.; Bakhmutov, V.G. Magnetostratigraphy of the Key Loess-Palaesol Sequence at Roxolany (Western Black Sea Region). In *Recent Advances in Rock Magnetism, Environmental Magnetism and Paleomagnetism*; Nurgaliev, D., Shcherbakov, V., Kosterov, A., Spassov, S., Eds.; Springer Geophysics; Springer International Publishing: Cham, Switzerland, 2019; pp. 371–382. [CrossRef]
231. Stephens, M.; Krzyszkowski, D.; Ivchenko, A.; Majewski, M. Palaeoclimate and Pedosedimentary Reconstruction of a Middle to Late Pleistocene Loess-Palaeosol Sequence, Prymorske, SW Ukraine. *Stud. Quat.* **2002**, *19*, 3–18.
232. Shovkoplyas, V.M.; Vozgrin, B.D.; Prylypko, S.K. Use of thermoluminescent analysis data in solving the problems of correlation of Upper Pleistocene deposits of glacial and non-glacial zones of Ukraine. *Miner. Resur. Ukrayiny* **2006**, *3*, 22–24. (In Ukrainian)
233. Tecsa, V.; Gerasimenko, N.; Veres, D.; Hambach, U.; Lehmkuhl, F.; Schulte, P.; Timar-Gabor, A. Revisiting the Chronostratigraphy of Late Pleistocene Loess-Paleosol Sequences in Southwestern Ukraine: OSL Dating of Kurortne Section. *Quat. Int.* **2020**, *542*, 65–79. [CrossRef]
234. Hlavatskyi, D.V.; Kuzina, D.M.; Gerasimenko, N.P.; Bakhmutov, V.G. Petromagnetism and paleomagnetism of Quaternary loess-soil sediments of Vyazivok section (Dnieper Lowland). *Geofiz. Zhurnal* **2016**, *38*, 186–193. [CrossRef]
235. Hlavatskyi, D.V.; Gerasimenko, N.P.; Bakhmutov, V.G.; Bonchkovskyi, O.S.; Poliachenko, I.B.; Shpyra, V.V.; Mychak, S.V.; Kravchuk, I.V.; Cherkes, S.I. Significance of the Ukrainian Loess-Palaeosol Sequences for Pleistocene Climate Reconstructions: Rock Magnetic, Palaeosol and Pollen Proxies. *Geofiz. Zhurnal* **2021**, *43*, 3–26. [CrossRef]
236. Veklich, M.F. Correlation of the Pleistocene Paleogeographical Stages: Ocean–Loess Areas–the Black Sea. In *Correlation of Paleogeographical Events: Continent–Shelf–Ocean*; Svitoch, A.A., Ed.; Moscow University Press: Moscow, Russia, 1995; pp. 27–33. (In Russian)
237. Vozgrin, B.D. Problems of stratigraphic subdivision and correlation of terrestrial deposits of the Antropogene of Ukraine. In *Regional Geological Studies in Ukraine and the Question of Creating a State Geologic Map*; The State Geological Survey, Ukrainian State Research Institute for Geological Survey: Kyiv, Ukraine, 2001; pp. 30–32.
238. Gerasimenko, N.P. (National Taras Shevchenko University of Kyiv, Faculty of Geography, Kyiv, Ukraine). Personal communication, 2021.
239. Kirschvink, J.L. The least squares line and plane and the analysis of palaeomagnetic data. *Geophys. J. Int.* **1980**, *62*, 699–718. [CrossRef]
240. Chadima, M.; Hrouda, F. Remasoft 3.0 a user-friendly paleomagnetic data browser and analyzer. *Trav. Geophys.* **2006**, *27*, 20–21.
241. Man, O. On the identification of magnetostratigraphic polarity zones. *Stud. Geophys. Geod.* **2008**, *52*, 173–186. [CrossRef]
242. Lisiecki, L.E.; Raymo, M.E. A Pliocene-Pleistocene Stack of 57 Globally Distributed Benthic δ^{18}O Records. *Paleoceanography* **2005**, *20*, PA1003. [CrossRef]
243. Railsback, L.B.; Gibbard, P.L.; Head, M.J.; Voarintsoa, N.R.G.; Toucanne, S. An Optimized Scheme of Lettered Marine Isotope Substages for the Last 1.0 Million Years, and the Climatostratigraphic Nature of Isotope Stages and Substages. *Quat. Sci. Rev.* **2015**, *111*, 94–106. [CrossRef]
244. Veklych, Y.M. (Ukrainian State Geological Research Institute, Kyiv, Ukraine). Personal communication, 2021.
245. Panin, P.G.; Timireva, S.N.; Konstantinov, E.A.; Kalinin, P.I.; Kononov, Y.M.; Alekseev, A.O.; Semenov, V.V. Plio-Pleistocene Paleosols: Loess-Paleosol Sequence Studied in the Beregovoye Section, the Crimean Peninsula. *Catena* **2019**, *172*, 590–618. [CrossRef]
246. Zhou, L.P.; Oldfield, F.; Wintle, A.G.; Robinson, S.G.; Wang, J.T. Partly Pedogenic Origin of Magnetic Variations in Chinese Loess. *Nature* **1990**, *346*, 737–739. [CrossRef]
247. Dearing, J.A.; Dann, R.J.L.; Hay, K.; Lees, J.A.; Loveland, P.J.; Maher, B.A.; O'Grady, K. Frequency-Dependent Susceptibility Measurements of Environmental Materials. *Geophys. J. Int.* **1996**, *124*, 228–240. [CrossRef]
248. Maher, B.A. Magnetic properties of some synthetic submicron magnetites. *Geophys. J.* **1988**, *94*, 83–96. [CrossRef]
249. Dunlop, D.J.; Xu, S. A comparison of methods of granulometry and domain structure determination. *EOS Trans. Am. Geophys.* **1993**, *74*, 203.
250. Dunlop, D.J. Magnetism in rocks. *J. Geophys. Res.* **1995**, *100*, 2161–2174. [CrossRef]
251. Stober, J.C.; Thompson, R. Palaeomagnetic secular variation studies of Finnish lake sediment and the carriers of remanence. *Earth Planet. Sci. Lett.* **1977**, *37*, 139–149. [CrossRef]
252. Bloemendal, J.; King, J.W.; Hall, F.R.; Doh, S.-J. Rock magnetism of Late Neogene and Pleistocene deep-sea sediments: Relationship to sediment source, diagenetic processes and sediment lithology. *J. Geophys. Res.* **1992**, *97*, 4361–4375. [CrossRef]
253. Robinson, S.G. The late Pleistocene paleoclimatic record of North Atlantic deep-sea sediments revealed by mineral-magnetic measurements. *Phys. Earth Planet. Inter.* **1986**, *42*, 22–47. [CrossRef]
254. Hrouda, F. Magnetic anisotropy of rock and its application in geology and geophysics. *Geophys. Surv.* **1982**, *5*, 37–82. [CrossRef]
255. Lagroix, F.; Banerjee, S.K. Paleowind direction from the magnetic fabric of loess profile in central Alaska. *Earth Planet. Sci. Lett.* **2002**, *195*, 99–102. [CrossRef]
256. Rees, A.I. The effect of depositional slopes on the anisotropy of magnetic susceptibility of laboratory deposited sands. *J. Geol.* **1966**, *74*, 856–867. [CrossRef]
257. Rees, A.I.; Woodal, W.A. The magnetic fabric of some laboratorydeposited sediments. *Earth Planet. Sci. Lett.* **1975**, *25*, 121–130. [CrossRef]

258. Ellwood, B.B. Bioturbation; minimal effects on the magnetic fabric of some natural and experimental sediments. *Earth Planet. Sci. Lett.* **1984**, *67*, 367–376. [CrossRef]
259. Bradák, B. Application of Anisotropy of Magnetic Susceptibility (AMS) for the Determination of Paleo-Wind Directions and Paleo-Environment during the Accumulation Period of Bag Tephra, Hungary. *Quat. Int.* **2009**, *198*, 77–84. [CrossRef]
260. Bradák, B.; Újvári, G.; Seto, Y.; Hyodo, M.; Végh, T. A Conceptual Magnetic Fabric Development Model for the Paks Loess in Hungary. *Aeolian Res.* **2018**, *30*, 20–31. [CrossRef]
261. Hlavatskyi, D.; Bakhmutov, V. Anisotropy of magnetic susceptibility of Pleistocene loess-paleosol sequences from Ukraine and its paleoenvironment implications. *Geophys. Res. Abstr.* **2019**, *21*, 1.
262. Nawrocki, J.; Bogucki, A.B.; Gozhik, P.; Łanczont, M.; Pańczyk, M.; Standzikowski, K.; Komar, M.; Rosowiecka, O.; Tomeniuk, O. Fluctuations of the Fennoscandian Ice Sheet Recorded in the Anisotropy of Magnetic Susceptibility of Periglacial Loess from Ukraine. *Boreas* **2019**, *48*, 940–952. [CrossRef]
263. Bakhmutov, V.G.; Glavatskiy, D.V. Problems of magnetostratigraphy of Pleistocene loess-soil deposits in the South of Ukraine. *Geofiz. Zhurnal* **2016**, *38*, 59–75. [CrossRef]
264. Butler, R.F. *Paleomagnetism: Magnetic Domains to Geologic Terranes*; Blackwell Scientific Publications: Boston, MA, USA, 1992; 319p.
265. Laj, C.; Channell, J.E.T. Geomagnetic Excursions. In *Treatise on Geophysics*; Kono, M., Ed.; Elsevier: Amsterdam, The Netherlands, 2007; pp. 373–416.
266. Channell, J.E.T.; Singer, B.S.; Jicha, B.R. Timing of Quaternary Geomagnetic Reversals and Excursions in Volcanic and Sedimentary Archives. *Quat. Sci. Rev.* **2020**, *228*, 106114. [CrossRef]
267. Zheng, H.; An, Z.; Shaw, J. New Contributions to Chinese Plio-Pleistocene Magnetostratigraphy. *Phys. Earth Planet. Inter.* **1992**, *70*, 146–153. [CrossRef]
268. Spassov, S.; Heller, F.; Evans, M.E.; Yue, L.P.; Ding, Z.L. The Matuyama/Brunhes Geomagnetic Polarity Transition at Lingtai and Baoji, Chinese Loess Plateau. *Phys. Chem. Earth Part A Solid Earth Geod.* **2001**, *26*, 899–904. [CrossRef]
269. Spassov, S.; Heller, F.; Evans, M.E.; Yue, L.P.; Dobeneck, T. von. A Lock-in Model for the Complex Matuyama-Brunhes Boundary Record of the Loess/Palaeosol Sequence at Lingtai (Central Chinese Loess Plateau). *Geophys. J. Int.* **2003**, *155*, 350–366. [CrossRef]
270. Pan, Y.X.; Zhu, R.X.; Liu, Q.S.; Guo, B.; Yue, L.P.; Wu, H.N. Geomagnetic Episodes of the Last 1.2 Myr Recorded in Chinese Loess. *Geophys. Res. Lett.* **2002**, *29*, 123-1–123-4. [CrossRef]
271. Yang, T.; Hyodo, M.; Yang, Z.; Li, H.; Maeda, M. Multiple Rapid Polarity Swings during the Matuyama-Brunhes Transition from Two High-Resolution Loess-Paleosol Records. *J. Geophys. Res. Solid Earth* **2010**, *115*, B05101. [CrossRef]
272. Pan, Q.; Xiao, G.; Zhao, Q.; Chen, R.; Ao, H.; Shen, Y.; Cheng, J.; Zhu, Z. The Jaramillo Subchron in Chinese Loess-Paleosol Sequences. *Palaeogeogr. Palaeoclim. Palaeoecol.* **2021**, *572*, 110423. [CrossRef]
273. Hyodo, M. Possibility of Reconstruction of the Past Geomagnetic Field from Homogeneous Sediments. *J. Geomag. Geoelec.* **1984**, *36*, 45–62. [CrossRef]
274. Hus, J.J.; Han, J. The Contribution of Loess Magnetism in China to the Retrieval of Past Global Changes—Some Problems. *Phys. Earth Planet. Inter.* **1992**, *70*, 154–168. [CrossRef]
275. Zhou, L.P.; Shackleton, N.J. Misleading Positions of Geomagnetic Reversal Boundaries in Eurasian Loess and Implications for Correlation between Continental and Marine Sedimentary Sequences. *Earth Planet. Sci. Lett.* **1999**, *168*, 117–130. [CrossRef]
276. Wang, X.; Yang, Z.; Løvlie, R.; Sun, Z.; Pei, J. A Magnetostratigraphic Reassessment of Correlation between Chinese Loess and Marine Oxygen Isotope Records over the Last 1.1Ma. *Phys. Earth Planet. Inter.* **2006**, *159*, 109–117. [CrossRef]
277. Jin, C.; Liu, Q. Revisiting the Stratigraphic Position of the Matuyama–Brunhes Geomagnetic Polarity Boundary in Chinese Loess. *Palaeogeogr. Palaeoclim. Palaeoecol.* **2011**, *299*, 309–317. [CrossRef]
278. Bol'shakov, V.A. The Use of the Rock Magnetic and Paleomagnetic Data for the Loess Plateau Deposits in China for Their Climatologic and Chronologic Correlation to the Oxygen Isotopic Timescale. *Izv. Phys. Solid Earth* **2017**, *53*, 293–310. [CrossRef]
279. Jin, C.; Liu, Q.; Xu, D.; Sun, J.; Li, C.; Zhang, Y.; Han, P.; Liang, W. A New Correlation between Chinese Loess and Deep-Sea $\delta^{18}O$ Records since the Middle Pleistocene. *Earth Planet. Sci. Lett.* **2019**, *506*, 441–454. [CrossRef]
280. Wang, X.; Løvlie, R.; Chen, Y.; Yang, Z.; Pei, J.; Tang, L. The Matuyama–Brunhes Polarity Reversal in Four Chinese Loess Records: High-Fidelity Recording of Geomagnetic Field Behavior or a Less than Reliable Chronostratigraphic Marker? *Quat. Sci. Rev.* **2014**, *101*, 61–76. [CrossRef]
281. Constantin, D.; Cameniţă, A.; Panaiotu, C.; Necula, C.; Codrea, V.; Timar-Gabor, A. Fine and Coarse-Quartz SAR-OSL Dating of Last Glacial Loess in Southern Romania. *Quat. Int.* **2015**, *357*, 33–43. [CrossRef]
282. Interglacials of the Last 800,000 Years. *Rev. Geophys.* **2016**, *54*, 162–219. [CrossRef]
283. Wieczorek, D.; Stachura, M.; Wachecka-Kotkowska, L.; Marks, L.; Krzyszkowski, D.; Zieliński, A.; Karaś, M. Similarities among Glacials and Interglacials in the LR04 Benthic Oxygen Isotope Stack over the Last 1.014 Million Years Revealed by Cluster Analysis and a DTW Algorithm. *Glob. Planet. Chang.* **2021**, *202*, 103521. [CrossRef]
284. Sirenko, O.A.; Matviishyna, Z.M.; Doroshkevych, S.P. New Materials for the Characteristics of Vegetation and Soils of the Lubny Stage of the Early Neopleistocene of Ukraine. *Zbirnyk Nauk. Pr. Inst. Geolohichnykh Nauk. NAN Ukrayiny* **2017**, *10*, 85–94. (In Ukrainian) [CrossRef]
285. Matviyishyna, Z. Micromorphology and pedogenesis of the Pleistocene loess-soil section of Pobuzhye Ukraine and their palaeoenvironmental implication. In *Quaternary Studies in Ukraine, Proceedings of the XVIII Congress of the International Assosiation*

on the Study of the Quaternary Period (INQUA), Bern, Switzerland, 21–27 July 2011; Gerasimenko, N.P., Gozhik, P.F., Dykan, N.I., Matviishyna, Z.M., Shelkoplyas, V.M., Vozgrin, B.D., Eds.; Institute of Geological Sciences NASU: Kyiv, Ukraine, 2011; pp. 55–66.
286. Varga, G. Changing Nature of Pleistocene Interglacials–Is It Recorded by Paleosoils in Hungary (Central Europe)? *Hung. Geogr. Bull.* **2015**, *64*, 317–326. [CrossRef]
287. Lu, H.; Jia, J.; Wang, Y.; Yin, Q.; Xia, D. The Cause of Extremely High Magnetic Susceptibility of the S5S1 Paleosol in the Central Chinese Loess Plateau. *Quat. Int.* **2018**, *493*, 252–257. [CrossRef]
288. Lu, H.; Yin, Q.; Jia, J.; Xia, D.; Gao, F.; Lyu, A.; Ma, Y.; Yang, F. Possible Link of an Exceptionally Strong East Asian Summer Monsoon to a La Niña-like Condition during the Interglacial MIS-13. *Quat. Sci. Rev.* **2020**, *227*, 106048. [CrossRef]
289. An, Z.S.; Liu, T.S.; Zhu, Y.Z.; Sun, F. The paleosol complex S5 in the China Loess Plateau—A record of climatic optimum during the last 1.2 Ma. *Geojournal* **1987**, *15*, 141–143. [CrossRef]
290. Clemens, S.C.; Prell, W.L.; Sun, Y.; Liu, Z.; Chen, G. Southern Hemisphere Forcing of Pliocene δ^{18}O and the Evolution of Indo-Asian Monsoons. *Paleoceanography* **2008**, *23*, PA4210. [CrossRef]
291. Guo, Z.T.; Berger, A.; Yin, Q.Z.; Qin, L. Strong Asymmetry of Hemispheric Climates during MIS-13 Inferred from Correlating China Loess and Antarctica Ice Records. *Clim. Past* **2009**, *5*, 21–31. [CrossRef]
292. Hao, Q.; Wang, L.; Oldfield, F.; Guo, Z. Extra-Long Interglacial in Northern Hemisphere during MISs 15-13 Arising from Limited Extent of Arctic Ice Sheets in Glacial MIS 14. *Sci. Rep.* **2015**, *5*, 12103. [CrossRef] [PubMed]
293. Sirenko, O.A.; Matviishyna, Z.M.; Doroshkevych, S.P. Development of Vegetation and Soils in the Central Part of the Prydniprovska Upland during the Shyrokyne and Martonosha Stages of the Eopleistocene–Early Neopleistocene. *Zbirnyk Nauk. Pr. Inst. Geolohichnykh Nauk. NAN Ukrayiny* **2019**, *12*, 59–67. (In Ukrainian) [CrossRef]
294. Hlavatskyi, D.V. Refined Magnetostratigraphic Position of the Shyrokyne Unit in Loess Sequences from Central Ukraine. *J. Geol. Geogr. Geoecol.* **2019**, *28*, 301–312. [CrossRef]
295. Song, Y.; Guo, Z.; Marković, S.; Hambach, U.; Deng, C.; Chang, L.; Wu, J.; Hao, Q. Magnetic Stratigraphy of the Danube Loess: A Composite Titel-Stari Slankamen Loess Section over the Last One Million Years in Vojvodina, Serbia. *J. Asian Earth Sci.* **2018**, *155*, 68–80. [CrossRef]
296. Hambach, U.; Jovanović, M.; Marković, S.B.; Nowaczyk, N.; Rolf, C. The Matuyama-Brunhes geomagnetic reversal in the Stari Slankamen loess section (Vojvodina, Serbia): Its detailed record and its stratigraphic position. *Geophys. Res. Abstr.* **2009**, *11*, 11498.
297. Williams, D.F.; Peck, J.; Karabanov, E.B.; Prokopenko, A.A.; Kravchinsky, V.; King, J.; Kuzmin, M.I. Lake Baikal Record of Continental Climate Response to Orbital Insolation During the Past 5 Million Years. *Science* **1997**, *278*, 1114–1117. [CrossRef]
298. Molodkov, A.; Bolikhovskaya, N. Climato-Chronostratigraphic Framework of Pleistocene Terrestrial and Marine Deposits of Northern Eurasia, Based on Pollen, Electron Spin Resonance, and Infrared Optically Stimulated Luminescence Analyses. *Est. J. Earth Sci.* **2010**, *59*, 49–62. [CrossRef]
299. Hlavatskyi, D.V.; Stepanchuk, V.N.; Kuzina, D.M.; Poliachenko, I.B.; Shpyra, V.V.; Skarboviychuk, T.V.; Yakukhno, V.I.; Bakhmutov, V.G. Rock Magnetic and Palaeomagnetic Studies of Loess-Palaesol Sections–Lower Palaeolithic Sites within the Southern Bug Valley (Medzhybizh, Holovchyntsi). *Geofiz. Zhurnal* **2021**, *43*, 3–37. [CrossRef]
300. Marković, S.B.; Heller, F.; Kukla, G.J.; Gaudenyi, T.; Jovanović, M.; Miljković, L. Magnetostratigraphy of the Stari Slankamen loess-paleosol sequences (Vojvodina, Serbia and Montenegro). *Zb. Rad. Departmana Geogr. Turiz. Hotel.* **2002**, *32*, 20–28. (In Serbian)
301. Hughes, P.D.; Gibbard, P.L.; Ehlers, J. The "Missing Glaciations" of the Middle Pleistocene. *Quat. Res.* **2020**, *96*, 161–183. [CrossRef]
302. Bol'shakov, V.A. On the Quantity of the Glacial–Interglacial Cycles of the Brunhes Chron Identified in the Deep-Water and Terrestrial Sections. *Izv. Phys. Solid Earth* **2015**, *51*, 630–650. [CrossRef]
303. Wacha, L.; Frechen, M. The Geochronology of the "Gorjanović Loess Section" in Vukovar, Croatia. *Quat. Int.* **2011**, *240*, 87–99. [CrossRef]
304. Timar-Gabor, A.; Panaiotu, C.; Vereș, D.; Necula, C.; Constantin, D. The Lower Danube Loess, New Age Constraints from Luminescence Dating, Magnetic Proxies and Isochronous Tephra Markers. In *Landform Dynamics and Evolution in Romania*; Radoane, M., Vespremeanu-Stroe, A., Eds.; Springer Geography; Springer International Publishing: Cham, Switzerland, 2017; pp. 679–697. [CrossRef]
305. Marković, S.B.; Stevens, T.; Mason, J.; Vandenberghe, J.; Yang, S.; Veres, D.; Újvári, G.; Timar-Gabor, A.; Zeeden, C.; Guo, Z.; et al. Loess Correlations–Between Myth and Reality. *Palaeogeogr. Palaeoclim. Palaeoecol.* **2018**, *509*, 4–23. [CrossRef]
306. Abbott, P.M.; Jensen, B.J.L.; Lowe, D.J.; Suzuki, T.; Veres, D. Crossing New Frontiers: Extending Tephrochronology as a Global Geoscientific Research Tool. *J. Quat. Sci.* **2020**, *35*, 1–8. [CrossRef]
307. Wintle, A.G.; Murray, A.S. A Review of Quartz Optically Stimulated Luminescence Characteristics and Their Relevance in Single-Aliquot Regeneration Dating Protocols. *Radiat. Meas.* **2006**, *41*, 369–391. [CrossRef]
308. Timar, A.; Vandenberghe, D.; Panaiotu, E.C.; Panaiotu, C.G.; Necula, C.; Cosma, C.; Van den Haute, P. Optical Dating of Romanian Loess Using Fine-Grained Quartz. *Quat. Geochronol.* **2010**, *5*, 143–148. [CrossRef]
309. Timar-Gabor, A.; Vandenberghe, D.A.G.; Vasiliniuc, S.; Panaoitu, C.E.; Panaiotu, C.G.; Dimofte, D.; Cosma, C. Optical Dating of Romanian Loess: A Comparison between Silt-Sized and Sand-Sized Quartz. *Quat. Int.* **2011**, *240*, 62–70. [CrossRef]
310. Timar-Gabor, A.; Wintle, A.G. On Natural and Laboratory Generated Dose Response Curves for Quartz of Different Grain Sizes from Romanian Loess. *Quat. Geochronol.* **2013**, *18*, 34–40. [CrossRef]

311. Zech, M.; Kreutzer, S.; Zech, R.; Goslar, T.; Meszner, S.; McIntyre, C.; Häggi, C.; Eglinton, T.; Faust, D.; Fuchs, M. Comparative 14C and OSL Dating of Loess-Paleosol Sequences to Evaluate Post-Depositional Contamination of n-Alkane Biomarkers. *Quat. Res.* **2017**, *87*, 180–189. [CrossRef]
312. Moska, P. Luminescence dating of Quaternary sediments–some practical aspects. *Stud. Quat.* **2019**, *36*, 161–169. [CrossRef]
313. Thiel, C.; Buylaert, J.-P.; Murray, A.; Terhorst, B.; Hofer, I.; Tsukamoto, S.; Frechen, M. Luminescence Dating of the Stratzing Loess Profile (Austria)–Testing the Potential of an Elevated Temperature Post-IR IRSL Protocol. *Quat. Int.* **2011**, *234*, 23–31. [CrossRef]
314. Buylaert, J.-P.; Jain, M.; Murray, A.S.; Thomsen, K.J.; Thiel, C.; Sohbati, R. A Robust Feldspar Luminescence Dating Method for Middle and Late Pleistocene Sediments. *Boreas* **2012**, *41*, 435–451. [CrossRef]
315. Novothny, Á.; Frechen, M.; Horváth, E.; Bradák, B.; Oches, E.A.; McCoy, W.D.; Stevens, T. Luminescence and Amino Acid Racemization Chronology of the Loess–Paleosol Sequence at Süttő, Hungary. *Quat. Int.* **2009**, *198*, 62–76. [CrossRef]
316. Balescu, S.; Lamothe, M.; Panaiotu, C.; Panaiotu, C. La chronologie IRSL des séquences lœssiques de l'est de la Roumanie. *Quaternaire* **2010**, *21*, 115–126. [CrossRef]
317. Balescu, S.; Jordanova, D.; Forget Brisson, L.; Hardy, F.; Huot, S.; Lamothe, M. Luminescence Chronology of the Northeastern Bulgarian Loess-Paleosol Sequences (Viatovo and Kaolinovo). *Quat. Int.* **2020**, *552*, 15–24. [CrossRef]
318. Schmidt, E.D.; Machalett, B.; Marković, S.B.; Tsukamoto, S.; Frechen, M. Luminescence Chronology of the Upper Part of the Stari Slankamen Loess Sequence (Vojvodina, Serbia). *Quat. Geochronol.* **2010**, *5*, 137–142. [CrossRef]
319. Moska, P.; Adamiec, G.; Jary, Z. OSL Dating and Lithological Characteristics of Loess Deposits from Biały Kościół. *Geochronometria* **2011**, *38*, 162–171. [CrossRef]
320. Moska, P.; Adamiec, G.; Jary, Z. High Resolution Dating of Loess Profile from Biały Kościół, South–West Poland. *Quat. Geochronol* **2012**, *10*, 87–93. [CrossRef]
321. Moska, P.; Adamiec, G.; Jary, Z.; Bluszcz, A.; Poręba, G.; Piotrowska, N.; Krawczyk, M.; Skurzyński, J. Luminescence Chronostratigraphy for the Loess Deposits in Złota, Poland. *Geochronometria* **2018**, *45*, 44–55. [CrossRef]
322. Moska, P.; Jary, Z.; Adamiec, G.; Bluszcz, A. Chronostratigraphy of a Loess-Palaeosol Sequence in Biały Kościół, Poland Using OSL and Radiocarbon Dating. *Quat. Int.* **2019**, *502*, 4–17. [CrossRef]
323. Schatz, A.-K.; Buylaert, J.-P.; Murray, A.; Stevens, T.; Scholten, T. Establishing a Luminescence Chronology for a Palaeosol-Loess Profile at Tokaj (Hungary): A Comparison of Quartz OSL and Polymineral IRSL Signals. *Quat. Geochronol.* **2012**, *10*, 68–74. [CrossRef]
324. Vasiliniuc, Ş.; Vandenberghe, D.A.G.; Timar-Gabor, A.; Panaiotu, C.; Cosma, C.; van den Haute, P. Testing the Potential of Elevated Temperature Post-IR IRSL Signals for Dating Romanian Loess. *Quat. Geochronol.* **2012**, *10*, 75–80. [CrossRef]
325. Fedorowicz, S.; Łanczont, M.; Bogucki, A.; Kusiak, J.; Mroczek, P.; Adamiec, G.; Bluszcz, A.; Moska, P.; Tracz, M. Loess-Paleosol Sequence at Korshiv (Ukraine): Chronology Based on Complementary and Parallel Dating (TL, OSL), and Litho-Pedosedimentary Analyses. *Quat. Int.* **2013**, *296*, 117–130. [CrossRef]
326. Constantin, D.; Begy, R.; Vasiliniuc, S.; Panaiotu, C.; Necula, C.; Codrea, V.; Timar-Gabor, A. High-Resolution OSL Dating of the Costineşti Section (Dobrogea, SE Romania) Using Fine and Coarse Quartz. *Quat. Int.* **2014**, *334–335*, 20–29. [CrossRef]
327. Constantin, D.; Mason, J.A.; Veres, D.; Hambach, U.; Panaiotu, C.; Zeeden, C.; Zhou, L.; Marković, S.B.; Gerasimenko, N.; Avram, A.; et al. OSL-Dating of the Pleistocene-Holocene Climatic Transition in Loess from China, Europe and North America, and Evidence for Accretionary Pedogenesis. *Earth-Sci. Rev.* **2021**, *221*, 103769. [CrossRef]
328. Murray, A.S.; Schmidt, E.D.; Stevens, T.; Buylaert, J.-P.; Marković, S.B.; Tsukamoto, S.; Frechen, M. Dating Middle Pleistocene Loess from Stari Slankamen (Vojvodina, Serbia)–Limitations Imposed by the Saturation Behaviour of an Elevated Temperature IRSL Signal. *Catena* **2014**, *117*, 34–42. [CrossRef]
329. Thiel, C.; Horváth, E.; Frechen, M. Revisiting the Loess/Palaeosol Sequence in Paks, Hungary: A Post-IR IRSL Based Chronology for the 'Young Loess Series'. *Quat. Int.* **2014**, *319*, 88–98. [CrossRef]
330. Újvári, G.; Molnár, M.; Novothny, Á.; Páll-Gergely, B.; Kovács, J.; Várhegyi, A. AMS 14C and OSL/IRSL Dating of the Dunaszekcső Loess Sequence (Hungary): Chronology for 20 to 150 Ka and Implications for Establishing Reliable Age–Depth Models for the Last 40 Ka. *Quat. Sci. Rev.* **2014**, *106*, 140–154. [CrossRef]
331. Zöller, L.; Richter, D.; Blanchard, H.; Einwögerer, T.; Händel, M.; Neugebauer-Maresch, C. Our Oldest Children: Age Constraints for the Krems-Wachtberg Site Obtained from Various Thermoluminescence Dating Approaches. *Quat. Int.* **2014**, *351*, 83–87. [CrossRef]
332. Chen, J.; Yang, T.; Matishov, G.G.; Velichko, A.A.; Zeng, B.; He, Y.; Shi, P.; Fan, Z.; Titov, V.V.; Borisova, O.K.; et al. A Luminescence Dating Study of Loess Deposits from the Beglitsa Section in the Sea of Azov, Russia. *Quat. Int.* **2018**, *478*, 27–37. [CrossRef]
333. Fedorowicz, S.; Łanczont, M.; Mroczek, P.; Bogucki, A.; Standzikowski, K.; Moska, P.; Kusiak, J.; Bluszcz, A. Luminescence Dating of the Volochysk Section—A Key Podolian Loess Site (Ukraine). *Geol. Q.* **2018**, *62*, 729–744. [CrossRef]
334. Veres, D.; Tecsa, V.; Gerasimenko, N.; Zeeden, C.; Hambach, U.; Timar-Gabor, A. Short-Term Soil Formation Events in Last Glacial East European Loess, Evidence from Multi-Method Luminescence Dating. *Quat. Sci. Rev.* **2018**, *200*, 34–51. [CrossRef]
335. Zhang, J.; Rolf, C.; Wacha, L.; Tsukamoto, S.; Durn, G.; Frechen, M. Luminescence Dating and Palaeomagnetic Age Constraint of a Last Glacial Loess-Palaeosol Sequence from Istria, Croatia. *Quat. Int.* **2018**, *494*, 19–33. [CrossRef]
336. Lomax, J.; Fuchs, M.; Antoine, P.; Rousseau, D.-D.; Lagroix, F.; Hatté, C.; Taylor, S.N.; Till, J.L.; Debret, M.; Moine, O.; et al. A Luminescence-Based Chronology for the Harletz Loess Sequence, Bulgaria. *Boreas* **2019**, *48*, 179–194. [CrossRef]

337. Avram, A.; Constantin, D.; Veres, D.; Kelemen, S.; Obreht, I.; Hambach, U.; Marković, S.B.; Timar-Gabor, A. Testing Polymineral Post-IR IRSL and Quartz SAR-OSL Protocols on Middle to Late Pleistocene Loess at Batajnica, Serbia. *Boreas* **2020**, *49*, 615–633. [CrossRef] [PubMed]
338. Fenn, K.; Durcan, J.A.; Thomas, D.S.G.; Banak, A. A 180 Ka Record of Environmental Change at Erdut (Croatia): A New Chronology for the Loess–Palaeosol Sequence and Its Implications for Environmental Interpretation. *J. Quat. Sci.* **2020**, *35*, 582–593. [CrossRef]
339. Fenn, K.; Durcan, J.A.; Thomas, D.S.G.; Millar, I.L.; Marković, S.B. Re-Analysis of Late Quaternary Dust Mass Accumulation Rates in Serbia Using New Luminescence Chronology for Loess–Palaeosol Sequence at Surduk. *Boreas* **2020**, *49*, 634–652. [CrossRef]
340. Perić, Z.M.; Marković, S.B.; Sipos, G.; Gavrilov, M.B.; Thiel, C.; Zeeden, C.; Murray, A.S. A Post-IR IRSL Chronology and Dust Mass Accumulation Rates of the Nosak Loess-Palaeosol Sequence in Northeastern Serbia. *Boreas* **2020**, *49*, 841–857. [CrossRef]
341. Perić, Z.M.; Marković, S.B.; Filyó, D.; Thiel, C.; Murray, A.S.; Gavrilov, M.B.; Nett, J.J.; Sipos, G. Quartz OSL and Polymineral Post IR–IRSL Dating of the Požarevac Loess–Palaeosol Sequence in North–Eastern Serbia. *Quat. Geochronol.* **2021**, *66*, 101216. [CrossRef]
342. Groza-Săcaciu, Ș.-M.; Panaiotu, C.; Timar-Gabor, A. Single Aliquot Regeneration (SAR) Optically Stimulated Luminescence Dating Protocols Using Different Grain-Sizes of Quartz: Revisiting the Chronology of Mircea Vodă Loess-Paleosol Master Section (Romania). *Methods Protoc.* **2020**, *3*, 19. [CrossRef]
343. Fedorowicz, S.; Woźniak, P.; Halas, S.; Łanczont, M.; Paszkowski, M.; Wójtowicz, A. Challenging K-Ar Dating of the Quaternary Tephra from Roxolany, Ukraine. *Mineral. Spec. Pap.* **2012**, *39*, 102–105.
344. Fedorowicz, S.; Łanczont, M.; Bogucki, A.; Woźniak, P.P.; Wróblewski, R.; Adamiec, G.; Bluszcz, A.; Moska, P. Isotope dating in Roksolany loess profile. In *Loess Cover of the North Black Sea Region, Proceedings of the XVIII Ukrainian-Polish Workshop, Roksolany, Ukraine, 8–13 September 2013*; Bogucki, A., Gozhik, P., Łanczont, M., Madejska, T., Yeovicheva, J., Eds.; KARTPOL s. c. Lublin: Lublin, Poland, 2013; pp. 65–68. (In Polish)
345. Constantin, D.; Veres, D.; Panaiotu, C.; Anechitei-Deacu, V.; Groza, S.M.; Begy, R.; Kelemen, S.; Buylaert, J.-P.; Hambach, U.; Marković, S.B.; et al. Luminescence Age Constraints on the Pleistocene-Holocene Transition Recorded in Loess Sequences across SE Europe. *Quat. Geochronol.* **2019**, *49*, 71–77. [CrossRef]
346. Kolfschoten, T.; Markova, A.K. Response of the European mammalian fauna to the mid-Pleistocene transition. In *Early–Middle Pleistocene Transitions: The Land–Ocean Evidence (Special Publications)*; Head, M.J., Gibbard, P.L., Eds.; Geological Society: London, UK, 2005; Volume 247, pp. 221–229.
347. Krokhmal, A.I. Eopleistocene sediments biostratification of central part of the northern Black Sea coastal. *Zbirnyk Nauk. Pr. Inst. Geolohichnykh Nauk. NAN Ukrayiny* **2009**, *2*, 194–199. (In Russian)
348. Krokhmal', O.; Rekovets, L.; Kovalchuk, O. An Updated Biochronology of Ukrainian Small Mammal Faunas of the Past 1.8 Million Years Based on Voles (Rodentia, Arvicolidae): A Review. *Boreas* **2021**, *50*, 619–630. [CrossRef]
349. Laag, C.; Hambach, U.; Botezatu, Y.; Baykal, A.; Veres, D.; Schönwetter, T.; Viola, J.; Zeeden, C.; Radaković, M.G.; Obreht, I.; et al. The geographical extent of the "L2-Tephra": A widespread marker horizon for the penultimate glacial (MIS 6) on the Balkan Peninsula. In *Crossing New Frontiers: INTAV International Field Conference on Tephrochronology "Tephra Hunt in Transylvania". Book of Abstracts*; Hambach, U., Veres, D., Eds.; International Union for Quaternary Research: Jena, Germany, 2018; p. 111.
350. Wulf, S.; Fedorowicz, S.; Veres, D.; Łanczont, M.; Karátson, D.; Gertisser, R.; Bormann, M.; Magyari, E.; Appelt, O.; Hambach, U.; et al. The 'Roxolany Tephra' (Ukraine)—New Evidence for an Origin from Ciomadul Volcano, East Carpathians. *J. Quat. Sci.* **2016**, *31*, 565–576. [CrossRef]
351. Łanczont, M.; Madeyska, T.; Bogucki, A.; Mroczek, P.; Hołub, B.; Łącka, B.; Fedorowicz, S.; Nawrocki, J.; Frankowski, Z.; Standzikowski, K. Abiotic environment of the Palaeolithic oecumene in the peri- and meta-Carpathian zone. In *Palaeolithic Oecumene in the Peri- and Meta-Carpathian Zone*; Łanczont, M., Madeyska, T., Eds.; Wydawnictwo UMCS: Lublin, Poland, 2015; pp. 434–435. (In Polish)
352. Molnár, K.; Lukács, R.; Dunkl, I.; Schmitt, A.K.; Kiss, B.; Seghedi, I.; Szepesi, J.; Harangi, S. Episodes of Dormancy and Eruption of the Late Pleistocene Ciomadul Volcanic Complex (Eastern Carpathians, Romania) Constrained by Zircon Geochronology. *J. Volcanol. Geotherm. Res.* **2019**, *373*, 133–147. [CrossRef]
353. Lukács, R.; Caricchi, L.; Schmitt, A.K.; Bachmann, O.; Karakas, O.; Guillong, M.; Molnár, K.; Seghedi, I.; Harangi, S. Zircon Geochronology Suggests a Long-Living and Active Magmatic System beneath the Ciomadul Volcanic Dome Field (Eastern-Central Europe). *Earth Planet. Sci. Lett.* **2021**, *565*, 116965. [CrossRef]
354. Harangi, S.; Molnár, K.; Schmitt, A.K.; Dunkl, I.; Seghedi, I.; Novothny, Á.; Molnár, M.; Kiss, B.; Ntaflos, T.; Mason, P.R.D.; et al. Fingerprinting the Late Pleistocene Tephras of Ciomadul Volcano, Eastern–Central Europe. *J. Quat. Sci.* **2020**, *35*, 232–244. [CrossRef]